



UNIVERSITÀ DEGLI STUDI DI PADOVA

DIPARTIMENTO DI INGEGNERIA CIVILE, EDILE ED AMBIENTALE  
*Department of Civil, Environmental and Architectural Engineering*

---

CORSO DI DOTTORATO IN  
SCIENZE DELL'INGEGNERIA CIVILE, AMBIENTALE E DELL'ARCHITETTURA

XXXIV CICLO

**Impact of agronomic activities on wellhead protection areas**

Tesi redatta con il contributo finanziario di Alto Trevigiano Servizi s.r.l.

Coordinatore:

**Ch.mo Prof. Carmelo Maiorana**

Supervisore:

**Ch.mo Prof. Paolo Salandin**

Dottorando:

**Leonardo Costa**

---

ANNO ACCADEMICO 2021-2022



## Summary

The interaction between agronomic practices and the use of groundwater for drinking water, poses a problem of coexistence between fundamental productive activities for most of the Italian and European territory. The relevance of the problem is evident, just to define methods and rules for the correct management of the underground resource, expressly provided for by the law (e.g. in Italy. D.Lgs n.152 of 3 April 2006), being the task of the Regions the identification of wellhead protection areas. Within the latter several activities are restricted, including agricultural activities carried out with the accumulation and use of chemical and natural fertilizers or pesticides. What is the decay of these substances in the first layers of the soil and their ability to alter the quality of the groundwater and / or to reach an intake work for drinking water is substantially unknown, and the alarms on the presumed danger for human health enhance the need to develop of a specific research. To this aim a diffuse activity has been developed on two typical areas of the Veneto piedemont territory interested by Prosecco vineyard, Valdobbiadene (TV) and Conegliano (TV). In these areas relevant well intakes guarantee the drinking water supply to large areas of the territory. Inside each of the two sites, the infiltration and the mobility of a tracer (KBr) and a Glyphosate based herbicide commonly involved in the vineyards protection, were locally monitored and verified in two areal parcels (25 m<sup>2</sup> each) subjected only to meteorological forcing. The study considered the infiltration process up to a depth of 70 cm, dependent on the pedologic properties of the shallower soil layers, the plant coverage and the root apparati, to obtain the calibration of a one-dimensional hydraulic model for each one of the four monitored parcels. This being the infiltration recognized as the driving mechanism of the pesticides movement. The modelling of the pesticide mobility, monitored together with and its principal metabolite on a temporal window of six months, resulted more complex suggesting a greater affinity of the observed chemical species to be adsorbed to

the soil matrix rather than be dissolved in water and transported toward the deeper layers of the soil. The different results observed between parcels of the same site, suggested a dependency of the pesticide vertical mobility on the heterogeneity of soil properties. To extend the experimental evidence to the scale of the wellhead protection area, a large series of tests has been developed in each site using a double ring infiltrometer and a 30 cm deep soil sampler to evaluate the spatial variability of the infiltration capacity, the soil organic content (TOC) and the soluble phosphorous concentration ( $PO_4^{3-}$ ), seeming the latter apparently correlated to the GLP adsorption. By this way we try to move from a point-wise to a field scale, where the soil properties are described by pedologic maps developed by regional authorities that can be combined with the amount of plant protection products distributed on the Treviso province, to define a vulnerability map of the investigated area. The research results are at the end organized in three subjects linked together: i) modeling of the in-situ experimental evidences of the injection subjected to natural meteorological forcing; ii) characterization of soil heterogeneity based on water infiltration analysis and basic chemical properties of the soil; iii) impact of the total amount of PPPs used in the province of Treviso in the wellhead protection area risk assessment.



## Symbols

**GLP** N-phosphonomethylglycine, Glyphosate

**AMPA** aminomethylphosphonic-acid

**KBr** Potassium Bromide

**ET** Evapotranspiration -  $ET_p$  potential ET

**$K_c$**  Crop coefficient

**$Z_e$**  Depth of influence of the active roots transpiration

**$K_f$**  Freundlich adsorption coefficient

**$K_{fs}$**  Field-saturated hydraulic conductivity

**$K_e$**  Effective hydraulic conductivity

## Acronym

**$SN_p$**  Settolo North parcel

**$SS_p$**  Settolo South parcel

**$CE_p$**  Colnù East parcel

**$CW_p$**  Colnù West parcel

**TV** Treviso province

**DOCG** Denomination of Controlled and Guaranteed Origin

**PPPs** Plant Protection Products

**DPC** Dead Plant Coverage

**BGL** Below Ground Level

**BRTSim** Bio-Reactive Transport Simulator

**PEST** model-independent Parameter ESTimator and uncertainty analysis

**SWAT** Sub-surface Water quality and Agricultural practices monitoring



# Contents

<b>1</b>	<b>Introduction</b>	<b>1</b>
1.1	Problem statement and purpose of the research work . . . . .	1
1.2	General information on wellhead protection areas and regulation . . . . .	5
1.2.1	Regulation on the sustainable use of plant protection products (PPPs) in agriculture . . . . .	10
1.3	Thesis outline . . . . .	13
<b>2</b>	<b>Materials and Methods</b>	<b>15</b>
2.1	The case study: the Province of Treviso and the hills of the Prosecco production . . . . .	15
2.2	Experimental activity and Data Collection . . . . .	18
2.2.1	Glyphosate, a broad-spectrum herbicide . . . . .	19
2.2.2	Experimental sites set-up . . . . .	22
2.2.3	Point-wise monitoring of a glyphosate-based herbicide evolution . . . . .	24
2.2.4	Surveys on the soil properties distribution at the field scale . . . . .	27
2.2.5	Groundwater quality monitoring . . . . .	32
2.2.6	Provincial scale data: PPPs sales and land use . . . . .	35
2.3	Modeling activity . . . . .	37
2.3.1	One-dimensional analysis of water and solutes infiltration . . . . .	38
2.3.1.1	Domain discretization, Boundary conditions . . . . .	39

2.3.1.2	Simulated scenarios . . . . .	41
2.3.2	Analysis of the soil properties spatial variability . . . . .	46
2.3.2.1	Tools for the analysis and the modeling of the surveys results . . . . .	46
2.3.3	Geospatial analysis of the PPPs distribution at provincial scale .	54
<b>3</b>	<b>Results and Discussion</b>	<b>57</b>
3.1	Pointwise-scale results . . . . .	57
3.1.1	Data collected by the meteorological stations . . . . .	57
3.1.2	Analysis of the data collected at the monitoring points . . . . .	58
3.1.2.1	Soil analyses . . . . .	58
3.1.2.2	Water quality from lab analyses . . . . .	62
3.1.3	Results of the numerical simulations . . . . .	65
3.1.3.1	Results of rainwater infiltration modelling . . . . .	65
3.1.3.2	Tracer evolution . . . . .	74
3.1.3.3	Glyphosate evolution . . . . .	77
3.1.4	Final remarks . . . . .	82
3.2	Field-scale results . . . . .	84
3.2.1	Results of the experimental surveys . . . . .	84
3.2.1.1	Soil sampling . . . . .	84
3.2.1.2	Infiltration tests . . . . .	88
3.2.2	Results of the infiltration tests modeling . . . . .	92
3.2.3	Results of the geostatistical analysis . . . . .	98
3.2.3.1	Estimation results . . . . .	105
3.2.4	Results of the groundwater quality monitoring activity . . . . .	112
3.2.5	Final remarks . . . . .	115
3.3	Province-scale results . . . . .	117

3.3.1	PPPs distribution analysis . . . . .	117
3.3.2	Hazard analysis results for the vine-specific PPPs . . . . .	120
3.3.3	Vulnerability of WHPAs . . . . .	123
3.3.4	Final remarks . . . . .	124
<b>4</b>	<b>Conclusions</b>	<b>125</b>



# List of Figures

1.1	Conceptual model of the problem. Limited information is available about the PPPs evolution in the first layers of soil and about their capability to reach drinking water resources. . . . .	3
2.1	The DOCG area of the Prosecco wine production. . . . .	16
2.2	Map of the Treviso province showing the locations of the pumping wells and the areas destined to vineyards. . . . .	16
2.3	Maps of the two experimental sites: a) Settolo, b) Colnù. The red arrows indicate the location of the two sites inside the Veneto region falling in the DOCG production area of Prosecco (light brown area). . . . .	22
2.4	Application of the solution containing the tracer and the glyphosate-based herbicide. (a) The tool used for the application of the solution featuring the concentrations listed in Table 2.3. (b) The application of the solution. . . . .	24
2.5	Correlation plots. Freundlich partition coefficient $K_f$ vs the tested soil chemical parameters in both the experimental sites (see section 2.2.3, Table 2.2). . . . .	29
2.6	Map of the infiltration tests developed at the experimental site of Colnù. . . . .	30
2.7	Map of the infiltration tests and the soil samplings developed at the experimental site of Settolo. . . . .	31

2.8	Functioning of the double-ring infiltrometer. Left: the double-ring infiltrometer. The purpose of the outer ring is to have the infiltrating water act as a buffer zone against infiltrating water straining away sideways from the inner ring. Right: System of measure adopted in each double-ring infiltrometer. Each inner ring has a synthetic measuring bridge (3), the measuring rod (1) with float (4) moves freely up and down through a small tube (2) in the measuring bridge. The float is positioned in the middle of the inner ring. The measuring rod moves freely through the tube and indicates the water level with a millimeter calibration. . . . .	32
2.9	Location of the probe in the Settolo area. Wellhead protection areas around the pumping wells are reported. They are defined by the isochrones (red area) and the geometric (white dotted line) criteria. . . . .	33
2.10	Installation of the Hydrolab HL4 multi-parametric probe. . . . .	34
2.11	Geometry of the model domain. . . . .	40
2.12	Composition of the total evapotranspiration ( $ET_{tot} = K_c * ET_p$ ). $K_c$ coefficient and resulting $ET_{tot}$ depending on simulated scenarios and experimental sites. . . . .	43
2.13	Distribution of the ET water flux withdrawal ( $m^3/s$ ) along $Z_e$ (30 cm). a) No pesticide effects on the transpiration activity of the plants roots (scenarios 2 and 3b). In this case the ET water flux withdrawal is always distributed along the first 30 centimeters of the unsaturated soil. b) Destructive herbicide effects on the transpiration activity of the plants roots (scenario 4). The ET water flux withdrawal take place from the ground-surface for five months after the herbicide application. . . . .	44
2.14	Scheme of the Green-Ampt model. . . . .	47



2.15	Graphical representations of the interpolation methods used to develop a preliminar exploratory data analysis. a) <i>Triangulation-based Natural Neighbor Interpolation</i> (NNI), b) <i>Thiessen Polygons</i> (TP), c) <i>Inverce Distance Weighting</i> (IDW). . . . .	49
2.16	List of parameters for the computation of the experimental variogram for a sparse sample. . . . .	50
2.17	a) Gaussian variogram model with its equation b) Scheme of the ellipse function for the range coefficients. . . . .	52
3.1	Daily precipitation (vertical blue bars) and temperatures (orange lines) measured by the two meteorological stations at Settolo and Colnù. . . .	58
3.2	Rainfall analysis. a) Comparison of monthly and annual precipitations observed at the two experimental sites. b) Histograms of rainfall intensity exceeding 5 mm/h. . . . .	59
3.3	Soil textures up to the depth of -0.70 m in each parcel of Settolo and Colnù sites (data from Mencaroni et al., 2021). . . . .	62
3.4	Results of the analysis performed on the collected water samples. (Data from Mencaroni et al., 2021). . . . .	64
3.5	Results of the rainfall infiltration modelling in terms of water content ( $\theta$ ) at the experimental parcel of Settolo North ( $SN_p$ ) compared with rainfall (P) and evatranspiration (ET) forcing. . . . .	66
3.6	Results of the rainfall infiltration modelling in terms of water content ( $\theta$ ) at the experimental parcel of Settolo South ( $SS_p$ ) compared with rainfall (P) and evatranspiration (ET) forcing. . . . .	67
3.7	Results of the rainfall infiltration modelling in terms of water content ( $\theta$ ) at the experimental parcel of Colnù East ( $CE_p$ ) compared with rainfall (P) and evapotranspiration (ET) forcing. . . . .	68

3.8	Results of the rainfall infiltration modelling in terms of water content ( $\theta$ ) at the experimental parcel of Colnù West ( $CW_p$ ) compared with rainfall (P) and evapotranspiration (ET) forcing. . . . .	69
3.9	Comparison between the Kling-Gupta efficiency coefficients (Gupta et al., 2009) calculated to evaluate the goodness of fit of the soil water-content trend modelled in the tested scenarios (Table 2.6). . . . .	70
3.10	Porosity ( $\varphi$ ) values from Table 3.2 vs depth ( $z$ ). Values of $\varphi$ were initially derived for all parcels using the ROSETTA code (a, b, c and d). Values of $\varphi'$ were derived from bulk densities for the Settolo site (a and b) and water content at saturation for the Colnù site (c and d). . . . .	71
3.11	Hydraulic parameters permeability $k$ and water retention curve coefficients $\alpha$ and $m$ vs depth $z$ . . . . .	72
3.12	Comparison between the tracer concentration values measured at the Settolo site and the results of the tracer infiltration modelling achieved for s2 (red line) and s4 (blue line). . . . .	75
3.13	Results of tracer infiltration modelling compared with water content behavior. Observed values are reported in green while the other lines are the s2 and s4 modelling results. . . . .	76
3.14	Comparison between the Freundlich model result for GLP water-soil partition for $SN_p$ using site-specific experimental data (Mencaroni et al. (2021) – blue line). Linear interpolation to obtain the coefficient $K_d$ for the BRTSim adsorption modelling is reported as dotted line. . . . .	77
3.15	Comparison between the GLP concentration values measured at the Settolo North parcel ( $SN_p$ ) and the results of the GLP infiltration modelling. . . . .	78
3.16	Comparison between the GLP concentration values measured at the Colnù East parcel ( $CE_p$ ) and the results of the GLP infiltration modelling. . . . .	79

3.17 Comparison between Glyphosate and KBr evolutions along the vertical in $SN_p$ and in $CE_p$ . . . . .	80
3.18 Soluble phosphorus $PO_4^{3-}$ concentrations in the topsoil of the Settolo site.	84
3.19 Total Organic Carbon (TOC) and the Volatile Solids (VS) spatial distri- butions at the Settolo site. . . . .	87
3.20 Overview of the infiltration tests results achieved at the Settolo site. The two macro-areas characterized by similar values of soil infiltration capac- ity are outlined in yellow, 'well area', and orange, 'south vineyards'. . .	89
3.21 Overview of the infiltration tests results achieved at the Colnù site . . .	91
3.22 Example of calibration result for the Green-Ampt model parameters, ini- tial water content $\theta_0$ , effective hydraulic conductivity, $K_e$ , and suction head at the wetting front $\psi_{wf}$ . Infiltration test n.116. . . . .	92
3.23 Nash-Sutcliffe Efficiency coefficients for the simulated infiltration tests at a) Settolo and b) Colnù. Figure b) also reports the infiltration test 69, presenting a significant variation in the infiltration rate in the first phases of the test. . . . .	93
3.24 Spatial characterization of the $\log K_{mod}$ distribution at a) the Settolo site b) the Colnù site. . . . .	95
3.25 Histogram of $\log K_{mod}$ obtained for the Settolo site. . . . .	97
3.26 Histogram of $\log K_{mod}$ obtained for the Colnù site. . . . .	97
3.27 Spatial interpolation of the $\log K_{mod}$ values at the Settolo site using the Thiessen Polygons method (TP). . . . .	100
3.28 Spatial interpolations of the modeled hydraulic conductivity, $K_{mod}$ , de- veloped for the Colnù site. . . . .	101
3.29 Spatial interpolation by Ordinary Kriging of the $\log K_{mod}$ values obtained at the Settolo site and Cross-validation result. . . . .	106

3.30	Spatial interpolation by Ordinary Kriging of the $\log K_{mod}$ values subdivided in the two macro-areas of the Settolo site and Cross-validation result.	108
3.31	Experimental variograms computed for the measure points inside a) the well area b) the south vineyards area . . . . .	111
3.32	Example of groundwater quality monitoring developed with the HL4 multi-parameter. . . . .	113
3.33	Example of depth profile measurement developed by dipping the HL4 multi-parameter probe in the borehole of installation. . . . .	114
3.34	Map of the PPPs sales spatial distribution and analysis of the class of use (bar-graphs <i>a</i> and <i>b</i> ). . . . .	118
3.35	Sale trends for the seven best-selling products. . . . .	119
3.36	Hazard maps developed for the wine-growing areas of the Treviso Province.	121
3.37	Vulnerability map for the wells of the Treviso Province. . . . .	122

# List of Tables

2.1	List of parameters observed by the probes of the meteorological stations and by the capacitive sensors. . . . .	23
2.2	Quantities obtained by laboratory analysis on the collected samples. . .	26
2.3	Concentration values and load values used for the application of the herbicide ( <i>he</i> ) on a 25 m <sup>2</sup> area and for the application of the tracer ( <i>tr</i> ) on a 7.5 m <sup>2</sup> area. . . . .	27
2.4	List of parameters measured by the HL4 multi-parameter probe. . . . .	34
2.5	Data about plant protection products, wells, and land use in the Treviso Province accompanied with sources. . . . .	35
2.6	Simulated scenarios for the one-dimensional modeling of the infiltration processes. . . . .	41
2.7	Flowrate values (Q) and concentration values (M) used in the Bromide-application simulation. . . . .	42
2.8	Information used for the development of the PPPs hazard-based classification. Retrieved from the CLP regulation EC 2008/1272. . . . .	55
3.1	Chemical analyses results (data from Mencaroni et al., 2021). . . . .	60
3.2	Physical analyses results (data from Mencaroni et al., 2021) and estimated soil porosity values. . . . .	61

3.3	Log-values of the linear partition coefficient $K_d$ [microg/g*ml/microg] used in the GLP evolution modeling (data from Mencaroni et al. (2021)).	81
3.4	Results of the analyses developed on the top-soil samples collected at the Settolo site. . . . .	85
3.5	Summary of the univariate statistics developed on the top-soil analyses results (Settolo site). . . . .	88
3.6	Infiltration tests modeling results. . . . .	96
3.7	Summary of the descriptive statistics developed on the hydraulic conductivity values obtained for the Settolo site. . . . .	98
3.8	Summary of the descriptive statistics developed on the hydraulic conductivity values obtained for the Colnù site. . . . .	98
3.9	Experimental Variograms computed along $0^\circ$ , $45^\circ$ , $90^\circ$ , $135^\circ$ directions and the parameters values used for the computations. . . . .	103
3.10	Experimental variogram and variogram model for the Settolo site (entire investigated area). . . . .	104
3.11	Parameters for the definition of the experimental variograms based on the values of $\log K_{mod}$ obtained in the well area and in the south vineyards area. . . . .	107
3.12	Experimental variogram and variogram model for the well area of the Settolo site. . . . .	109
3.13	Experimental variogram and variogram model for the south vineyards area of the Settolo site. . . . .	110
3.14	Features and Hazard classification for the best-selling products in the wine-growing areas of the Treviso province . . . . .	120

# Chapter 1

## Introduction

### 1.1 Problem statement and purpose of the research work

Worldwide agricultural practices are commonly developed in areas where groundwater is extracted for drinking water supply, raising relevant questions about the interactions that might occur. Both activities provide vital elements in each of our lives and for other countless productive sectors, but high rates of groundwater demand for irrigation (Siebert et al., 2010), application of fertilizers (Burri et al., 2019), and integrated defenses developed on the chemical plant protection products basis (Arias-Estévez et al., 2008), are all factors that could significantly affect the quality of groundwater.

From the point of view of those who manage the wells supplying drinking water to thousand of inhabitants, groundwater vulnerability to plant protection products (PPPs) has gain more and more relevance since the recent environmental monitoring activities have revealed a diffuse presence of these products in all the inland fresh-water bodies (Tang et al. 2021, and ISPRA, 2020).

In fact, among the water bodies that are exploited as sources for drinking water supply, aquifers are certainly the most fragile due to the large water residence times. A diffuse groundwater contamination could require from weeks to decades for a complete

restoration impeding in this way the use of the water source. Moreover, the impact of groundwater contamination in most cases is not limited to the aquifer itself but affects also the fed springs and water streams (Conant et al., 2004).

In the last thirty years, the problem has been debated at different legislative levels. European Union, Italian Parliament, and Regional authorities, in this order, have set new and more stringent regulations to preserve and improve the quality of the drinking water (see following section 1.2). One of the applied measures to prevent the extraction and the distribution of contaminated groundwater from wells is the establishment of the wellhead protection areas (WHPAs). In these areas a large number of activities are limited or forbidden in order to move away any possible source of point-wise or diffuse pollution from the well location. A generally accepted definition of WHPAs is on the basis of the isochrones, linear envelopes around the well characterized by the same travel time (Stauffer et al., 2005). In this method, distances within the capture area of the well are directly linked to the residence of water and solutes. Depending on the characteristics of these latter, the proper identification of the WHPA boundaries is therefore equivalent to impose a solutes residence time higher than a minimum pre-determined value. This period of time can be linked to the so-called self-purification capacity of the soil, or to the times necessary for implementation of protective measures by the well manager. However, even if this concept has been discussed for a long time, the proper definition of the majority of WHPAs has not been accomplished yet due in most cases to the lack of the necessary information on the well site. For these cases, the currently adopted method is still the geometrical one, permitted by regulation, that is the outlining of a 200 m radius - circular area around the well. This solution is inspired to the simplified groundwater-flow model based on the hypotheses of complete homogeneity and isotropy of the soil and on the presence of a widespread and circular feeding of the aquifer. It goes without saying that in this manner the results are completely generic and inadequate in almost all cases (see section 2.2.5).



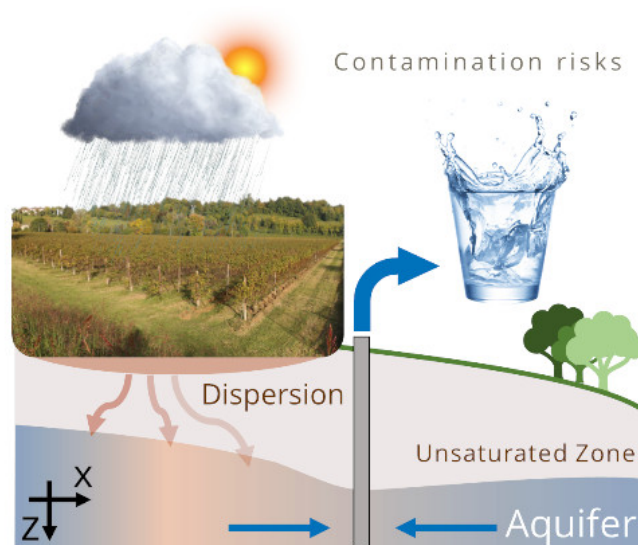


Figure 1.1: Conceptual model of the problem. Limited information is available about the PPPs evolution in the first layers of soil and about their capability to reach drinking water resources.

In parallel to the legislative efforts for water quality preservation, PPPs have been subjected to regulations too reducing by more than 50 % the number of approved active substances in pesticides. In this sector, the actions of the European Commission are not only aimed at the reduction of the potentially harmful PPPs, but also at the adoption of biological-based products capable in the future to substitute the current chemical-based integrated defenses. This recognizing that in a contest of increasing concern for the effects of the global climate change and the increasing lands exploitation, the development of sustainable agronomic practices has become mandatory. However, in the mean time that the agronomic activities evolve in a such way to preserve (or even increase) the actual productivity in a more sustainable way, it is still recognized the relevance to study the mechanisms governing the evolution in the environment of the PPPs active substances still allowed.

Going back to WHPAs, it can be assumed that a contamination process by PPPs starts from the ground-surface and that its evolution is affected by the physical-chemical pro-

cesses that occurs in the unsaturated zone in addition to the transport phenomena that take place in the saturated aquifer, e.g. Crestani et al. (2015a) and Zovi et al. (2017). Products such as chemical fertilizers, herbicides and pesticides undergo significant changes in crossing the topsoil layer, the so-called root zone. Their chemical peculiarities intersect with the microbiological activities and the pedo-climatic properties of the territorial context, giving rise to phenomena of adsorption, volatility and leaching. These processes determine the environmental fate of the fraction of PPPs residues reaching the soil, considerably influencing the prevention and the protection measures (e.g., the WHPAs definition and limitations within them) to be adopted for the maintenance and improvement of the qualitative characteristics of groundwater intended for human consumption (Figure 1.1).

The purpose of this thesis work was to understand the interactions between plant protection products used in agricultural activities and the unsaturated soil of the wellhead protection areas, starting from experimental data and available geographical information collected at different scales connected each other: i) point-wise scale, ii) field scale, and iii) provincial scale. At the point-wise scale (characteristic length  $L = 10^0m$ ), the analysis regarded the leaching capability of PPPs residues, from the ground and subjected to hydrological forcing only. At the field scale,  $L = 10^2m$ , the spatial heterogeneity of the soil properties affecting this leaching capability and of the infiltration velocities, was accounted to spatially extend the point-wise scale results. At the provincial scale,  $L = 10^4m$ , a preliminary link was tested between the evidences ascertained at the two lower scales and the distribution of PPPs on the territory, based on geographical information of public domain. In this research work, the acquired information are aimed at improving the definition of WHPAs by understanding how the PPPs evolution in the unsaturated soil vary their geometric characteristics and therefore their extension in an agricultural territory. This based on physical-chemical processes and not purely geometrical solutions.

## 1.2 General information on wellhead protection areas and regulation

Hereinafter a summary of the regulations in charge established for the definition of the wellhead protection areas (or safeguard zone, as referred to by the European legislation) and on the protection of groundwater intended for human consumption is reported. The purpose of this section is not to provide an in-depth analysis of the current regulation, since this is not the purpose of this thesis work, but only an overview on how the legislators at different levels tackle the problem stated above.

**Directive 2000/60/EC** The European Directive, also called Water Framework Directive, WFD, established a framework for Community action in the field of water policy. The WFD was aimed at the protection and the sustainable management of the freshwater resources, defined by the same directive in the first article as *inland surface waters, transitional waters, coastal waters and groundwater*. In the same article, the purpose of the framework for this latter resource of our interest, is explained as follows:

*(d) to ensure the progressive reduction of pollution of groundwater and prevents its further pollution (...)*

For this reason, the Directive introduced the concept of "safeguard zone" that was then transposed in the Italian regulation, by the D.lgs 152/2006. The directive article established that:

*Article 7*

*Waters used for the abstraction of drinking water*

*1. Member States shall identify, within each river basin district:*

- all bodies of water used for the abstraction of water intended for human consumption providing more than 10 m<sup>3</sup> a day as an average or serving more than 50 persons, and*

- *those bodies of water intended for such future use.*

*Member States shall monitor, in accordance with Annex V, those bodies of water which according to Annex V, provide more than 100 m<sup>3</sup> a day as an average.*

2. *For each body of water identified under paragraph 1, (...) , Member States shall ensure that under the water treatment regime applied, and in accordance with Community legislation, the resulting water will meet the requirements of Directive 80/778/EEC as amended by Directive 98/83/EC.*

3. *Member States shall ensure the necessary protection for the bodies of water identified with the aim of avoiding deterioration in their quality in order to reduce the level of purification treatment required in the production of drinking water. Member States may establish safeguard zones for those bodies of water.*

Within the WFD, article 17 stated the adoption of the more detailed directive reported in the following paragraph, indicating *strategies to prevent and control pollution of groundwater* aimed at *achieving the objective of good groundwater chemical status in accordance with Article 4(1)(b)* of the former directive.

**Directive 2006/118/EC** This directive had a more "technical" character and integrated the fifth annex of the WFD complementing the already indicated provisions for the prevention and the limitation of pollutants inputs into groundwater. It was transposed in the Italian legislation by the D.lgs 30/2009 and established the following criteria:

- a) criteria for the assessment of good groundwater chemical status; and
- b) criteria for the identification and reversal of significant and sustained upward trends and for the definition of starting points for trend reversals.

It was of interest for the development of the experimental activities of this research work, the content of the first annex of the Directive, reported hereinafter.

*For the purposes of assessing groundwater chemical status in accordance with Article 4 (Procedure for assessing groundwater chemical status, writer's note), the following groundwater quality standards will be the quality standards referred to in Table 2.3.2 in Annex V to Directive 2000/60/EC and established in accordance with Article 17 of that Directive.*

<i>Pollutant</i>	<i>Quality standards</i>
<i>Nitrates</i>	<i>50 mg/l</i>
<i>Active substances in pesticides, including their relevant metabolites, degradation and reaction products</i>	<i>0.1 µg/l <sup>(1)</sup></i> <i>0,5 µg/l (total) <sup>(2)</sup></i>

*(1): 'Pesticides' means plant protection products and biocidal products as defined in Article 2 of Directive 91/414/EEC and in Article 2 of Directive 98/8/EC, respectively.*

*(2): 'Total' means the sum of all individual pesticides detected and quantified in the monitoring procedure, including their relevant metabolites, degradation and reaction products.*

The reported table shows the maximum limits allowed in the groundwater for Nitrates and PPPs, both strictly related to agricultural sources of pollution. Particular attention had been paid in setting a limit of 0.5 µg/l to the mixtures of PPPs active substances that could be detected during a groundwater quality survey, being in most cases unknown the real hazard of these mixtures in the environment.

**Directives 91/676/EEC and 2020/2184/EC** Even if not directly correlated to the concept of safeguard zone mentioned in the first two directives, Directives 91/676/EEC and 2020/2184/EC establish important guidelines for the Member States in regulating the monitoring of groundwater quality in agricultural territories and the quality stan-

dards for drinking water intended for human consumption. In details, the antecedent one concerned the protection of waters against pollution caused by nitrates from agricultural sources. The innovative character of this directive consisted more than twenty years ago of recognizing for the first time in the European territory, the pressure coming from the increasing use of fertilizers in agricultural activities on the freshwater bodies, groundwater included. The more recent directory constitutes a recast for clarity purpose of the multiple times amended 98/83/EC, which was more than twenty years ago an important update itself of the Directive 80/778/EEC. Directive 2020/2184/EC is worth to be mentioned here because, without substituting the WFD, poses itself the important objective to

*protect human health from the adverse effects of any contamination of water intended for human consumption by ensuring that it is wholesome and clean, and to improve access to water intended for human consumption*

concerning in this way an other important driving force of this research work: the human health protection against hazardous chemical species such as the PPPs active substances that may reach the drinking water resource.

**D.lgs 152/2006 - art.94** The Directives listed above were fully transposed in the Italian regulation always exceeding the imposed terms of time. The concept of the safeguard zone, only outlined without entering in details in Directives 2000/60 and 2006/118, was established by the article 94 of the legislative decree (D.lgs) 152/2006, the well-known decree concerning an all-encompassing framework in the Italian environmental law. What essentially the article 94 does is to delegate the task of properly define the extension of the wellhead protection areas to the regions. The national regulation limits itself, in the point 6 of the article, to the definition of the already mentioned geometrical method - 200 m radius circular area around the well - in absence of a specific definition by the interested region. Regarding the prohibited activities within the areas, the article set

important limitations for agronomic activities:

- it is forbidden the *accumulation of chemical fertilizers, fertilizers or pesticides*
- it is forbidden the *spreading of chemical fertilizers, fertilizers or pesticides, unless the use of these substances is carried out based on the indications of a specific use plan that takes into account the nature of the soils, compatible crops, the agronomic techniques used and the vulnerability of the water resources*

The outlining of the *specific use plan* for PPPs and the action to take for the activities already present in the area, are both established in the fifth point of the article. The former is again a task of the regions. The latter consist, when possible, in the removal of the forbidden activities. In the case of the agricultural activities, this last sentence constitutes a delicate issue because in most cases the extension of the wellhead protection areas coincides with a large surface of the cultivated territories.

**Resolution of the regional council of the Veneto region, 1621/2019** In the Veneto Region, the task to provide a technical framework for the definition of the well-head protection area, has been only recently accomplished. Without entering in details on the suggested methods, comprising also the isochrones criterion above mentioned, resolution 1621/2019 establishes in particular that

*useful data for the definition of the wellhead protection zone must be based on experimental surveys and site-specific.*

In the list of the site-characterization parameters, even if only briefly expressed, permeability of the unsaturated part of the soil and extension of areas presenting preferential infiltration pathways are suggested. Therefore, the regional regulation leaves a gap to be filled with the study of the mechanisms governing the evolution of solutes in the unsaturated soil, as this work tends to do.

### 1.2.1 Regulation on the sustainable use of plant protection products (PPPs) in agriculture

#### Definitions

A 'pesticide' is something that prevents, destroys, or controls a harmful organism ('pest') or disease, or protects plants or plant products during production, storage and transport. The term includes, amongst others: herbicides, fungicides, insecticides, acaricides, nematocides, molluscicides, growth regulators, repellents, rodenticides and biocides.

Plant protection products are 'pesticides' that protect crops or desirable or useful plants.

An active substance is any chemical, plant extract, pheromone or micro-organism (including viruses), that is contained in a Plant protection product and has action against 'pests' or on plants, parts of plants or plant products.

What is the difference between pesticides and plant protection products?

The most common use of pesticides is in the form of plant protection products.

The term 'pesticide' is often used interchangeably with 'plant protection product', however, pesticide is a broader term that also covers non plant/crop uses, for example biocides.

(Directorate-General, Health and Food Safety, EU)

PPPs (chemical and non-chemical) are essential for food production. Every year around 400'000 tons of active substances of plant protection products are distributed on the European Union territories to i) protect plants or plant products against pests/diseases, before or after harvest, ii) influence the life processes of plants (such as substances influencing their growth, excluding nutrients), iii) preserve plant products, and iv) destroy



or prevent growth of undesired plants or parts of plants. Usually the fraction of active substance in a PPP is around 20% to 30% in weight, increasing to approximately 2 million tons the quantity of complete products - containing other ingredients increasing their effectiveness - that are sold and distributed on the EU agricultural soils in one year. Integrated defenses can be developed using non-chemical PPPs. However, this measures alone cannot satisfy the needs of all the agricultural producers, being still more expensive, less performing, and less persistent respect to the traditional products. In few words they still requires more applications during the treatment periods at higher costs. To reduce the bio-accumulation, the toxicity, and the environmental impact of chemical-based PPPs, in 2009 EU countries were required to implement the Directive 2009/128/EC by adopting National Action Plans (NAPs) for the sustainable use of plant protection products. The Directive established specific actions that are:

training of users, advisors and distributors

inspection of pesticide application equipment

the prohibition of aerial spraying

the protection of the aquatic environment and drinking water

limitation of pesticide use in sensitive areas

information and awareness raising about pesticide risks

systems for gathering information on pesticide acute poisoning incidents, as well as chronic poisoning developments, where available

In Italy, the NAP was formally established with the legislative decree 150/2012. However, the national regulation embedding the technical annexes which contained the indications for the regions, was published in 2014 only with the decree of the ministry of agricultural, food and forestry policies January the 22<sup>nd</sup>, 2014. In the Veneto Region,

the actions delegated to the regions were transposed with the resolution of the regional council of the Veneto region 111/2014.

It is worth reporting that in the national regulation five different fates of PPPs in the environment are recognized. These are i) drift given by the wind, ii) volatilization, driven by the evaporation process, iii) runoff due to the superficial flow of water in numerous streams along a slope, iv) adsorption, depending on the active substance and the chemical properties of the soil and, v) leaching depending on the soil permeability. In the national guidelines, particular prominence is given to the control and the prevention of the drift phenomenon. This is achieved by using anti-drift nozzles regulating the dimension of the solution drops sprayed on the plants, by planning the treatments in days characterized by low wind conditions, by protecting the environmental bodies at the boundaries of the cultivation with the delineation of the so-called "buffer-strips" around the cultivated land plots. Drift-control practices are suggested in arboreal crops like the vine cultivation, for which, however, indications about the amount of PPP to be used per hectare are not always clear. This because there are still many uncertainties on how to control the drift in hilly territories, being different, in that environment, the agricultural practices developed to improve the productivity. Moreover, in most cases the latest technologies (i.e. tunnel sprayer for drift recovery) are not used and this results in the loss in the environment of 30% to 40% of the treatment solution, that may reach the ground and be subjected to infiltration.

Regarding this latter process, less information is given by the national guidelines on how to limit the PPPs leaching process, giving only few suggestion on products to be avoided within highly permeable areas. This also because, as already stated above, few information are currently available on the real capacity of PPPs to reach groundwater and possibly alter freshwater bodies destined to drinking water supply.

### 1.3 Thesis outline

The research activities developed in this thesis work are presented in the following two chapters: 2) Materials and Methods, and 3) Results and Discussion. In the first section of the former, the case-study - the Province of Treviso and the hills of the Prosecco production - according to which all the analyses were applied, is presented. In the following two sections, the experimental activities, the data collection, and the tools used in the modeling activity of the experimental evidences and the collected information, are subdivided in each section according to the analyzed scale and described. This in order to understand the results reported in the following chapter. In this latter, the sections are subdivided according to the scales in which they were achieved.



## Chapter 2

# Materials and Methods

### 2.1 The case study: the Province of Treviso and the hills of the Prosecco production

In the north-eastern Italy the most diffused agricultural activities, together with other productive activities (e.g., Dal Ferro et al., 2016), interacts with the wellhead protection areas located in the territory. This is manifest in the piedmont and in the medium-high plain areas of the Treviso province (Veneto, Italy), where the favorable soil and climate conditions for the growth of the Glera-grape variety have brought, in the last decades, to a continuous increase of land cover for vineyards for the Prosecco wine production. This has mainly happened in a hilly area of 8400 hectares, named hills of Prosecco (Figure 2.1), classified through the label of denomination of controlled and guaranteed origin (DOCG - European Regulation CE n. 479/2008) and recently recognized as a UNESCO heritage. The increasing offer of this typical wine, from 60 million bottles to 92.1 million bottles in the last ten years, requires intensive agronomic strategies of defense, from fungi, bacteria, and viruses, and phyto-regulation (e.g. fertilizers) to keep up with an intense productivity. Nowadays, this can be only achieved using chemical-based PPPs, and this is confirmed by the sales data collected in the province at the municipal-

2.1. The case study: the Province of Treviso and the hills of the Prosecco production

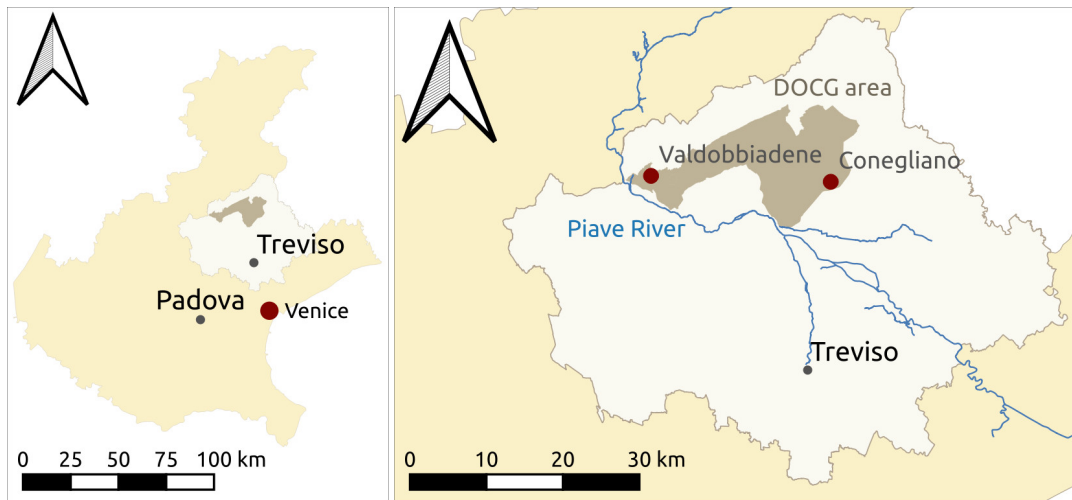


Figure 2.1: The DOCG area of the Prosecco wine production.

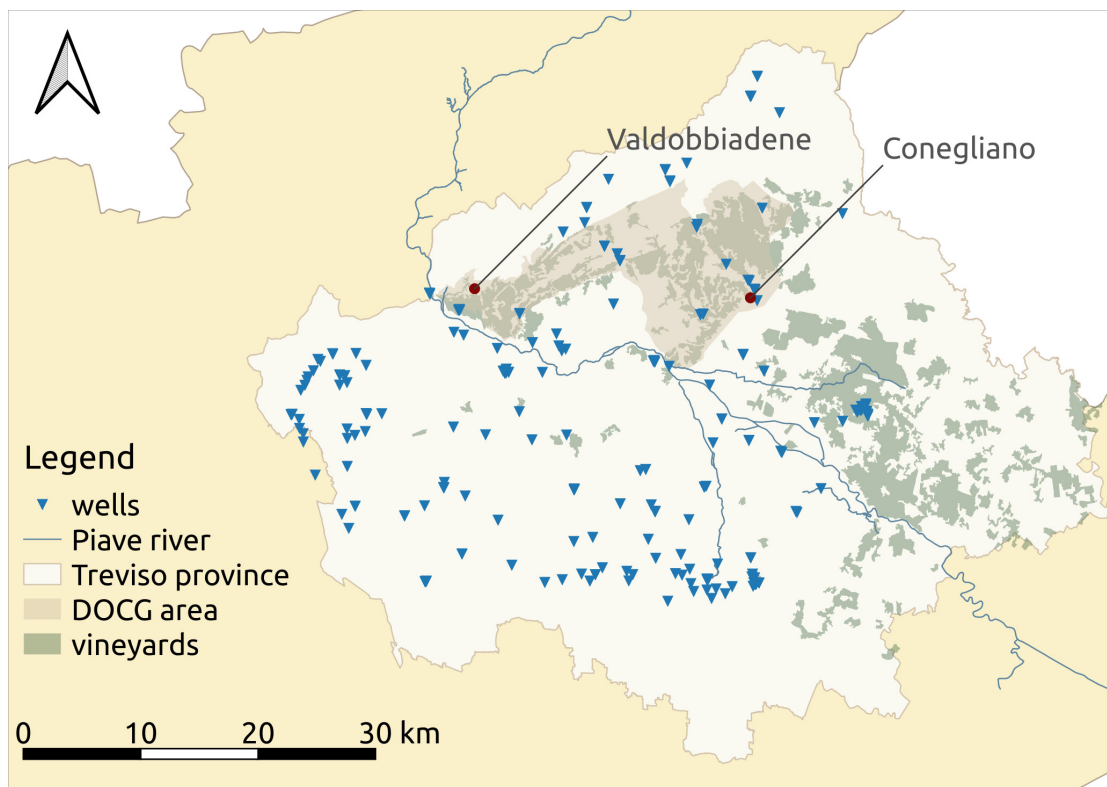


Figure 2.2: Map of the Treviso province showing the locations of the pumping wells and the areas destined to vineyards.

scale (ARPAV, 2020). More than ten million units (liters or kilograms depending on the PPP formulation) have been sold in 2019 in the province of Treviso and among these, 910 thousand units (approximately 10%) were used in the DOCG territories. Uncertainties about the environmental fate of the PPPs residues after the application, in particular their capacity to infiltrate the soil and reach the local aquifers exploited for drinking water supply, and about the harmfulness of PPPs mixtures (e.g. fungicides, pesticides, and fertilizers are commonly used together in a single vine treatment), has raised concerns about possible alterations of the groundwater quality and risks for the human health. This fact is of absolute relevance considering that in the Treviso province a volume of 101.5 million cubic meters of water is extracted every year from wells to supply drinking water to a population of approximately 900,000 inhabitants (Trentin T., 2021) and that round 60 % of this volume is supplied from the Prosecco area. The two reasons that make this territory strategic for drinking water extraction are i) the abundance of good-quality groundwater accessible already from the shallower aquifers, ii) the elevation of the wells respect to the distribution network. These are fundamental in terms of economical and environmental sustainability because both the water purification and the pumping are processes characterized by high costs of operation and require large amounts of energy. A loss of an aquifer as drinking water resource in this area due to PPP contamination, would have such an high impact difficult to properly estimate. This difficult coexistence pushed us to focus our attention on this area and to choose it as case-study.

## 2.2 Experimental activity and Data Collection

To understand the mechanisms and the forcing governing the evolution of PPPs reaching ground surface within WHPAs, the experimental activity has been developed at two different scales, point-wise scale and field scale. In both cases, the activities were carried out in the three and a half year-period 2018-2021 in two sites named Settolo and Colnù, located in two municipalities of the DOCG Prosecco production area, Valdobbiene and Conegliano. Both sites are surrounded by vineyards, although presenting slightly different soil properties and being subjected to non-identical hydrologic conditions. More importantly, they host two systems of wells supplying up to 240 l/s (Settolo) and up to 30 l/s (Colnù) of drinking water, to 40÷50 and 5÷6 thousand inhabitants respectively. The activities developed at the point-wise scale have been part of the project SWAT (Subsurface Water quality and Agricultural practices monitoring), carried out in the two-years period 2018-2020 by the CIR Centre of Hydrology 'DINO TONINI' with the collaboration of the two local integrated water-cycle companies, Alto Trevigiano Servizi and Piave Servizi. The experimental campaign of the project was aimed at understanding the evolution and the leaching capability of the broad spectrum herbicide Glyphosate (GLP, N-phosphonomethyl-glycine), being this active substance largely used in the study area since its introduction in the market in 1974, until 2019. In that year GLP was banned from the DOCG area due to numerous concerns about its potential harmfulness (for Research on Cancer, 2017), but it remained approved for use in the EU territory until 15 December 2022 (EU2017/2324 of December 12th, 2017). This latter reason, joint with limited information available about the herbicide persistence in the environment, made further study on this active substance necessary. The in-depth description of the SWAT monitoring and laboratory activities are available in Carretta et al. (2019) and (Mencaroni et al., 2021) while hereinafter the experimental activities not directly developed within the thesis work are summarized to grant a clear under-



standing of the mathematically described physical processes. In fact, the modelling activity presented in this work, and reported in section 2.3, could have not been developed regardless a clear picture of the phenomena to be simulate.

The experimental activity at the field scale regarded two aspects, i) the study of the spatial distribution of the soil properties affecting the GLP leachability and ii) the monitoring of the groundwater quality based on index parameters. It required logistic support by the two local integrated water-cycle companies but it was fully developed by the author with the fundamental help, during the most demanding talks, of two extremely good collaborators.

At the provincial scale, data collection has been developed to obtain a preliminary map of the Treviso WHPAs vulnerability in a geographical information system (GIS), based on the amounts of PPPs sold in the same territory in the period 2012-2019. Sale data at the municipal scale (the province of Treviso counts 94 municipalities) have been collected by query to the Regional Environmental Agency, ARPAV, being the public data available by law through the agency publication medium, grouped per provinces and hence limited, both in terms of accuracy and geographical resolution.

### **2.2.1 Glyphosate, a broad-spectrum herbicide**

The diffusion of glyphosate (GLP, N-phosphonomethylglycine,  $C_3H_8NPO_5$ ) as a post-emergence herbicide suitable for a large variety of crops, has been supported worldwide since its introduction in 1974 due to its claimed effectiveness, biodegradability and apparent low mobility (Baylis, 2000). However, thanks to the development of new quantification techniques GLP has been identified in a increasing number of environmental monitoring programs. The results achieved in the analysis of GLP residues distribution in the european agricultural topsoils (Silva et al., 2018) and the global-scale hazard analysis correlated to its persistence (Maggi et al., 2020), provided a worrying picture related to the consequences of its widespread use. Along with the long-standing dispute about

the negative effects on human health (Székács and Darvas, 2018), limited information is available on its mobility and decay in groundwater. GLP and its principal degradation metabolite, aminomethylphosphonic-acid (AMPA), have been commonly detected in both surface and subsurface waters by field surveys (e.g. Battaglin et al. 2014). Peruzzo et al. (2008) developed a field survey in a 25 km<sup>2</sup> area interested by intensive soybean cultivations analyzing GLP concentrations in soil, sediments and surface water along a period of 2 years. By comparing the trend of the pesticide concentration in the collected samples with the occurrence of the herbicide applications, the sowings and the observed rainfalls events, a strong correlation between precipitations and GLP concentration in surface waters was ascertained. To study the distribution of GLP and AMPA residues at the catchment scale, Aparicio et al. (2013) carried out a survey at different locations of an agricultural basin located in the southeast of the Province of Buenos Aires. The results show that high mass-fractions of the herbicide and its metabolite were both present in soils subjected to agricultural activity. In the stream samples the concentrations of the two chemicals were found to be higher in suspended particles and sediments than in water. This evidence has been broadly verified in other research works concerning the quality of water coming from agricultural-plots subjected to surface runoff. Napoli et al. (2016) developed a balance to evaluate the herbicide loss caused by soil erosion in a vineyard located in Florence (Italy) observing that rainfall, occurring within a month after the treatment of the vineyard, can cause the transport of high concentrations of GLP and AMPA. Other studies on GLP mobility and persistence in field conditions have been provided by Todorovic et al. (2014) and Poiger et al. (2017). The first investigated the influence of heavy erosive precipitations falling immediately after the application of the GLP formulation Roundup Max<sup>®</sup>. ascertaining the main effects of soil structure and preferential flows on the dissipation of the herbicide and AMPA. The second study was carried out analyzing the concentrations of GLP and AMPA in more than 1000 samples collected from groundwater, surface water, streams, lakes and effluents from wastewa-

ter treatment plants in the province of Zurich. GLP was detected in surface waters at elevated concentrations for a much longer part of the year than other herbicides. The particulate-facilitated transport as principal mechanism for the GLP movement was also verified in soil-flume laboratory experiments developed by Yang et al. (2015) and Bento et al. (2018). In the first case, experiments conducted in an artificial rain-simulation facility confirmed the risks for GLP offsite transport when rainfall occurs shortly after its application on bare loess soil before and after sowing. The second study analysed the redistribution of GLP and AMPA on the soil surface and quantified the transport to off-target areas driven by water erosion. The amounts being transported, re-adsorbed and deposited onto adjacent off-target areas were considerable (8 - 18% of the applied GLP after four rain events). Moreover, the particle-bound transport of the two chemicals resulted mostly associated with the content of organic-matter and the presence of clay minerals, easily and rapidly transported with runoff. Tang et al. (2019) achieved a similar evidence by developing a series of microcosm experiments on soil samples characterized by a different GLP exposure history. Also in this case, the adsorption of GLP to suspended mineral particle was observed in samples with higher fractions of silt and clay. The study assessed the various factor affecting the herbicide biodegradation to simulate the biochemical reactions of GLP degradation also applying the numerical model BRTSim (Maggi, 2006). Laboratory evidences on GLP biodegradation along with field data of precipitation and water-table dynamics were implemented in the research work of la Cecilia et al. (2018) developed using the same model. The study numerically assessed the biodegradation and the infiltration of GLP and AMPA in a vineyard and in a wheat field located in the Po river Valley, Italy. The model used literature data for the sorption dynamics, public database data for the soils characteristics and relationship estimations from physical properties for the hydraulic parameters. GLP and Bromide infiltration experiments were conducted by Okada et al. (2014, 2016) under controlled laboratory conditions using undisturbed soil columns collected in agricultural fields lo-

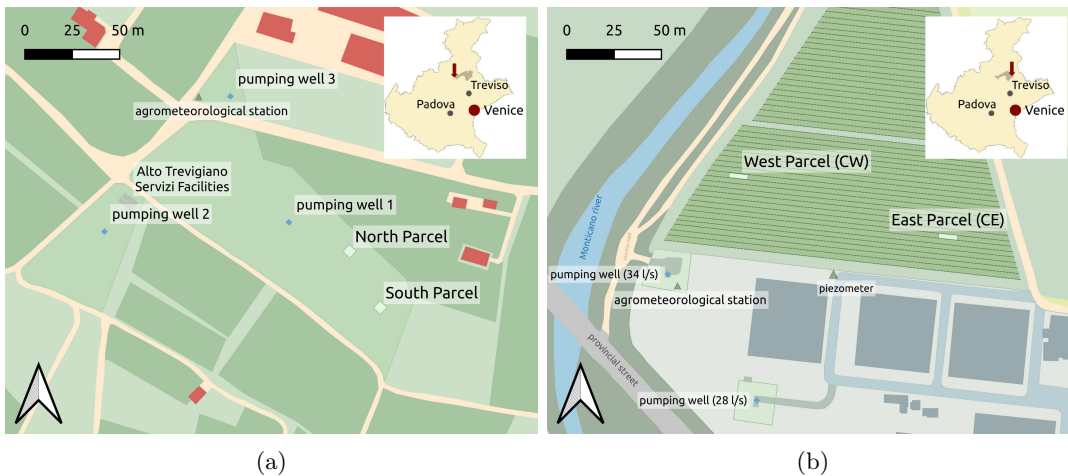


Figure 2.3: Maps of the two experimental sites: a) Settolo, b) Colnù. The red arrows indicate the location of the two sites inside the Veneto region falling in the DOCG production area of Prosecco (light brown area).

cated in the Còrdoba and Buenos Aires provinces, Argentina. The strong retention of glyphosate to the soil matrix was the dominant factor influencing glyphosate mobility in the soil profile. However, the two studies acknowledge a possible underestimation of the GLP leaching concentrations that could occur in the field under rain water condition, considering that GLP's leaching mechanism is mainly via particle facilitated transport. It's manifest that a broad list of studies have been developed to evaluate the presence of GLP in ecosystems or its offsite dispersion by runoff after erosive precipitation events, while less attention is devoted to the subsurface environment where GLP evolution is affected by physical infiltration processes dominated by heterogeneity of the formations and preferential transport pathways (Kjær et al., 2011).

### 2.2.2 Experimental sites set-up

To study the GLP evolution subjected to the hydrological forcing only, two experimental sites were organized in October 2018 in two areas, Settolo - Valdobbiadene and Colnù - Conegliano, hosting two systems of wells and surrounded by vineyards for Prosecco production, cultivated on different soil properties and hydrological conditions. The sites

Table 2.1: List of parameters observed by the probes of the meteorological stations and by the capacitive sensors.

<b>probe</b>	<b>measure</b>	<b>id</b>	<b>unit</b>
Tipping bucket rain gauge	precipitation	P	count
Barometer	atmospheric pressure	$P_{\text{atm}}$	mbar
	relative humidity	RH	%
	temperature	T	$^{\circ}\text{C}$
Thermometer & Hygrometer	dew-point	$T_d$	$^{\circ}\text{C}$
	wind temperature	$T_w$	$^{\circ}\text{C}$
	wind velocity	$v_w$	m/s
Anemometer	wind direction	D	compass degrees
Pyranometer	solar radiation	$E_e$	$\text{W}/\text{m}^2$
Two electrodes capacitive sensors	Volumetric Water Content	$\theta(z)$	%
	Temperature	$T(z)$	$^{\circ}\text{C}$

consisted of an agrometeorological station (DeltaOHM, Italy) and an underground system composed by multi-parametric sensors (HD3910.1, DeltaOHM, Italy), porous water samplers (SPE20, UMS, Germany) and pan lysimeters. The agrometeorological stations were equipped with standard sensors suitable for the measurement and evaluation of the hydrological forcing (Table 2.1). Multi-parametric sensors and pore water samplers were installed at three depths, 0.10 m, 0.30 m, and 0.70 m, to gauge temperature  $T$  ( $^{\circ}\text{C}$ ) and volumetric water content  $\theta$  (%), and to collect soil pore solution. At Settolo due to the presence of large gravel deposits starting from a depth of 0.50 m, it was not feasible to install the pore water sampler at 70 cm, which was replaced with a pan lysimeter. The soil monitoring equipment was installed in two 25 m<sup>2</sup> size plots per site named Settolo North Parcel ( $\text{SN}_p$ ) and Settolo South Parcel ( $\text{SS}_p$ ) for the Settolo site and Colnù East Parcel ( $\text{CE}_p$ ) and Colnù West Parcel ( $\text{CW}_p$ ) for the Colnù site. The two monitoring stations were positioned at reciprocal distances of 30 m and 115 m within the Settolo and the Colnù sites respectively.



Figure 2.4: Application of the solution containing the tracer and the glyphosate-based herbicide. (a) The tool used for the application of the solution featuring the concentrations listed in Table 2.3. (b) The application of the solution.

### 2.2.3 Point-wise monitoring of a glyphosate-based herbicide evolution

In August 2018 a preliminary sampling campaign with the collection of undisturbed core samples of the first meter of soil had been developed to obtain information on physical and chemical properties (Table 2.2). The core samples were collected just outside the site parcels to prevent the creation of preferential infiltration pathways within the areas selected for the monitoring activity. The core samples were collected with a tractor powered hydraulic sampler just outside the site parcels to prevent the creation of preferential infiltration pathways within the areas selected for the monitoring activity. During the sample preparation at the DAFNAE laboratories, the soil samples, having known internal diameter (6.9 cm) and therefore volume, were subdivided in three layers each, 0.00-0.15 m, 0.15-0.40 m, and 0.40-0.70 m for Colnù, and 0.00-0.15 m, 0.15-0.40 m, and 0.40-0.50 m for Settolo. Then, the analyses were performed for each sample section. At the purpose of the successive one-dimensional analysis, both soil texture and soil bulk density were used to estimate the physical soil properties and the hydraulic parameters necessary to simulate the rainwater and the tracer infiltration processes and the vertical GLP evolution (see sections 2.3.1 and 2.3.1.2). The former was determined by using a

particle size analyzer (Mastersizer 2000, Malvern Panalytical Ltd, Spectris Company) according to Bittelli et al. (2019). The latter was measured by drying the soil sample in a ventilated oven at 105 °C and by dividing the resulting weight by the known initial volume of the sample (Dal Ferro N., 2022, private communication).

In November 2018 the applications of a tracer and an herbicide, commonly involved in the protection of the vineyards from weeds and other unwanted plant species, were performed on the four plots. The tracer, potassium bromide (KBr), was applied on a 7.5 m<sup>2</sup> area in the center of each site plot while the pesticide was applied on the whole plot area. The pesticide applied on the four plots was the commercial herbicide Chikara Duo' containing glyphosate (GLP - 28.8%) and flazasulfuron. Its application was carried out simulating the pesticide spreading mechanism of a boom sprayer through a manually conducted tool equipped with an air-actuated nozzle spray bar. For both Chikara and potassium bromide a spatially uniform step-injection (about 10 seconds) was developed. The concentrations used for the application on the four parcels are listed in the Table 2.3. The water samples were collected by connecting, after each rainfall event, a vacuum pump (Vacuum Porter, Meter Group) to the porous cups and the pan lysimeters. They were stored in plastic bottles (Nalgene) to avoid any adsorption phenomenon of the investigated chemicals. Table 2.2 reports the parameters from the analysis on the collected samples. The presence of GLP and AMPA was recognized in terms of concentration and mass fraction by analyzing the water samples and the soil samples through specifically developed laboratory procedures (Carretta et al., 2019). Adsorption analyses were developed on three sections of each core sample (0.00 to -0.15 m, -0.15 m to -0.40 m, -0.40 m to -0.70 m) to quantify the fraction of GLP adsorbed to the soil particles. From the laboratory analyses developed on soil samples, the value of the Freundlich adsorption coefficient  $K_f$  obtained from simple interpolation of the well-known relationship

$$Q_e = K_f \times C_e^{(1/n)} \quad (2.1)$$

Table 2.2: Quantities obtained by laboratory analysis on the collected samples.

quantity	id	unit
soil samples		
soil texture *	-	%
skeleton	-	%
soil pH <sup>+</sup>	pH	\
organic carbon **	OC	% <sub>ds</sub> <sup>1</sup>
total nitrogen **	N <sub>tot</sub>	% <sub>ds</sub> <sup>1</sup>
available phosphorous <sup>x</sup>	P <sub>Olsen</sub>	mg/kg
electric conductivity <sup>+</sup>	EC	μS/cm
cation exchange capacity <sup>*</sup>	CEC	meq/100g
hydraulic conductivity at saturation **	K <sub>sat</sub>	cm/h
soil bulk density <sup>†</sup>	BD	g/cm <sup>3</sup>
porosity	φ	%
water retention curve	pF - curve	\
Freundlich adsorption coefficient <sup>o</sup>	K <sub>f</sub>	μg <sup>(1-1/n)</sup> ml <sup>1/n</sup> g <sup>-1</sup>
glyphosate mass fraction	w <sub>GLP</sub>	μg/kg
aminomethylphosphonic-acid mass fraction	w <sub>AMPA</sub>	μg/kg
water samples		
glyphosate concentration	C <sub>GLP</sub>	μg/l
aminomethylphosphonic-acid concentration	C <sub>AMPA</sub>	μg/l
bromide concentration	C <sub>Br</sub>	mg/l

\* measured with particle size analyzer (Mastersizer 2000, Malvern Panalytical Ltd, Spectris Company)

<sup>+</sup> measured by an electrode in soil suspensions with a soil to water ratio of 1:2.5 (w/v).

\*\* measured with flash combustion method (CNS-analyzer, vario MACRO cube, Elementar Analysensysteme GmbH).

<sup>1</sup> percentage of the dry sample.

<sup>x</sup> measured with the Olsen method.

<sup>\*</sup> measured using the BaCl<sub>2</sub>-triethanolamine method.

\*\* measured with constant head permeameter test.

<sup>†</sup> 105 °C oven-dry bulk density

<sup>o</sup> measured with Batch Equilibrium Method (OECD, 2000). Chemical standard of glyphosate acid (98.6% purity) was purchased from Dr. Ehrenstorfer (LGC Labor GmbH, Augsburg, Germany).

where  $Q_e$  is the amount of GLP adsorbed to soil particles ( $\mu\text{g/g}$ ),  $C_e$  is the GLP concentration in water ( $\mu\text{g/mL}$ ) and  $n$  is the regression constant. According to the assumed unit of measure, the obtained value of  $K_f$  is expressed in terms of  $\mu\text{g}^{(1-1/n)}\text{ml}^{1/n}\text{g}^{-1}$ .

The variables listed in Table 2.1, were observed and acquired by the meteorological stations and by the multi-parametric capacitive sensors with a frequency of one measure every 5 to 15 minutes.



Table 2.3: Concentration values and load values used for the application of the herbicide (*he*) on a 25 m<sup>2</sup> area and for the application of the tracer (*tr*) on a 7.5 m<sup>2</sup> area.

	Settolo		Colnù		unit
	North	South	East	West	
$C_{he}$	17.14	17.14	17.14	17.14	g/l
$L_{he}$	0.16	0.16	0.18	0.24	g/m <sup>2</sup>
$C_{tr}$	112.72	112.08	106.91	106.91	g/l
$L_{tr}$	10.37	10.76	10.26	9.55	g/m <sup>2</sup>

#### 2.2.4 Surveys on the soil properties distribution at the field scale

The surveys consisted of distributed tests for soil infiltration capacity ( $f$ ), [m/s], and soil samplings to measure the mass fractions of volatile solids (VS), [% Total Solids (TS)], total organic carbon (TOC), [%TS], and soluble phosphorous ( $w_{PO_4^{3-}}$ ), [mgP/kgTS].

Phosphorus concentration was evaluated within the experimental site after the results of a correlation analysis developed between the values of the soil chemical parameters observed during the monitoring activity of the GLP degradation, and the Freundlich partition coefficients  $K_f$ , obtained for the soils of the two experimental sites.

Figure 2.5 reports the results of the analysis, showing only a mild anti-correlation of the water-soil partition coefficient - indicating the amount of herbicide remaining in water-solution and the amount adsorbed - with the available phosphorus observed with the Olsen method. This measure provides an estimate of the pool of phosphorus accessible for plant uptake as 'available phosphorus'. By measuring the Olsen P levels, it is possible to estimate how much phosphorus is sitting in soil solution and a proportion of that sorbed to soil colloid surfaces.

According to the mild anti-correlation found with site-specific data, higher phosphorus concentration values correspond to lower  $K_f$  values, increasing the risk of glyphosate mobility in case of high phosphorus soil-content. Despite previous studies have discussed a similar correlation only at high nutrient concentrations, the analysis was developed

anyway, also to collect further information of the spatial variability of the soil properties at the field scale.

Being recognized as the dominant sorbent for most pesticides in soil (Wauchope et al., 2002), and being ascertained the validity of prediction techniques for glyphosate sorption using clay, CEC, and soil organic content concentration values as predictors of the Freundlich coefficient  $K_f$  (e.g. Dollinger et al., 2015), the total organic content (TOC) was also evaluated within the Settolo site.

At the Colnù site the surveys were developed within an area of 1.75 ha, equal to the surface of the two contiguous vineyards located north-east of the system of pumping wells. At the Settolo site the surveys were developed within an area of 2 ha containing the well buffer zone (0.8 ha) and four vineyards characterized by surfaces ranging from 0.1 to 0.5 ha. In each site, two surveys were performed inside the monitoring parcels set-up for the point-wise scale experimental activities,  $CE_p$  -  $CW_p$  and  $SN_p$  -  $SS_p$  respectively, while the remaining ones were spatially distributed maintaining reciprocal distances ranging between 15 and 50 meters within the Colnù site, and between 10 and 40 meters within the Settolo site. Figures 2.6 and 2.7 report the distribution of the surveys within the two sites. The infiltration tests were 54 in total, 17 at Colnù and 37 at Settolo, and they were carried out during five site inspections in the period from June the 30<sup>th</sup> to August the 7<sup>th</sup>, 2020, at the Colnù site and during thirteen site inspections in the period from July the 2<sup>nd</sup> to November 11<sup>th</sup>, 2021, at the Settolo site. They were developed using a set of three double-ring infiltrometers (Eijkelkamp Soil & Water - Figure 2.8) to evaluate both the infiltration curve starting from the non-homogeneous soil-saturation condition (i.e., as it was the soil at the moment of the test), and the field-saturated hydraulic conductivity ( $K_{fs}$ ). For each infiltration test, the preparation at the selected position within the site, consisted of the vertical insertion of the rings up to 5 cm into the soil. At the beginning of the infiltration test, both rings of the infiltrometer were filled with water and the water level  $h$  inside the inner ring was continuously monitored,

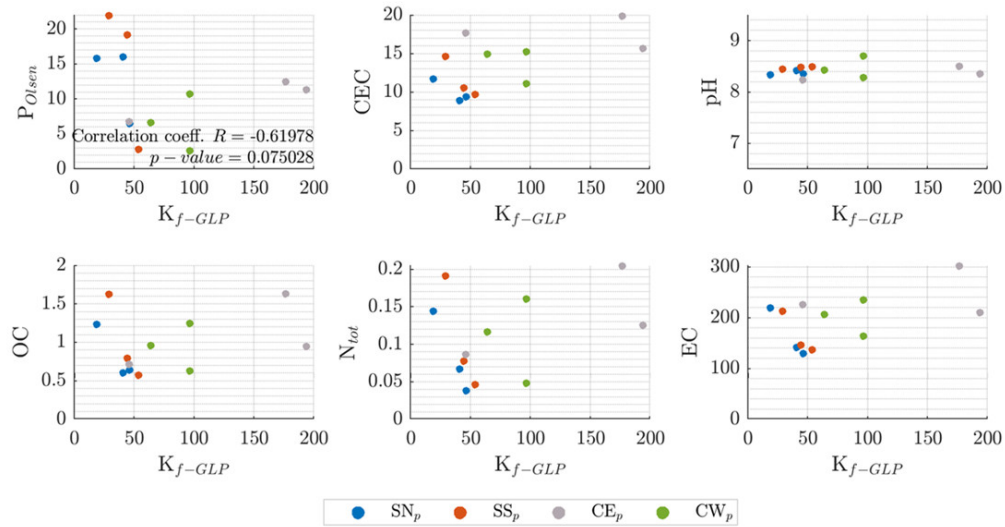


Figure 2.5: Correlation plots. Freundlich partition coefficient  $K_f$  vs the tested soil chemical parameters in both the experimental sites (see section 2.2.3, Table 2.2).

by means of short-intervals  $\Delta t_i$  reading of the measuring rod, to determine the initial slope of the infiltration curve. Afterward, the measuring rod was monitored at constant intervals, 30 to 600 seconds depending on the infiltration rate  $f(h, t)$  (Equation 2.2), to verify the reaching of a constant rate assumed close to  $K_{fs}$ .

$$f(h, t) = \frac{h_{i+1} - h_i}{t_{i+1} - t_i} = \frac{\Delta h}{\Delta t} \quad (2.2)$$

When necessary, the infiltrometer rings were refilled to maintain the water levels even and above zero. This procedure permitted to start a new infiltration test having others still running, thus improving the efficiency of the experimental activity with the simultaneous monitoring of all the three double-ring infiltrometers. In both sites the water needed for the infiltration tests, from 50 to more than 500 liters depending on the soil infiltration capacity, was supplied by the integrated water-cycle company manager of the system of wells, and transported to the tests positions by means of one half-inch HDPE-pipe, a 50-liters water tank, and 6 buckets. The monitoring of each infiltration test running required almost 3 hours.

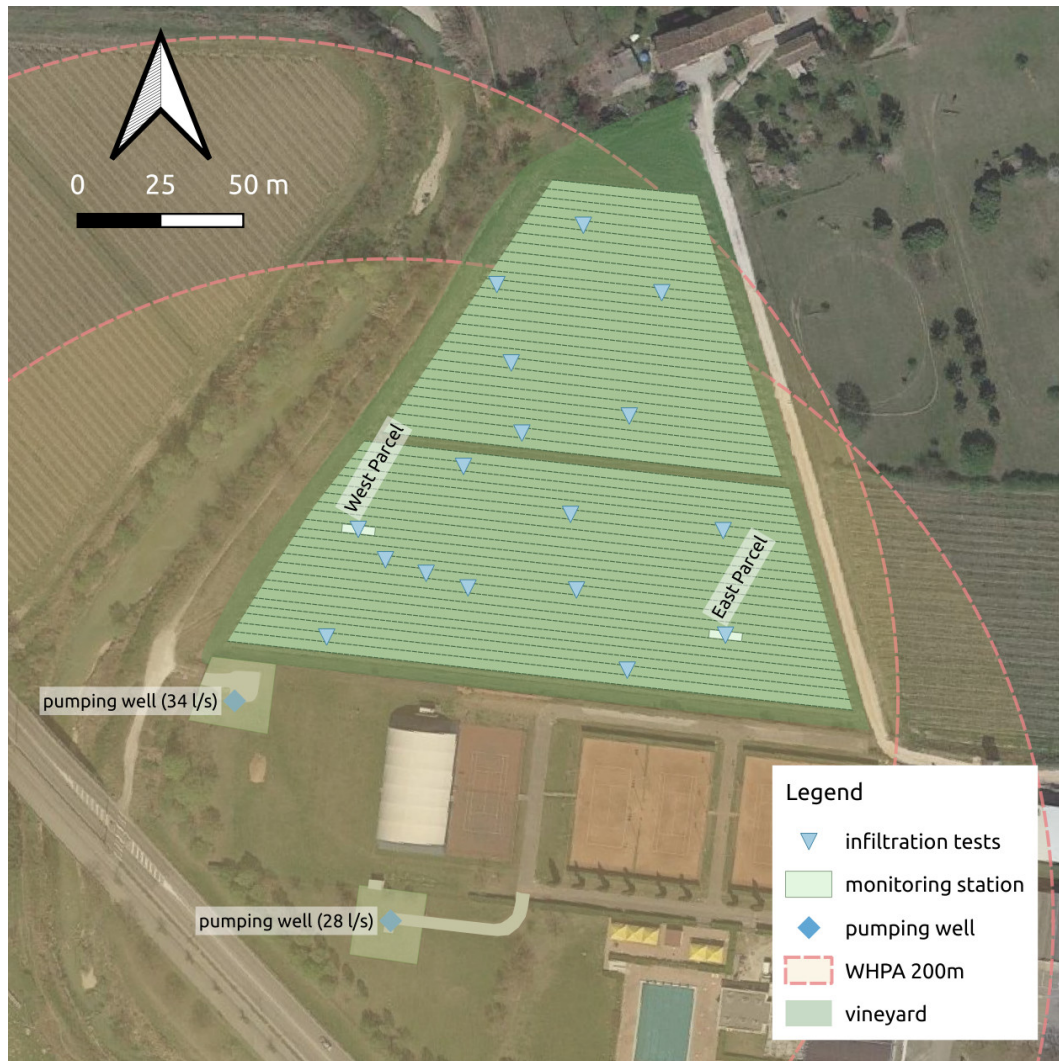


Figure 2.6: Map of the infiltration tests developed at the experimental site of Colnù.

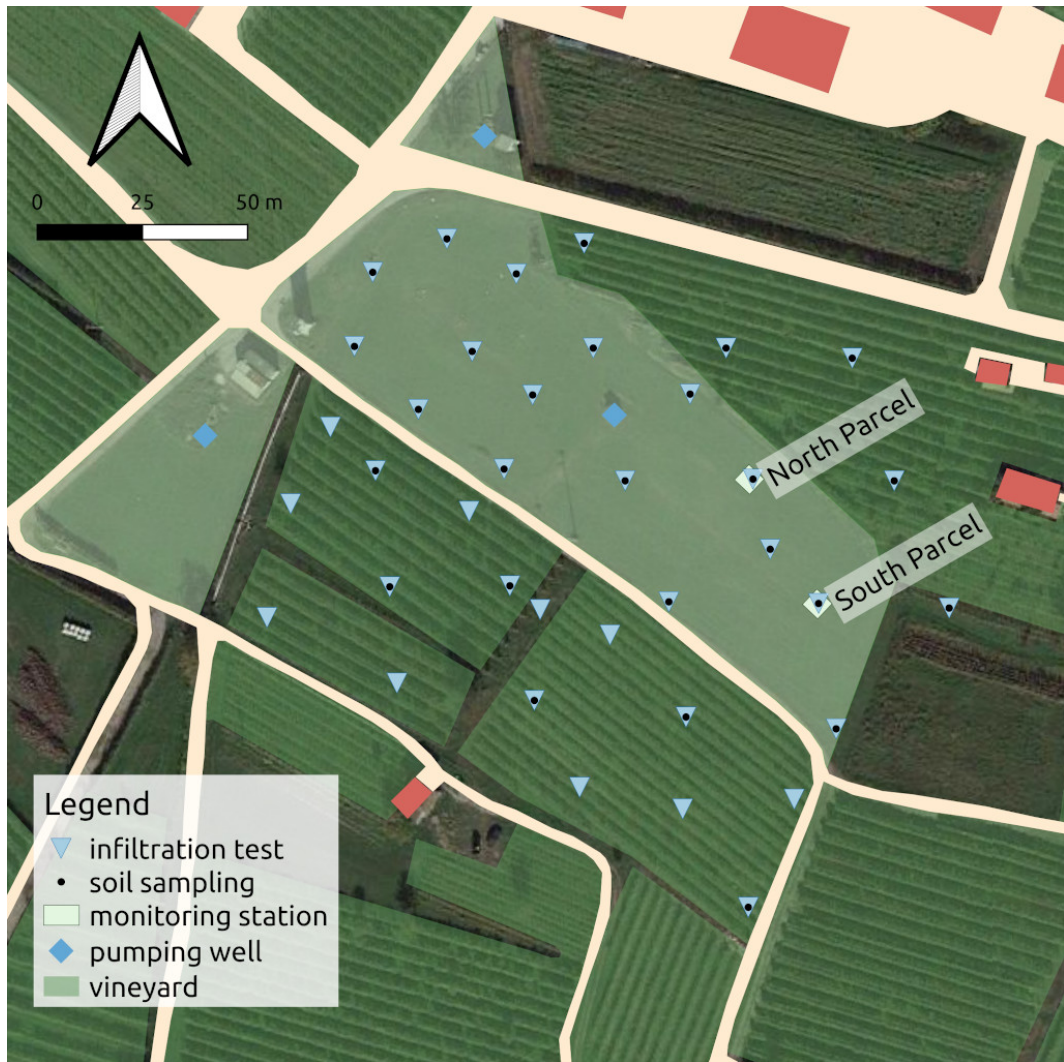


Figure 2.7: Map of the infiltration tests and the soil samplings developed at the experimental site of Settolo.



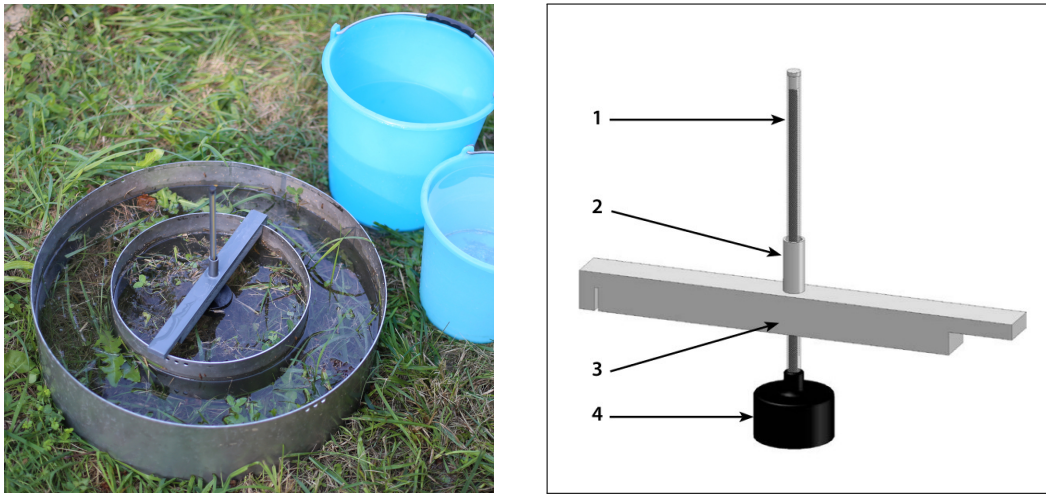


Figure 2.8: Functioning of the double-ring infiltrometer. Left: the double-ring infiltrometer. The purpose of the outer ring is to have the infiltrating water act as a buffer zone against infiltrating water straining away sideways from the inner ring. Right: System of measure adopted in each double-ring infiltrometer. Each inner ring has a synthetic measuring bridge (3), the measuring rod (1) with float (4) moves freely up and down through a small tube (2) in the measuring bridge. The float is positioned in the middle of the inner ring. The measuring rod moves freely through the tube and indicates the water level with a millimeter calibration.

The soil sampling activity regarded the Settolo site only where 27 samples were collected in September the 15<sup>th</sup> and October the 14<sup>th</sup>, 2021, in the same positions of part of the infiltration tests. To collect a significant portion of the topsoil layer, the sampling was performed by means of a 1-inch core sampler up to a depth of 0.40 m. Since no reacting or bio-degradable species were aimed to be measured, after the sampling the core samplers were sealed and stored at room temperature without particular precautions. The soil samples were then analyzed in the laboratory of environmental engineering of the University of Padova.

### 2.2.5 Groundwater quality monitoring

The monitoring activity has been developed at the Settolo site by collecting data on the conditions of the phreatic aquifer exploited by the base-well.

Starting from October 2018, information on the general underground flow paths have

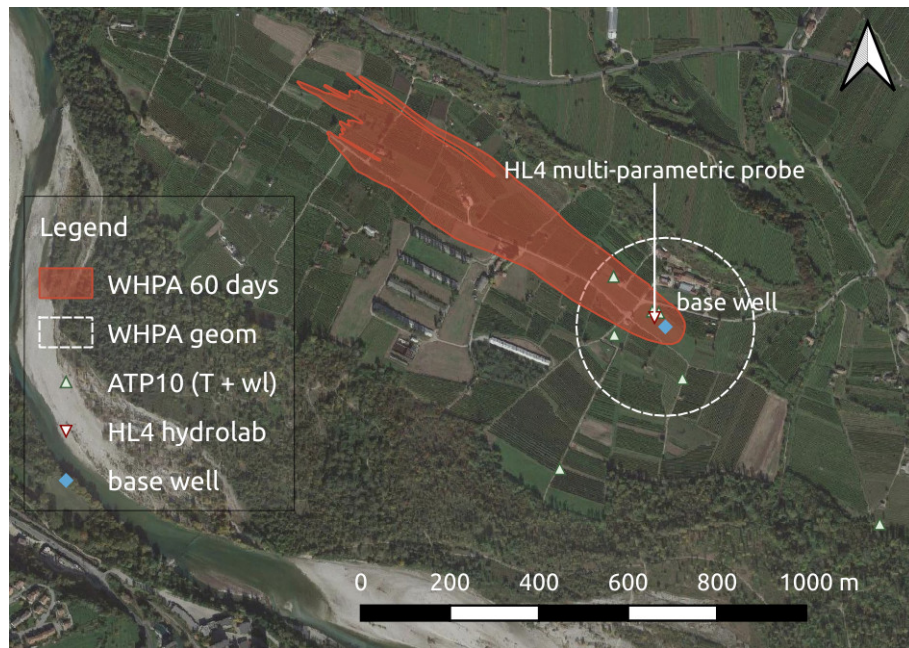


Figure 2.9: Location of the probe in the Settolo area. Wellhead protection areas around the pumping wells are reported. They are defined by the isochrones (red area) and the geometric (white dotted line) criteria.

been retrieved by managing seven probes (Beaver ATP10) installed in as many 35 meter-depth boreholes. The probes measure values of water depth and temperature every 10 minutes, and are part of a larger monitoring network set-up in the same area in 2008 (PRIN 2007). Detailed information on the research project is available at <http://settolo.dicea.unipd.it/>.

In February 2020, the knowledge of the groundwater behavior within the site, permitted the proper positioning of a multi-parametric probe, Ott-Hydrolab HL4, to monitor the quality of the groundwater extracted by the base-well (Figure 2.9). The probe is currently maintained operative thirty meters upstream to the base-well, at a depth of 10 meters BGL in an already-existing borehole. It is equipped with the five sensors and the two selective ions electrodes (ISE) listed in Table 2.4 working synergistically and requiring substitution of the electrode tips and calibration for all the systems of measure at regular intervals of 90 days. Along with the standard water quality in-



Figure 2.10: Installation of the Hydrolab HL4 multi-parametric probe.

Table 2.4: List of parameters measured by the HL4 multi-parameter probe.

sensor/electrode	id	unit
Depth	z	[m]
Temperature	T	[m]
Conductivity	$\sigma$	[ $\mu\text{S}/\text{cm}$ ]
water pH	pH	[ ]
Oxidation-Reduction Potential	ORP	[mV]
ISE Ammonium Ion	$\text{NH}_4^+$	[mgN- $\text{NH}_4^+/\text{l}$ ]
ISE Nitrate	$\text{NO}_3$	[mgN- $\text{NO}_3/\text{l}$ ]



Table 2.5: Data about plant protection products, wells, and land use in the Treviso Province accompanied with sources.

<b>Data</b>	<b>Source</b>
PPPs sale data	Prevention, Food Safety, Veterinary Department, Veneto Region (ARPAV elaboration)
PPPs use in vineyard	2019 Winemaking Protocol, Consortium for the Prosecco DOCG protection
PPPs safety data sheets	<i>Fitogest</i> technical consultation site
wells features and location	Alto Trevigiano Servizi and Piave Servizi
cartographic data	Veneto Region Superior Institute for Protection and Environmental Research (ISPRA)
land use	Corine Land Cover 2018 (CLC18)

dicators, conductivity, temperature, and pH, the index parameter oxidation-reduction potential, ORP, was selected to verify the presence of any ongoing-pollution phenomena while ammonium ion,  $\text{NH}_4^+$  and nitrate,  $\text{NO}_3^-$ , were selected as indexes of aged and diffused groundwater contamination caused by phyto-regulators and fertilizers (Burkart and Stoner, 2008). In fact, Nitrogen is the principal nutrient in the vast majority of fertilizers produced and sold worldwide, due to its positive impact on the plants leaves growth. In details, ammonium ion was selected because ammonia is the main nitrogen-based straight fertilizer while nitrate derived from fertilizers is highly soluble in water and can easily leach through the soil into groundwater (Allison, 1966), as well as being notoriously harmful for the human health.

### 2.2.6 Provincial scale data: PPPs sales and land use

Table 2.5 reports the sources of the data used for the WHPAs vulnerability assessment in the Treviso Province. Regarding the agronomic practices involved in the cultivation of the Glera - grape variety for the Prosecco production, the data has been collected based on the technical source commonly consulted by the insiders, the Winemaking Protocol (*Protocollo Vitivinicolo* in Italian language). This document is drawn up every

year and consists of numerous suggestions on vine cultivation. It reports the updated defense practices to be adopted against all the common diseases acknowledged in viticulture, botrytis, iodine, esca, downy mildew, and indicates the PPPs that can be used to eradicate them. The principal insecticides and generic herbicides to control pests and weeds are indicated too. In a similar manner, the information about the harmfulness of all the vine-specific PPPs was singularly retrieved from the safety sheet of each product, available in the technical consultation site *Fitogest*.

## 2.3 Modeling activity

The information achieved at the three investigated scales were studied using respectively i) physically-based models, ii) geostatistical estimation techniques, and iii) geospatial analyses.

At the point-wise scale, the data collected at the four monitoring parcels of the two experimental sites were used to calibrate/validate a one-dimensional transport model for unsaturated soil and to test its capability to simulate the GLP evolution subjected to the hydrological forcing only. The modeling steps followed considering the uncertainties of real cases (e.g. heterogeneity of the physico-chemical properties of the soil, control on the herbicide drift during application) and in the measurements control, were *i)* rainwater infiltration, *ii)* solute transport, *iii)* evolution of reactive solutes. At the same scale, the results of each infiltration test were analyzed with a simpler infiltration model to obtain additional information on the soil hydraulic properties and on the soil initial conditions at the beginning of the tests. The ensemble of results coming from the distributed surveys developed at each site, were then geo-statistically analyzed to extend the experimental evidences retrieved at the point-wise scale to the field scale. The geospatial analysis of the geographical data collected at the provincial scale was developed to identify possible interactions occurring between the vine cultivation and the soil of the WHPAs based on the reciprocal locations and extensions.

### 2.3.1 One-dimensional analysis of water and solutes infiltration

A one-dimensional transport model for unsaturated soil (Bioreactive Transport Simulator - BRTSim) (Maggi, 2006), was adopted to simulate the rainwater infiltration, the tracer evolution and the glyphosate evolution processes up to the depth of 0.70 m BGL. BRTSim is a finite-volumes computational solver for biogeochemical reaction-advection-dispersion processes in porous and non-porous media. It finds suitable applications to describe water flow in soils, to track transport and dispersion of aqueous chemicals and to assess their chemical equilibrium and their decomposition rates in both chemical and biochemical reactions. The model, for which a detailed description is available in both Maggi (2006) and la Cecilia et al. (2018), was chosen for its capability to handle the numerous biochemical reactions and physical processes characterizing the root zone and affecting the GLP evolution by biodegradation, dispersion, and sorption-desorption dynamics. BRTSim solves a multiphase flow problem over a defined domain (see the following section § 2.3.1.1) considering the three phases, (i) solid phase (M), (ii) liquid phase (L) and (iii) gas phase (G). A fourth independent phase (the biological phase B) is also accounted for given its interactions with L and G phases. M phase is not assumed to undergo dynamic changes within the solving domain. For the other three phases L, G and B, the model computes the mass conservation law

$$\frac{\partial M_\beta}{\partial t} = \int_\Gamma \rho_{\beta e} v_\beta d\Gamma + \int_V \rho_{\beta e} u_\beta dV \pm \int_V f_\beta r_\beta \rho_{\beta e} dV, \quad \text{for } \beta = L, G, B, \quad (2.3)$$

in each volume of the solving domain where  $\rho_{\beta e}$  is the effective phase density (accounting for the effect of dissolved species),  $v_\beta$  corresponds to the Darcy's velocity of phase  $\beta$  through the surface  $\Gamma$  of a volume toward an adjacent volume,  $u_\beta$  is the rate of production and destruction of phase  $\beta$  in that volume, and  $r_\beta$  is the exchange rate between the L and B phases, with  $f_\beta$  the coefficient of conversion. Among the experimental data, the water content observations collected at the depths 0.10 m, 0.30 m

and 0.70 m were used to calibrate/validate the infiltration model, while bromide and GLP concentration data were used only to test the predictive capabilities of the coupled infiltration-advection/dispersion model. The hydraulic parameters, soil porosity  $\varphi$ , permeability  $k$  and retention curve coefficients -  $\alpha$  and  $n$  (van Genuchten, 1980), were initially estimated from soil-textures using the ROSETTA code (Schaap et al., 2001) and then were calibrated working with PEST (Doherty and Hunt, 2010) to minimize the difference between modelled and observed  $\theta$  values. The Kling-Gupta efficiency coefficient (KGE) (Gupta et al., 2009) was used to evaluate the goodness of fit of the developed simulations to the measured  $\theta$  trends. In the assessment of the model efficiency, KGE gives more weight to similar behaviors between observed and modelled trends rather than the squared errors computed between observed and modelled values (see Gupta et al. (2009)). This peculiarity makes this metric more suitable for hydrological models where the physical quantities are often characterized, as in this case, by peaks and high variability. The hydrological forcing, considered as main driving mechanism for rainwater and solutes infiltration, was modelled starting from the rainfall depths acquired by the rain gauges and the variables observed by the two agro-meteorological stations. The evapotranspiration forcing (ET) was developed using the single crop coefficient approach  $ET_{tot} = K_c \times ET_p$  provided by (Allen et al., 1998) being the potential evapotranspiration (ET<sub>p</sub>) assessed using the Penman-Monteith equation. The crop coefficient  $K_c$  [ \ ] was differently assumed depending on the vitality of the vegetation cover, and the glyphosate herbicide effects (dead plant coverage - DPC). The depth of influence of the active-roots transpiration  $Z_e$ [cm] was assumed according to the time behavior of  $K_c$  (Allen et al., 1998).

### 2.3.1.1 Domain discretization, Boundary conditions

The model domain, shown in Figure 2.11, is a box subdivided in seventeen elements of thicknesses  $\Delta_i$  and volumes  $\Delta_i * A_t$ , being  $A_t = 25 \text{ m}^2$  considering the infiltration

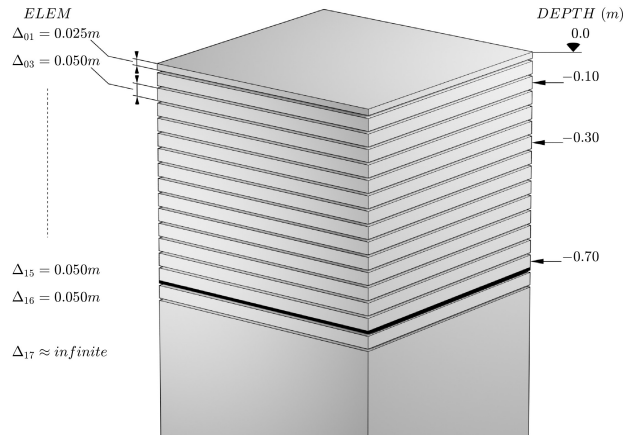


Figure 2.11: Geometry of the model domain.

modelling of water and glyphosate and  $A_t = 7.5 \text{ m}^2$  for the tracer. For each element, the following features have been defined. (i) Depth, volume, interface areas with the adjacent elements and distances between upper and lower centers of mass (nodes). (ii) Soil texture and hydraulic properties (absolute permeability  $k$ , Van Genuchten retention curve coefficients  $\alpha$  and  $n$  and residual liquid and gas saturations). (iii) Initial conditions of soil saturation, soil temperature and gas pressure. The thickness of the surficial element has been set equal to 0.025 m while for the other elements has been set equal to 0.05 m to obtain the correspondence between the third, seventh, fifteenth elements central nodes and the capacitive sensors and the water pore samplers depths installed at -0.10, 0.30 and -0.70 meters. Neumann's (second type) boundary conditions were set at the surface of the domain and at the bottom of the lower domain element by imposing a material flux equal to zero. A free water drainage condition at 0.70 m BGL was simulated by assigning a nearly infinite volume to the seventeenth element (Maggi, 2019, personal communication). Uniform conditions have been imposed at the beginning of a spin-up period of 90 days during which the first 30 days of hydrological forcing were repeated for three times to mitigate the influence of the initial values on the model results. In detail, the soil saturation was set equal to 98% for the elements from  $\Delta_{01}$  to  $\Delta_{15}$  and

Table 2.6: Simulated scenarios for the one-dimensional modeling of the infiltration processes.

scenario	$\varphi'$ [ % ]		calibration						validation	tracer sim.
	Settolo	Colnù	$t_{cal}$ [ d ]	$Z_e$ [cm]	$K_c$ [ \ ]	$k$ [m <sup>2</sup> ]	parameters $\alpha$ [ \ ]	$m$ [ \ ]	$t_{val}$ [ d ]	
0	from the ROSETTA code		no	none	const	- parameters from the ROSETTA code -			93	none
1	derived from bulk density	$\theta_{max}$	156	"	"	calibrated	calibrated	calibrated	"	"
2	"	"	"	30.0	time varying	"	"	"	"	YES
3a	"	"	"	none	const	from lab analysis			"	none
3b	"	"	"	30.0	time varying	"	"	"	"	"
4	"	"	"	time varying	"	"	calibrated	calibrated	"	YES

$\varphi'$ : maximum volumetric water content

$\theta_{max}$ : maximum volumetric water content measured on-site

60% for the elements  $\Delta_{16}$  and  $\Delta_{17}$ , the soil temperature was considered constant along the vertical direction and equal to the daily mean temperature of the first day of the simulated period and the gas pressure was set equal to the daily averaged atmospheric pressure gauged by the meteorological station in the first day of the simulated period.

### 2.3.1.2 Simulated scenarios

The scenarios reported in Table 2.6 were developed by varying the parameters  $Z_e$ ,  $K_c$ ,  $k$ ,  $\alpha$  and  $n$  to test the influence of each parameter on the modelling of the infiltration process, also using water retention curves deduced from laboratory analyses. The numerical code also required the definition of the maximum volumetric water content that can be reached under the forcing conditions. Theoretically this value corresponds to the porosity  $\varphi$ , but during the infiltration process that takes place in field conditions, bubbles of air entrapped in the soil matrix play a fundamental role, reducing the maximum volumetric water content to a value  $\varphi' \leq \varphi$ . In a first approximation (scenario 0)  $\varphi'$  was set equal to  $\varphi$ , being the latter deduced from the soil texture by means of the Rosetta code (Schaap et al., 2001). In the other scenarios, a most proper  $\varphi'$  value was estimated based on the measured maximum volumetric water content values or on the bulk densities when the former gave unphysical values. Starting from the scenario 0 where rough hydraulic parameters were set based on the Rosetta code, the scenarios differ each other by increasing the complexity of the simulated physical processes. All

Table 2.7: Flowrate values (Q) and concentration values (M) used in the Bromide-application simulation.

index	7.5 m <sup>2</sup> areal parcels				unit
	Settolo North	South	Colnù East West		
Q <sub>Br</sub>	0.069	0.072	0.072	0.067	L/s
M <sub>Br</sub>	1.411	1.403	1.338	1.338	mol/l

the scenarios considered the rainwater infiltration process simulation while the simulation of the tracer and the glyphosate transport process were developed in the scenarios performing better in terms of water infiltration (scenarios 2 and 4). Hereinafter, a brief description of each is provided focusing the attention on the introduced variations.

**Scenario 0.** The water infiltration process was simulated implementing the soil hydraulic parameters obtained through the ROSETTA code where the crop coefficient  $K_c$  was assumed constant and equal to unit, meaning that all  $ET_p$  contributed to the total evapotranspiration ( $ET_{tot}$ ).

**Scenario 1.** The values of  $\varphi'$  for the soil layers of the Colnù site were derived from the maximum water content measured in the field by the capacitive sensors. The corresponding values for the soil layers of the Settolo site were extrapolated starting from the bulk densities of the collected soil samples due to spikes in maximum water content value. The hydraulic parameters  $\alpha$ ,  $n$  and  $k$  were calibrated along a 156-day period discarding  $\theta$  values observed when the soil temperatures were gauged below 0 °C. The crop coefficient  $K_c$  was assumed constant and equal to one (Figure 2.12).

**Scenario 2.** The simulations were developed considering constant values for  $Z_e$  and a time varying  $K_c$  according to Allen et al. (1998).  $Z_e$  was set equal to 30 cm to simulate the transpiration carried out by the root apparatus of the grass coverage. Thus, the  $ET_{tot}$  water flux was simulated as a water withdrawal proportionally distributed along a depth of 30 cm, and  $K_c$  was assumed equal to 0.9 until the pesticide application and equal to 0.3 for the next three months (Allen et al., 1998). The hydraulic parameters of



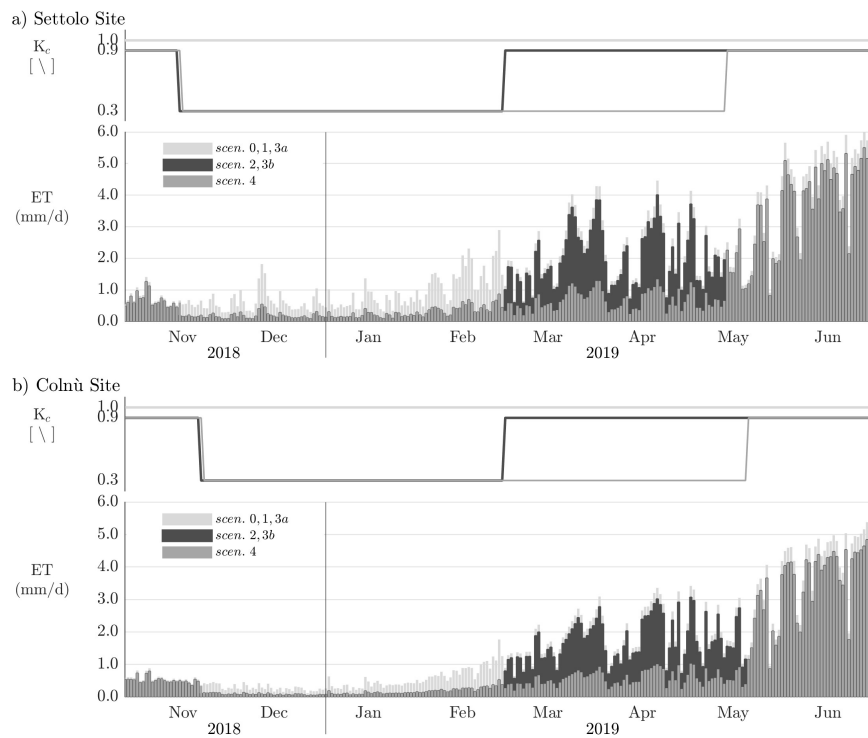


Figure 2.12: Composition of the total evapotranspiration ( $ET_{tot} = K_c * ET_p$ ).  $K_c$  coefficient and resulting  $ET_{tot}$  depending on simulated scenarios and experimental sites.

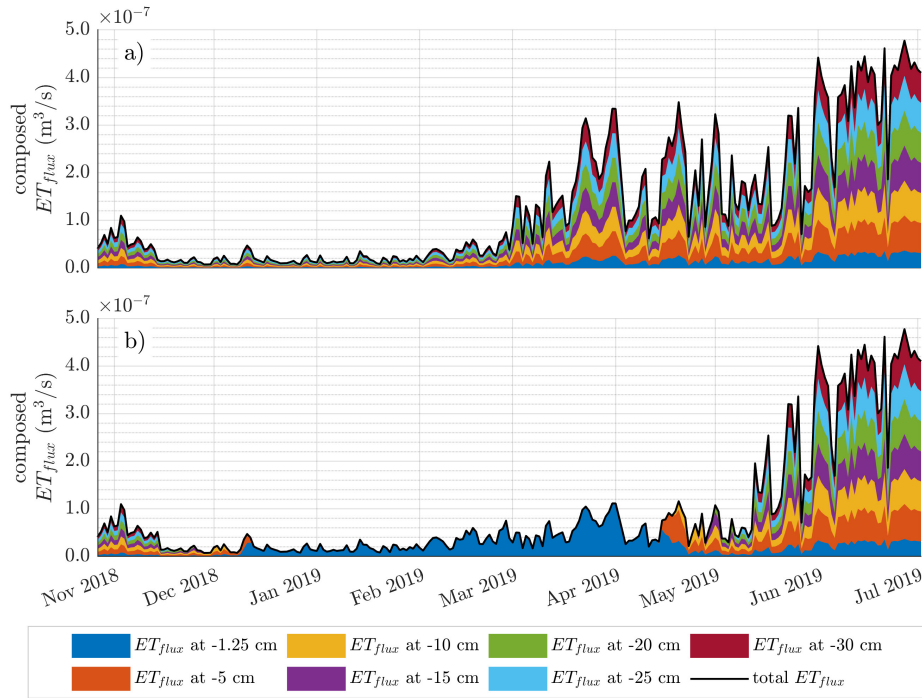


Figure 2.13: Distribution of the ET water flux withdrawal ( $\text{m}^3/\text{s}$ ) along  $Z_e$  (30 cm).  
 a) No pesticide effects on the transpiration activity of the plants roots (scenarios 2 and 3b). In this case the ET water flux withdrawal is always distributed along the first 30 centimeters of the unsaturated soil.  
 b) Destructive herbicide effects on the transpiration activity of the plants roots (scenario 4). The ET water flux withdrawal take place from the ground-surface for five months after the herbicide application.

the soil were calibrated along a 156-day period. The potassium bromide application was modelled as a 10 second step-injection and the diffusion coefficient  $D_s$  was set equal to  $1E-0.9 \text{ m}^2/\text{s}$ . Table 2.7 reports the fluxes and the molar concentrations of the injected solution for each parcel and implemented in the transport model.

**Scenarios 3a and 3b.** The retention curve coefficients  $\alpha$  and  $n$  were derived by fitting the experimental water-retention curves obtained from the soil samples collected in the field (Table 2.2 and section 2.2.3).

**Scenario 4.** To account for the pesticide effects on the plant roots, the simulations were developed assuming a DPC period of six months ( $K_c = 0.3$ ) since the parcel treatment. Moreover,  $Z_e$  was reduced from 0.30m (Scenario 2) to 0.0125m being the water withdrawal limited at the surface during the DPC period.

### 2.3.2 Analysis of the soil properties spatial variability

The spatial analysis on the experimental results obtained with the distributed surveys at the two sites, was developed by using the tools hereinafter described. This, to retrieve additional information on the soil properties not measured both at the scale of the single survey (point-wise), and within the areas extending between the surveys positions. The first issue was tackled by numerical analysis of the infiltration tests results. The second one, by applying to the ensembles of data spatially distributed, both two-dimensional interpolation methods and geostatistical tools for structural analyses and estimation (De Marsily, 1986).

#### 2.3.2.1 Tools for the analysis and the modeling of the surveys results

**Green-Ampt model** To estimate the initial soil water content  $\theta_0$  and the effective hydraulic conductivity, commonly referred in literature to as  $K_e$ , with  $K_e \approx 0.5 \cdot K_{sat,lab}$  according to Bouwer (1966), each infiltration test data have been analyzed using the Green-Ampt model (Green and Ampt, 1911).

Being us aware of the limitations of using the Green-Ampt (GA) model in the case of soils presenting non-homogeneous profiles along the vertical (e.g. Childs and Bybordi 1969 and Moore and Eigel 1981), the model was chosen for the interpretative analysis of the infiltration tests results obtained at the two experimental sites. This, because the infiltration tests were developed in areas characterized by unknown pedological properties, so that the choice of the Green-Ampt model limited the number of requested soil-hydraulic parameters to the only effective suction head  $\psi$ .

The model is derived from the simplified picture of infiltration reported in Figure 2.14 and is based on the hypothesis of a sharp wetting front dividing soil of moisture content  $\theta_0$  below from saturated soil with moisture content equal to the porosity  $\varphi$  above (Shaw, 2005). Following this scheme, the increase in the water stored in the soil for a unit cross section as a result of infiltration is  $L(\varphi - \theta_0)$ . This quantity is set by definition as equal

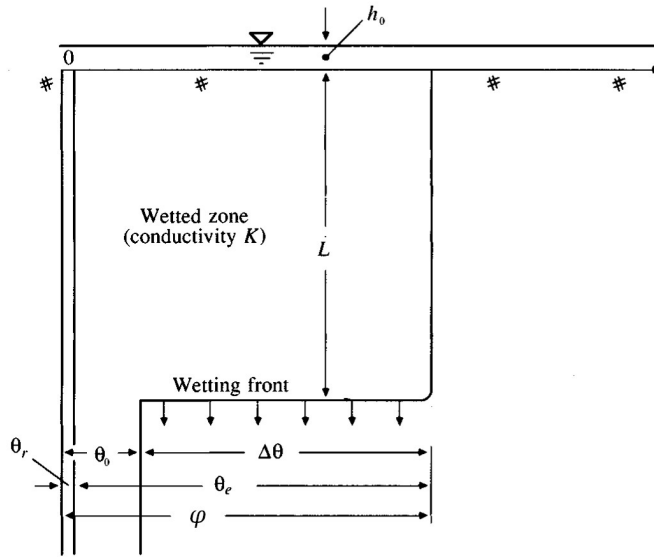


Figure 2.14: Scheme of the Green-Ampt model.

to the cumulative depth of water infiltrated into the soil

$$F(t) = L(\varphi - \theta_0) = L\Delta\theta \quad (2.4)$$

Considering the momentum, the Darcy flux  $q$  expressed by the Darcy's law

$$q = -K \frac{\partial h}{\partial z} = -f \quad (2.5)$$

is assumed constant along the depth and equal to  $-f$ , being the infiltration rate positive downward. Considering two points, 1 and 2, located respectively at the ground surface and just below the wetting front, Equation 2.5 can be approximated by

$$f = K \left[ \frac{h_1 - h_2}{z_1 - z_2} \right] \quad (2.6)$$

where  $h_1$  is equal to the initial ponding depth  $h_0$ . Being the head  $h_2$  equal to the depth of the wetting front  $-L$  increased by the wetting front soil suction head  $-\psi_{wf}$ ,

the Darcy's law for the system can therefore be rewritten as follows:

$$f = K \left[ \frac{h_0 - (-\psi_{wf} - L)}{L} \right] \quad (2.7)$$

From the definition of the cumulative infiltration depth, substitution of 2.4 into 2.7 gives

$$f = \frac{dF}{dt} = K \left[ \frac{h_0 + \psi_{wf} + F(t)/\Delta\theta}{F(t)/\Delta\theta} \right] \quad (2.8)$$

considering also that the infiltration rate can be written as  $f = dF/dt$  and 2.8 can be expressed as a differential equation in the one unknown F. At this point, the initial ponding is often neglected (e.g. Chow et al.,1988, Endreny, 2006) and the integration of the 2.8 between two time steps,  $t - 1$  and  $t$ , leads to

$$F_t = F_{t-1} + K_e \Delta t + \psi_{wf} \Delta\theta \cdot \log \left( \frac{\psi_{wf} \Delta\theta + F_t}{\psi_{wf} \Delta\theta + F_{t-1}} \right) \quad (2.9)$$

However, this was not the case, since the initial ponding depth  $h_0$  was set equal to the water level  $h_0^*$  measured inside the infiltrometer after each refilling managed to avoid the complete drainage of the system (see § 2.2.4). Therefore, the integration of the 2.8 that was used for the experimental data analysis accounting for the initial ponding depth, is the following:

$$F_t = F_{t-1} + K_e \Delta t (1 - \Delta\theta) + \frac{h_0^* + F^* + \psi_{wf}}{1 - \Delta\theta} \cdot \log \left( \frac{(h_0^* + F^* + \psi_{wf}) + F_t (1 - \Delta\theta)}{(h_0^* + F^* + \psi_{wf}) + F_{t-1} (1 - \Delta\theta)} \right) \quad (2.10)$$

The numerical solution of the equation 2.10 was achieved by using the *Newton Raphson iteration method*. The Green-Ampt model parameters, initial soil water content  $\theta_0$ , wetting front soil suction head  $-\psi_{wf}$ , and the effective hydraulic conductivity  $K_e$ , were calibrated by minimizing the difference between the measured water level  $h$  values and the modeled ones. These latter were computed at each time interval starting from the

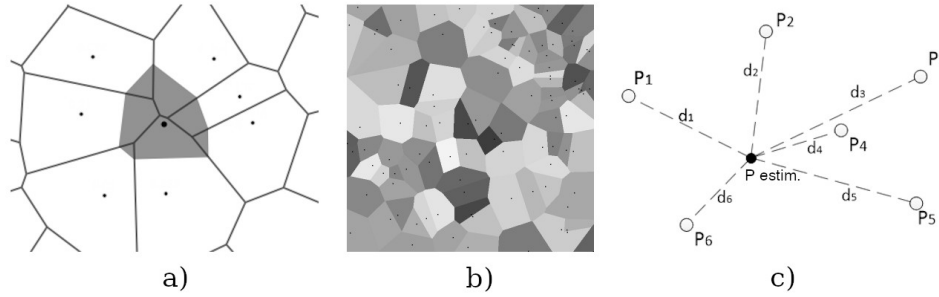


Figure 2.15: Graphical representations of the interpolation methods used to develop a preliminar exploratory data analysis. a) *Triangulation-based Natural Neighbor Interpolation* (NNI), b) *Thiessen Polygons* (TP), c) *Inverce Distance Weighting* (IDW).

numerical solution of 2.10 and according to

$$h_t^{mod} = h_0^* - \frac{dF^{mod}}{dt} \approx h_0^* - \frac{\Delta F^{mod}}{\Delta t} \quad (2.11)$$

Hereinafter the effective hydraulic conductivity  $K_e$  calibrated with the Green-Ampt model will be referred to as  $K_{mod}$  (modeled hydraulic conductivity).

**Exploratory data analysis and spatial characterization** The spatial distributions, i.e. how the data look plotted in a 2D representation, of the modeled  $K_{mod}$  values, and of the investigated soil-chemical properties, % VS, % TOC, and  $w_{PO_4^{3-}}$ , at the distributed survey positions within the two experimental sites, was analyzed in the open-source (Free and Open Source Software - FOSS) GIS gui QGIS<sup>®</sup>.

Three spatial interpolations of  $K_{mod}$  were tested for the Colnù site, using *Triangulation-based Natural Neighbor Interpolation* (NNI) and *Thiessen Polygons* (TP) methods (Sibson, 1981; Thiessen, 1911; Voronoi, 1908a,b) combined together, and *Inverce Distance Weighting* (IDW) method (Shepard, 1968). The NNI method was implemented through the MATLAB<sup>®</sup> function *griddata* and then the interpolation result was extended to the borders of the two vineyards of the site by means of the TP method. The IDW method was applied using the QGIS dedicated tool. For both sites, the spatial characterization

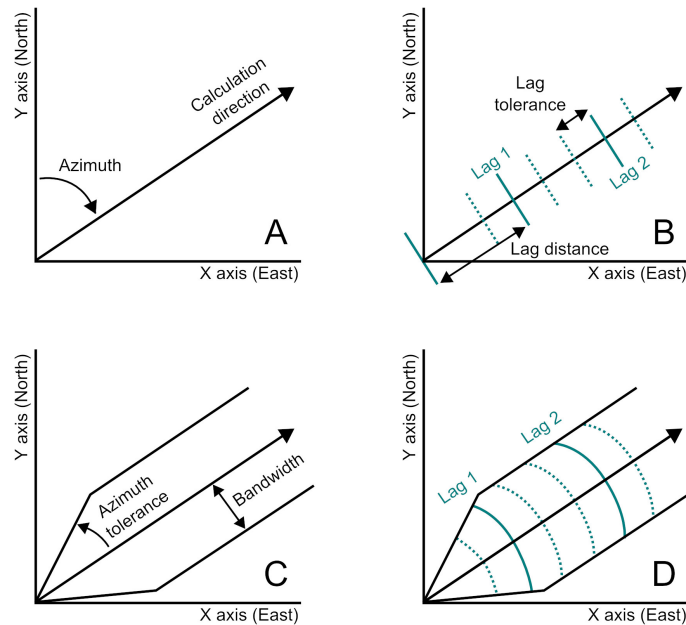


Figure 2.16: List of parameters for the computation of the experimental variogram for a sparse sample.

of the surveys results was also developed in QGIS using *rule based symbology*. The TP method was applied to the  $K_{mod}$  values only to acquire preliminary information on the spatial correlation length and on the presence of any recognizable pattern of the soil property within the experimental sites.

**Univariate analysis** Univariate statistics were developed for each site on both the values and the natural logarithms of  $K_{mod}$  for to determine measures of position and spread. The same was developed for the values of the soil parameters observed from the collected soil samples at the Settolo site. This to evaluate the presence of any different spatial distribution of the quantities between the plots of the site destined to vine cultivation or buffer area around the well. The  $\log K_{mod}$  values were subdivided in frequency classes and plotted in two histograms showing also the cumulative distribution function *cdf*.



**Structural analysis: characterization of spatial continuity** A preliminary spatial correlation analysis of the soil hydraulic conductivity values was developed for the Settolo site, assuming the correlation dependent on the mutual distance of the experimental points in the domain, i.e., avoiding any dependency of correlation on their position in space (hypothesis of stationarity). This hypothesis permits the development of an experimental variogram (Isaaks and Srivastava, 1989) to characterize the spatial continuity of the soil property within the investigated area of the experimental site (section 2.2.4). The computation of the variogram (sometimes also referred to as the semivariogram) from a sparse sample, as for this case, requires the discrete approximation

$$\gamma(\vec{h}) \approx \frac{1}{2N(\vec{h})_{\vec{u}_1 - \vec{u}_2 = \vec{h} \pm \Delta\vec{h}}} \sum (z(\vec{u}_1) - z(\vec{u}_2))^2 \quad (2.12)$$

where  $N$  is the total number of realizations,  $\vec{u}_1$  and  $\vec{u}_2$  are the positions of the two single realizations  $z(\vec{u}_1)$  and  $z(\vec{u}_2)$  of the regionalized variable  $z(\vec{u})$ , and  $\vec{h} = \vec{u}_1 - \vec{u}_2$  is the separation vector.

This approximation assumes that the data are not disposed on a regular grid, making it difficult to find many pairs of data separated exactly by  $\vec{h}$ . For this reason, the value of the variogram for a given value of  $\vec{h}$  is approximated by the semi-average of the squared difference of all pairs which are separated by a vector that falls within  $\vec{h} \pm \Delta\vec{h}$ , in which  $\Delta\vec{h}$  is a tolerance vector (lag tolerance), large enough, to ensure that the number of pairs  $N(\vec{h})$  is acceptable. In practice, it is customary to specify the number of directions (azimuth angles - Figure 2.16A) in which to compute the variogram, and then decide a lag tolerance (Figure 2.16B) and an angular tolerance (azimuth tolerance) plus a maximum bandwidth (Figure 2.16C), to estimate the variogram value from the data (Deutsch, 2015).

In the case of the experimental site of Settolo, the variogram-computation parameters were initially estimated based on the data spatial characterization above mentioned, and

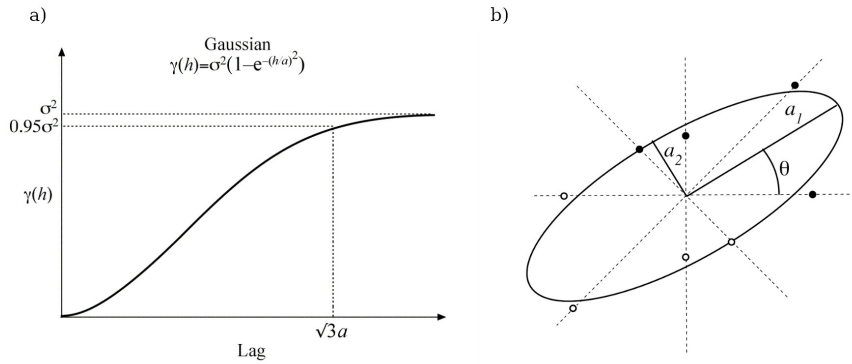


Figure 2.17: a) Gaussian variogram model with its equation b) Scheme of the ellipse function for the range coefficients.

then refined using the code *Stanford Geostatistical Modeling Software* SGeMS.

To determine the value of the variogram for distances or directions different from the ones for which it has been computed, a Gaussian variogram model (Figure 2.17a) was developed in SGeMS by fitting the experimental variogram along four azimuths,  $0^\circ$ ,  $45^\circ$ ,  $90^\circ$ , and  $135^\circ$ . The fitting was developed by varying the model coefficients i) sill ( $= 0.95\sigma^2$ ), ii) range ( $= \sqrt{3}a$ ), that is the distance beyond which data pairs are not correlated, and iii) nugget effect (not reported in Figure 2.17a). The range coefficient  $a$  was differently adjusted along the computation directions, hence assuming a non-isotropic distribution of the correlated values. In practice an ellipse function  $a(\theta)$ , where  $\theta$  is the angle of the semi-major axis with the x-axis, was fitted to the range coefficients by defining its major and minor semi-axes and their orientation.

In the case of the experimental site of Colnù, both the experimental variogram and the variogram model were developed, in a first attempt, using the code *System for Automated Geoscientific Analyses* (SAGA). This, also to test the out-of-the-box tool for geostatistical analyses implemented in the FOSS QGIS gui.

**Estimation** The modeling of the soil hydraulic conductivity spatial correlation in both the experimental sites, permitted a preliminary estimation of the  $\log K$  distribution over

the Settolo investigated areas with the *Ordinary Kriging* (OK) algorithm interpolator. For the Settolo site, the geostatistical *logK* estimation was developed on a grid covering the entire surveys area (section 2.2.4) and having  $1 \times 1$  meters cells. At this purpose, The OK algorithm implementation available in the code SGeMS (Remy et al., 2009) was used. On the other hand, the cross-validation for the variogram model used in the *logK* estimation at the Settolo site was developed from scratch. By cross-validation we refer to an exercise in which kriging estimates are computed at data locations using all data except the datum co-located at the estimation location. In this way, the performance of kriging can be compared against actual measurements. This was done by setting up a Python script for the error computation between real and estimated *logK* values at each *i-th* test position not considered in the *i-th* ordinary kriging developed on the basis of the remaining  $N - 1$  realizations.






### 2.3.3 Geospatial analysis of the PPPs distribution at provincial scale

The analysis of the PPPs sale data collected in the province of Treviso in the period 2012-2019, was developed in three phases connected each other.

1. Identification of the PPPs involved in the vine cultivation through the information reported in the Wine-making Protocol 2019 and creation of a database containing all the vineyard-specific PPPs.
2. Hazard analysis and classification of the vineyard-specific PPPs based on the CLP pictograms and statements (summarized in Table 2.8) contained in their safety sheets.
3. Geographical combination of i) vineyards extension retrieved from the land-use geospatial data (CLC18), ii) position of the WHPAs, and iii) spatial distribution of the vineyard-specific PPPs.

The latter phase required the relevant assumption that PPPs were used in the same municipality of sale or in the neighboring ones. Regarding the hazard classification for vineyard-specific PPPs, it was developed by assigning to each product an additional hazard class ranging from 1 to 5, where 1 stands for low hazard and 5 very high hazard. Hazard class 5 was assigned to the products showing on their labels both the GHS ids GHS06 and GHS08 while hazard class 1 was assigned to the ones with no CLP pictograms or hazard statements. From the network of wells extracting drinking water, only wells exploiting phreatic aquifers were considered. This, to account with a higher probability, for possible pollution phenomenon due to PPPs infiltration occurring at distances from the wells lower than the characteristic length of the field scale ( $L \sim 10^2 m$ ). WHPAs on the territory were defined by means of the geometric criteria according to the national regulation, i.e., as circular areas around the wells having radius of 200 meters.

Table 2.8: Information used for the development of the PPPs hazard-based classification. Retrieved from the CLP regulation EC 2008/1272.

Pictogram	Global ID	Hazard statement and [class]
Health Hazard		
	GHS05	Severe skin burns [1A, 1B, 1C] Eye damage [1]
	GHS06	Fatal or Toxic (if swallowed, in contact with skin, if inhaled) [1, 2, 3]
	GHS07	Toxic (if swallowed, in contact with skin, if inhaled) [4] Skin irritation [2] Eye irritation [2] Allergic skin reaction [1] May cause respiratory irritation [ \ ]
	GHS08	May cause respiratory irritation [1] May cause genetic defects [1A, 1B, 1C] May cause cancer [1A, 1B, 2] Eye irritation [2] May damage fertility or the unborn child [1A, 1B, 2] Causes damage to organs [1, 2] May be fatal if swallowed and enters airways [1]
Environmental Hazard		
	GHS09	Toxic to aquatic life with long lasting effects



## Chapter 3

# Results and Discussion

### 3.1 Pointwise-scale results

In this section the experimental evidence and the modeling results achieved at the pointwise scale in the period 2018-2019 are presented.

#### 3.1.1 Data collected by the meteorological stations

The first two months of the simulations period were characterized by abundant precipitations ( $P_{max} \geq 50$  mm/d and  $P_{max} \geq 20$  mm/d observed in late October and in the second half of November respectively) while scarce rainfall depths were observed during the remaining part of the meteorologic winter (Figures 3.1a and 3.1b). In 2019, the more relevant precipitations fell at both the experimental sites in spring and in autumn seasons when the annual maximum percentages of rainy days (almost 50 %) were recorded. Comparable daily mean temperatures are recorded in each site, from  $-1.4$  °C to  $29.9$  °C at the Settolo site and from  $-3.5$  °C to  $28.8$  °C at the Colnù site, being the mean values along the entire period were  $13.6$  °C and  $13.0$  °C respectively. Figure 3.2a shows the monthly behavior and the total amount of rainfall data from October 2018 to September 2019. Settolo was mostly affected by rain precipitations in each month,

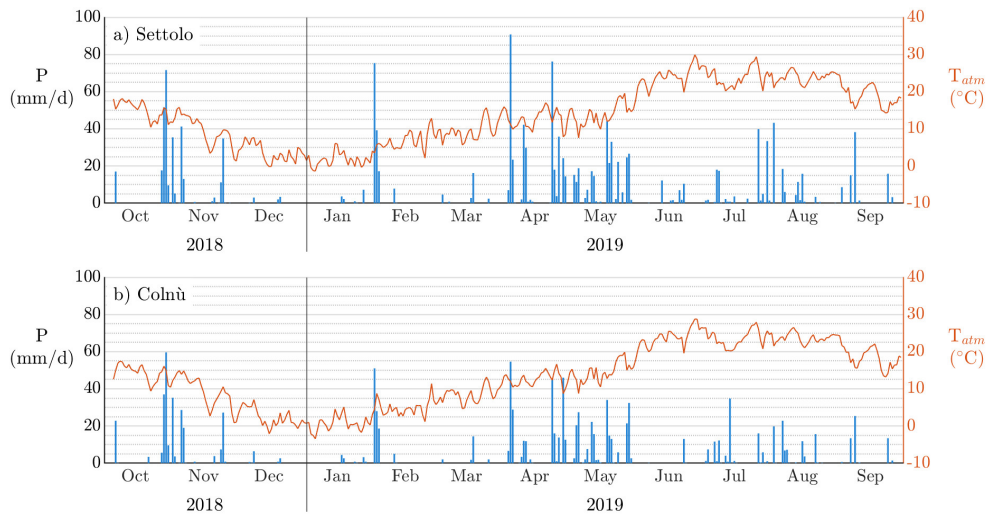


Figure 3.1: Daily precipitation (vertical blue bars) and temperatures (orange lines) measured by the two meteorological stations at Settolo and Colnù.

with the cumulate rainfall of about 1.3 times the cumulate depth of rainfall observed at Colnù, although the number of rainy days is almost equal. Moreover, Figure 3.2b shows that the number of occurrences of rainfall intensity exceeding 5 mm/h was higher in Settolo than in Colnù.

### 3.1.2 Analysis of the data collected at the monitoring points

#### 3.1.2.1 Soil analyses

Table 3.1 and 3.2 report the results obtained by laboratory analysis on the soil samples collected at the site parcels of Settolo and Colnù. Below both tables, the footnotes indicate the thickness of the analyzed soil layers, additional information on the units of measures (when needed), and the measure methodology adopted for the laboratory analyses. Figure 3.3 shows the soil textures in the two experimental sites and the differences observed in terms of sand, silt and clay percentages. Up to a depth of 0.50 m, the soil of the Settolo site is more sandy while at Colnù it's more silty (Figure 3.3). Slight differences were observed inside the same experimental site too, the two shallower



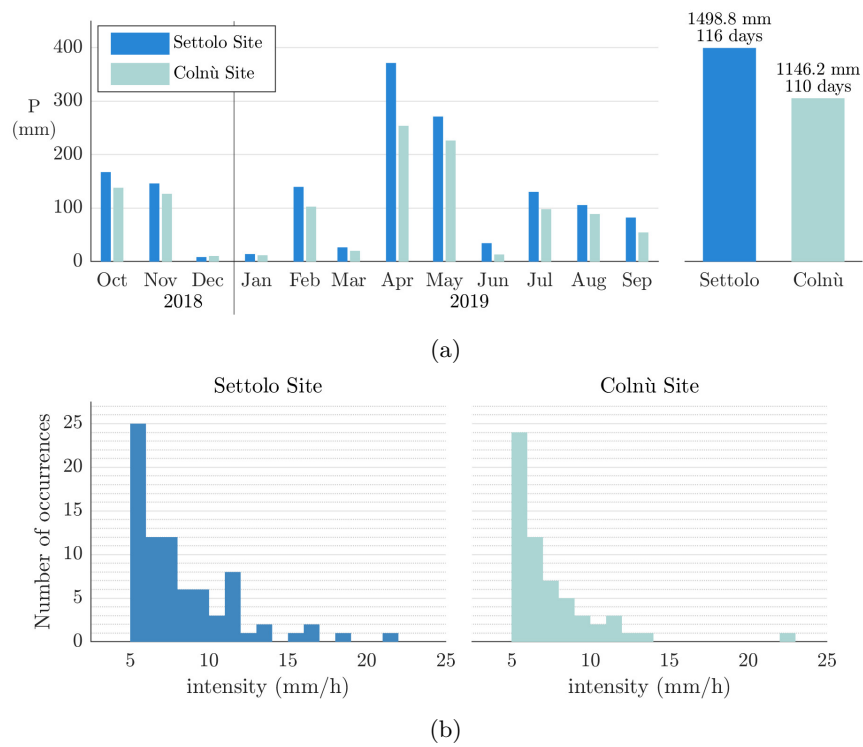


Figure 3.2: Rainfall analysis. a) Comparison of monthly and annual precipitations observed at the two experimental sites. b) Histograms of rainfall intensity exceeding 5 mm/h.

### 3.1. Pointwise-scale results

Table 3.1: Chemical analyses results (data from Mencaroni et al., 2021).

parcel	soil layer	OC <sup>1*</sup> % <sub>ds</sub>	N <sub>tot</sub> <sup>2*</sup> % <sub>ds</sub>	pH <sup>+</sup> \	EC <sup>3+</sup> μS/cm	P <sub>Olsen</sub> <sup>4</sup> mg/kg	CEC <sup>5</sup> meq/100g	K <sub>f</sub> <sup>6°</sup>	1/n <sup>7</sup>	R <sup>2</sup>
SN <sub>p</sub>	L1 <sub>S</sub>	1.239	0.144	8.34	220.0	15.876	11.733	18.7	0.61	0.975
	L2 <sub>S</sub>	0.566	0.070	8.51	151.1	8.327	9.446	40.4	0.78	0.989
	L3 <sub>S</sub>	0.655	0.065	8.34	133.2	23.754	8.430	45.9	0.82	0.986
	L4 <sub>S</sub>	0.644	0.039	8.36	130.2	6.508	9.410	35.0	0.74	
	mean st. dev.	0.776 0.269	0.080 0.039	8.39 0.071	158.6 36.3	13.62 6.83	9.755 1.213	11.7	0.091	
SS <sub>p</sub>	L1 <sub>S</sub>	1.632	0.192	8.45	214.0	21.956	14.639	29.0	0.79	0.998
	L2 <sub>S</sub>	0.911	0.095	8.48	151.6	22.227	11.499	44.1	0.84	0.995
	L3 <sub>S</sub>	0.685	0.061	8.49	142.5	16.203	9.699	53.5	0.86	0.988
	L4 <sub>S</sub>	0.579	0.047	8.50	137.4	2.880	9.712	42.2	0.83	
	mean st. dev.	0.952 0.411	0.099 0.056	8.48 0.019	161.4 30.8	15.82 7.85	11.387 2.015	10.1	0.029	
site	mean	0.864	0.089	8.43	160.0	14.716	10.571	38.6	0.78	
	st. dev.	0.358	0.05	0.07	33.7	7.436	1.853	11.5	0.082	
CE <sub>p</sub>	L1 <sub>C</sub>	1.638	0.205	8.51	303.0	12.521	19.911	176.4	0.82	0.995
	L2 <sub>C</sub>	0.898	0.122	8.31	216.0	9.799	15.520	193.6	0.78	0.960
	L3 <sub>C</sub>	1.005	0.129	8.42	205.0	12.957	15.890	229.4	0.73	0.986
	L4 <sub>C</sub>	0.717	0.087	8.24	227.0	6.824	17.683	199.8	0.78	
	mean st. dev.	1.065 0.347	0.136 0.043	8.37 0.103	237.8 38.5	10.525 2.456	17.251 1.740	22.077	0.037	
CW <sub>p</sub>	L1 <sub>C</sub>	1.251	0.161	8.29	236.0	10.733	15.264	96.3	0.84	0.978
	L2 <sub>C</sub>	1.107	0.119	8.44	211.0	6.796	14.830	63.8	0.58	0.970
	L3 <sub>C</sub>	0.820	0.115	8.43	204.0	6.491	15.130	96.4	0.71	0.999
	L4 <sub>C</sub>	0.632	0.049	8.71	164.4	2.644	11.128	85.5	0.71	
	mean st. dev.	0.953 0.242	0.111 0.04	8.468 0.152	203.9 25.7	6.666 2.862	14.088 1.716	15.3	0.106	
site	mean	1.009	0.123	8.419	220.8	8.596	15.669	142.7	0.74	
	st. dev.	0.304	0.043	0.139	36.8	3.291	2.343	60.2	0.086	

L1<sub>S</sub> = L1<sub>C</sub> = 0.00m → -0.15m, L2<sub>S</sub> = L2<sub>C</sub> = -0.15m → -0.25m, L3<sub>S</sub> = L3<sub>C</sub> = -0.25m → -0.40m  
L4<sub>S</sub> = -0.40m → -0.50m, L4<sub>C</sub> = -0.40m → -0.70m

<sup>1</sup> Organic Carbon expressed as weight percentage of the dry sample.

\* measured with flash combustion method (CNS-analyzer, vario MACRO cube, Elementar Analysensysteme GmbH).

<sup>2</sup> Total Nitrogen expressed as weight percentage of the dry sample.

<sup>+</sup> measured by an electrode in soil suspensions with a soil to water ratio of 1:2.5 (w/v).

<sup>3</sup> Electric conductivity.

<sup>4</sup> Available Phosphorus measured with the Olsen method.

<sup>5</sup> Cation Exchange Capacity, measured using the BaCl<sub>2</sub>-triethanolamine method.

<sup>6</sup> K<sub>f</sub> expressed in μg<sup>(1-1/n)</sup>ml<sup>1/n</sup>g<sup>-1</sup>.

<sup>°</sup> measured with Batch Equilibrium Method (OECD, 2000). Chemical standard of glyphosate acid (98.6% purity) was purchased from Dr. Ehrenstorfer (LGC Labor GmbH, Augsburg, Germany).

<sup>7</sup> Exponent of the Freundlich adsorption model.

Table 3.2: Physical analyses results (data from Mencaroni et al., 2021) and estimated soil porosity values.

parcel	soil layer	$K_{sat}^{**}$ m/s	BD <sup>1</sup> g/cm <sup>3</sup>	skeleton %	sand <sup>2*</sup> %	silt <sup>2*</sup> %	clay <sup>2*</sup> %	$\varphi^3$ from Rosetta	$\varphi'^4$ BD derived	$\varphi'^4$ = $\theta_{max}$
SN <sub>p</sub>	L1 <sub>S</sub>	8.87E-06	1.372	23.36	53.66	34.14	12.20	0.389	0.482	0.400
	L2 <sub>S</sub>	7.88E-05	1.341	19.16	43.55	40.27	16.18	0.398	0.494	0.423
	L3 <sub>S</sub>	8.02E-06	1.483	8.43	51.62	34.09	14.29	0.391	0.440	0.453
	L4 <sub>S</sub>	-	-	8.75	46.02	37.56	16.42	0.396	0.440	0.423
	L5 <sub>S</sub>	-	-	-	-	-	-	0.387	0.440	0.406
	mean st. dev.	3.19E-05 4.06E-05	1.399 0.061	14.93 6.508	48.72 4.091	36.51 2.586	14.77 1.701			
SS <sub>p</sub>	L1 <sub>S</sub>	1.55E-03	1.089	8.81	46.60	41.21	12.19	0.394	0.589	0.662
	L2 <sub>S</sub>	7.21E-06	1.384	15.01	46.66	38.66	14.69	0.394	0.478	0.582
	L3 <sub>S</sub>	1.33E-06	1.443	8.56	49.46	35.47	15.07	0.393	0.456	0.501
	L4 <sub>S</sub>	-	-	15.64	51.52	33.30	15.18	0.392	0.456	0.428
	L5 <sub>S</sub>	-	-	-	-	-	-	0.387	0.456	0.355
	mean st. dev.	5.19E-04 8.92E-04	1.305 0.154	12.00 3.331	48.56 2.063	37.16 3.015	14.28 1.221			
site	mean	2.76E-04	1.352	13.47	48.64	36.84	14.53			
	st. dev.	6.25E-04	0.126	5.372	3.241	2.827	1.501			
CE <sub>p</sub>	L1 <sub>C</sub>	1.18E-04	1.345	1.17	32.19	52.23	15.57	0.411	0.492	0.423
	L2 <sub>C</sub>	1.72E-05	1.344	2.81	33.20	49.88	16.92	0.410	0.493	0.422
	L3 <sub>C</sub>	3.05E-06	1.353	1.50	33.25	49.29	17.46	0.410	0.489	0.420
	L4 <sub>C</sub>	3.82E-06	1.487	0.56	31.92	47.29	20.79	0.416	0.439	0.444
	mean	8.03E-06	1.382	1.51	32.64	49.67	17.69			
	st. dev.	7.96E-06	0.06	0.821	0.591	1.763	1.919			
CW <sub>p</sub>	L1 <sub>C</sub>	5.81E-04	1.398	2.64	37.17	47.81	15.02	0.404	0.473	0.404
	L2 <sub>C</sub>	1.05E-05	1.452	1.18	38.60	44.23	17.17	0.404	0.452	0.408
	L3 <sub>C</sub>	9.97E-05	1.318	1.22	38.52	45.01	16.47	0.403	0.503	0.412
	L4 <sub>C</sub>	1.02E-06	1.544	0.66	43.51	38.03	18.46	0.401	0.417	0.401
	mean	3.71E-05	1.428	1.42	39.45	43.77	16.78			
	st. dev.	5.44E-05	0.082	0.734	2.413	3.571	1.24			
site	mean	1.04E-04	1.405	1.47	36.05	46.72	17.23			
	st. dev.	1.98E-04	0.076	0.78	3.83	4.08	1.67			

L1<sub>S</sub> = L1<sub>C</sub> = 0.00m → -0.15m , L2<sub>S</sub> = L2<sub>C</sub> = -0.15m → -0.25m, L3<sub>S</sub> = L3<sub>C</sub> = -0.25m → -0.40m

L4<sub>S</sub> = -0.40m → -0.50m, L4<sub>C</sub> = -0.40m → -0.70m

L5<sub>S</sub> = -0.50m → -0.70m

\*\* measured with constant head permeameter test.

<sup>1</sup> 105 °C oven-dry bulk density

<sup>2</sup> Sand, Silt, and Clay are expressed as percentages of the dry sample without the skeleton.

\* measured with particle size analyzer (Mastersizer 2000, Malvern Panalytical Ltd, Spectris Company) according to Bittelli et al. (2019)

<sup>3</sup> Porosity values estimated by the Rosetta code and used in the Scenario 0 of the rainwater infiltration simulation (see Section 2.3.1.2).

<sup>4</sup> Values of the maximum volumetric water content  $\varphi' \leq \varphi$ , estimated on the basis of the bulk density values or on the on-site maximum volumetric water content values (see Section 2.3.1.2).

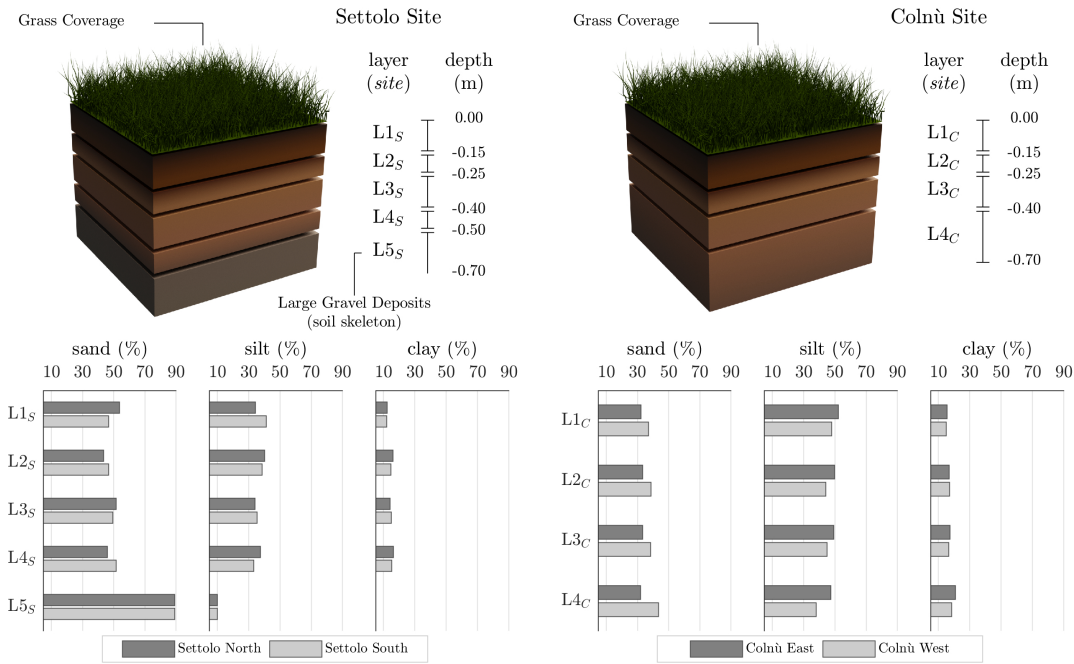


Figure 3.3: Soil textures up to the depth of -0.70 m in each parcel of Settolo and Colnù sites (data from Mencaroni et al., 2021).

L1<sub>S</sub> soil layers of the Settolo parcels and the two deeper L4<sub>C</sub> soil layers of the Colnù parcels. The soil sampling in the former site was limited to the first 50 cm due to the presence of coarse material, so that the texture of the Settolo L5<sub>S</sub> layers was derived from previous survey (Crestani et al., 2015b). Textures for these layers were set equal to 89 % sand, 10 % silt and 1 % clay.

### 3.1.2.2 Water quality from lab analyses

Figure 3.4 shows a general overview of the results achieved by the laboratory analysis on the water samples collected which is described in the details in Mencaroni et al. (2021). The water-quality surveys developed up to a depth of 0.70 m provided complex evidence concerning the infiltration of the potassium bromide and the mobility of glyphosate. Data from the Settolo site are reported on the left column while the ones from the Colnù site on the right column. The variation along the time of the

bromide concentration is represented as colored areas (gray and pink to distinguish the two parcels of each experimental site) and refer to the left vertical axes. Glyphosate and AMPA are distinguished by symbols. The units of measure are reported on the right axes being three orders of magnitude less than the bromide concentration. The applied tracer mass ( $\text{Br}^-$ ) was conserved along the vertical direction up to a depth of 0.30 m while, below that limit, the mass was strongly reduced, likely by loss through paths different from the vertical one. At -0.10 m (Figure 3.4a and Figure 3.4d) the concentrations of tracer in both the experimental sites remained high during the first three months (November 2018 to January 2019) due to the absence of consistent rainfalls until the beginning of February 2019 when a sudden drop is manifest. At -0.30 m (Figure 3.4b and Figure 3.4e) a similar behavior was observed only at the Colnù East, while at the West site parcel the maximum concentration peak occurred in the second half of March 2019. At -0.70 m (Figure 3.4c and Figure 3.4f) the tracer concentrations are low compared to the previous ones and as already stated, a dramatic reduction of the applied tracer mass is evident. The temporal profiles show peaks shifted toward the second half of the sampling period. The vertical behavior of the herbicide concentrations seems to be strongly site-specific, manifesting different distribution and values on time in the experimental sites. At the Settolo site the glyphosate-based pesticide shows increasing concentrations from the shallower sampling point to up -0.70 m. The experimental observations highlight an opposite trend for the Colnù site where the higher herbicide concentrations at the depth of 0.10 m gradually decreases toward the deeper sampling points. After two months from the application, AMPA was found in both sites: at -0.10 m in the Colnù site and at -0.30 m in the Settolo site. Regardless the depth, the maximum values measured in both sites were close to 7.5  $\mu\text{g}/\text{l}$ , ranging most part of the samplings between concentrations of 1.5  $\mu\text{g}/\text{l}$  and 4  $\mu\text{g}/\text{l}$ .

3.1. Pointwise-scale results

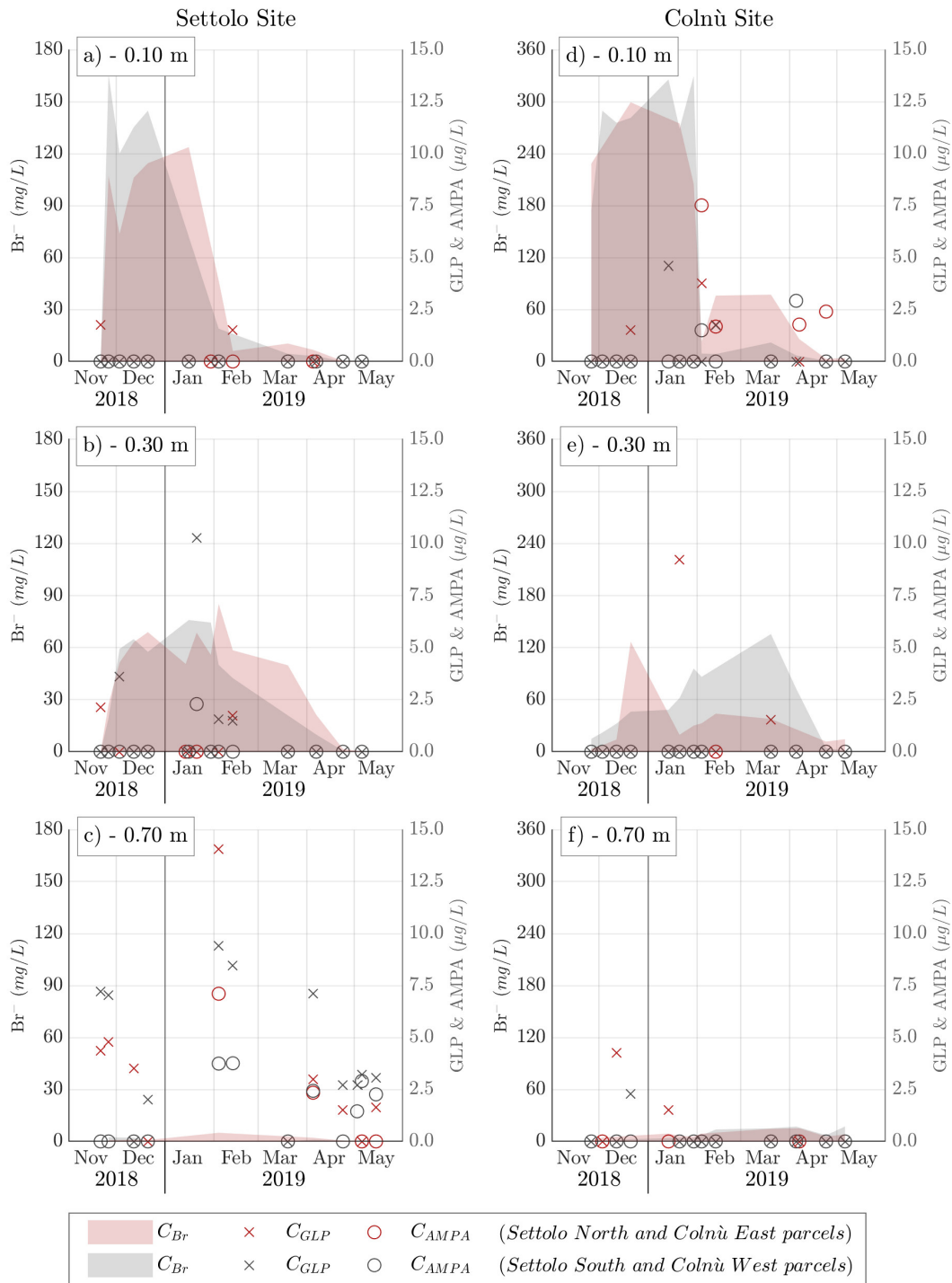


Figure 3.4: Results of the analysis performed on the collected water samples. (Data from Mencaroni et al., 2021).

### 3.1.3 Results of the numerical simulations

#### 3.1.3.1 Results of rainwater infiltration modelling

The results of the rainwater infiltration modelling, obtained from the scenarios described in section 2.3.1.2, are compared each other in Figures 3.5, 3.6, 3.7, and 3.8 along with the behaviors of rainfall and evapotranspiration daily values. The graphs reported in the figures consider three depths (0.10 m, 0.30 m, and 0.70 m) and two groups of scenarios: 1) simulations developed on the basis of estimated or calibrated hydraulic parameters ( $s_0$ ,  $s_1$ ,  $s_2$  and  $s_4$ ) and 2) simulations developed based on laboratory-derived hydraulic parameters ( $s_{3a}$  and  $s_{3b}$ ). In Scenario 0 the hydraulic parameters were estimated by the Rosetta code, on the basis of the soil texture, and then used in the model without calibration. The uncalibrated model reproduced the behavior of the soil water-content gauged on site, showing both peaks and tails similar to the ones measured by the capacitive sensors. However, the experimental water content  $\theta$  levels appeared in most cases underestimated by the model, like at -0.70 m of the  $SN_p$  parcel where the modelled trends were up to 50% shifted down (3.5). Relevant differences between simulated and observed  $\theta$  values resulted in  $SS_p$  and in  $CE_p$  parcels too (i.e., in three out of four parcels) and suggested that the offset was probably due to the lack of calibration. Therefore, the estimation of the hydraulic parameters along a time window of 156 days. As expected, the calibration reduced the gap between modelled and observed  $\theta$  values already from  $s_1$  but making worse the simulated water content behavior at 0.70 m. Assuming a time varying  $K_c$  and  $Z_e = 0.30$  m the simulation of the  $\theta$  trends improved in the dry periods occurring until March 2019 (Figures 3.5 - 3.7 and Figure 2.12). The modelled  $\theta$  peaks were shorter and better reproduced the experimental data, however, the water content observed in the period between the second half of March 2019 and the first half of April 2019 resulted underestimated. This gap was reduced in  $s_4$  at all depths by assuming  $Z_e$  variable in time (2.13). This also generally improved the simulation at -0.70 m, but

### 3.1. Pointwise-scale results

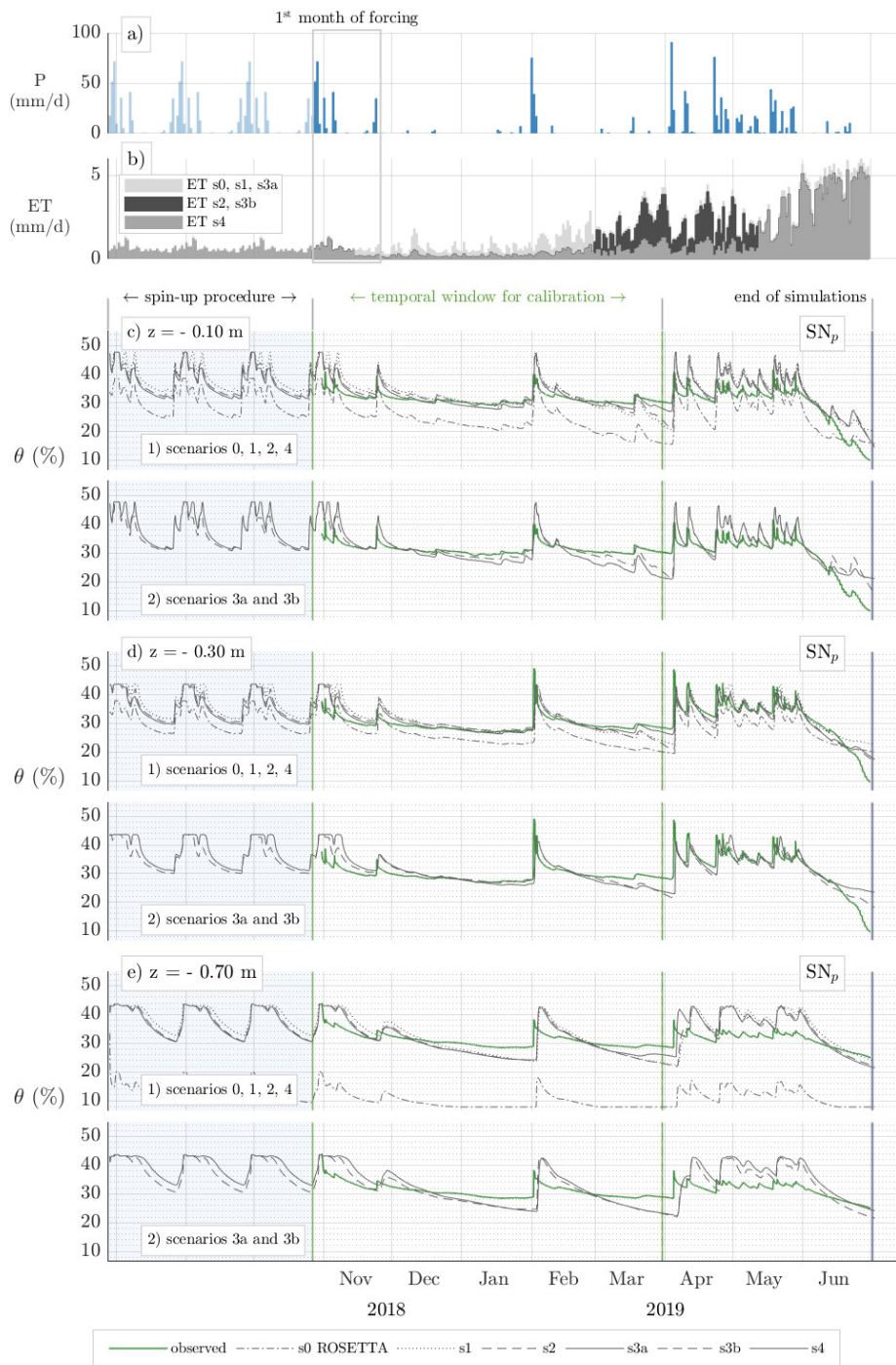


Figure 3.5: Results of the rainfall infiltration modelling in terms of water content ( $\theta$ ) at the experimental parcel of Settolo North ( $SN_p$ ) compared with rainfall (P) and evatranspiration (ET) forcing.



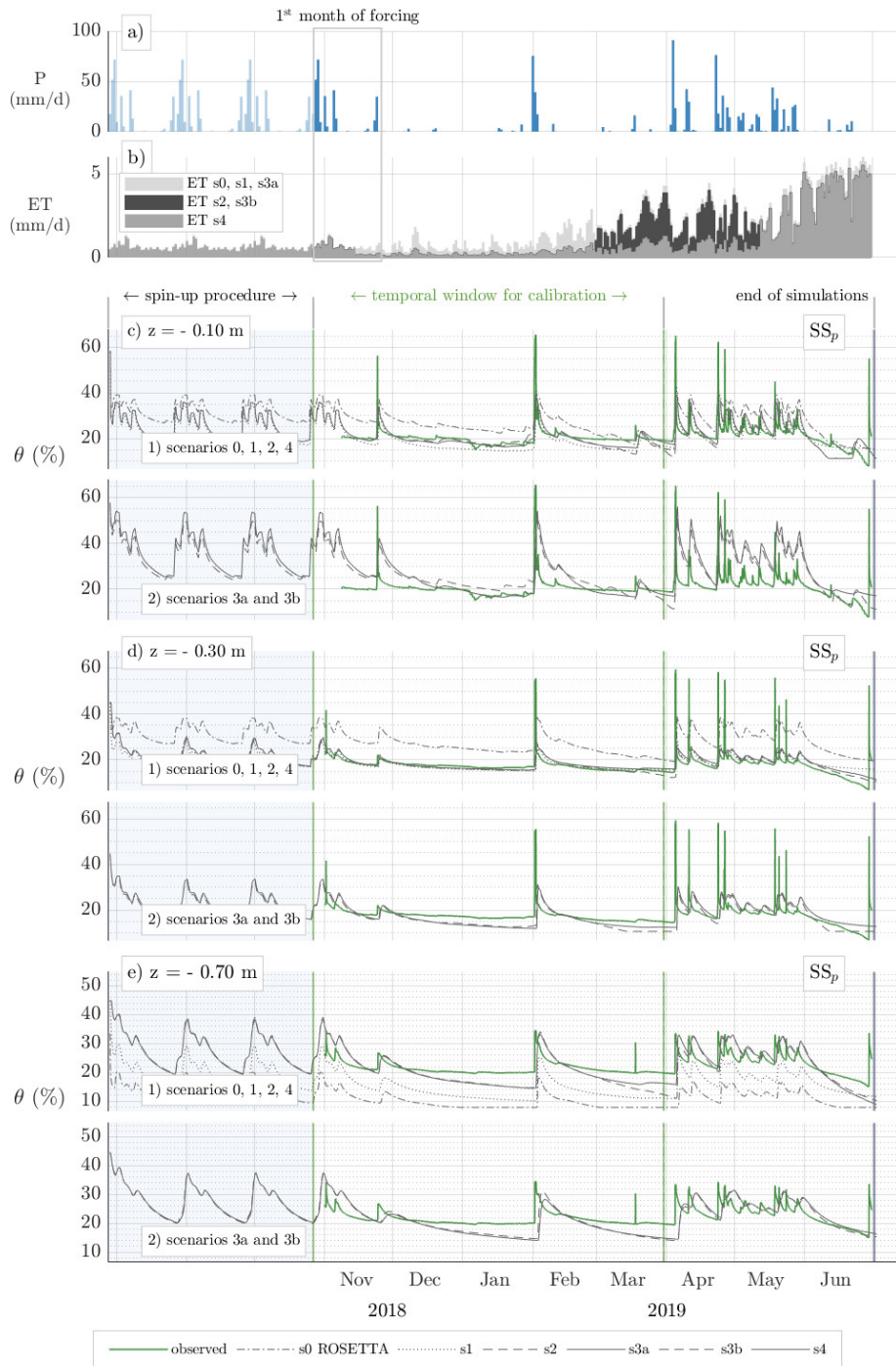


Figure 3.6: Results of the rainfall infiltration modelling in terms of water content ( $\theta$ ) at the experimental parcel of Settolo South ( $SS_p$ ) compared with rainfall (P) and evatranspiration (ET) forcing.

### 3.1. Pointwise-scale results

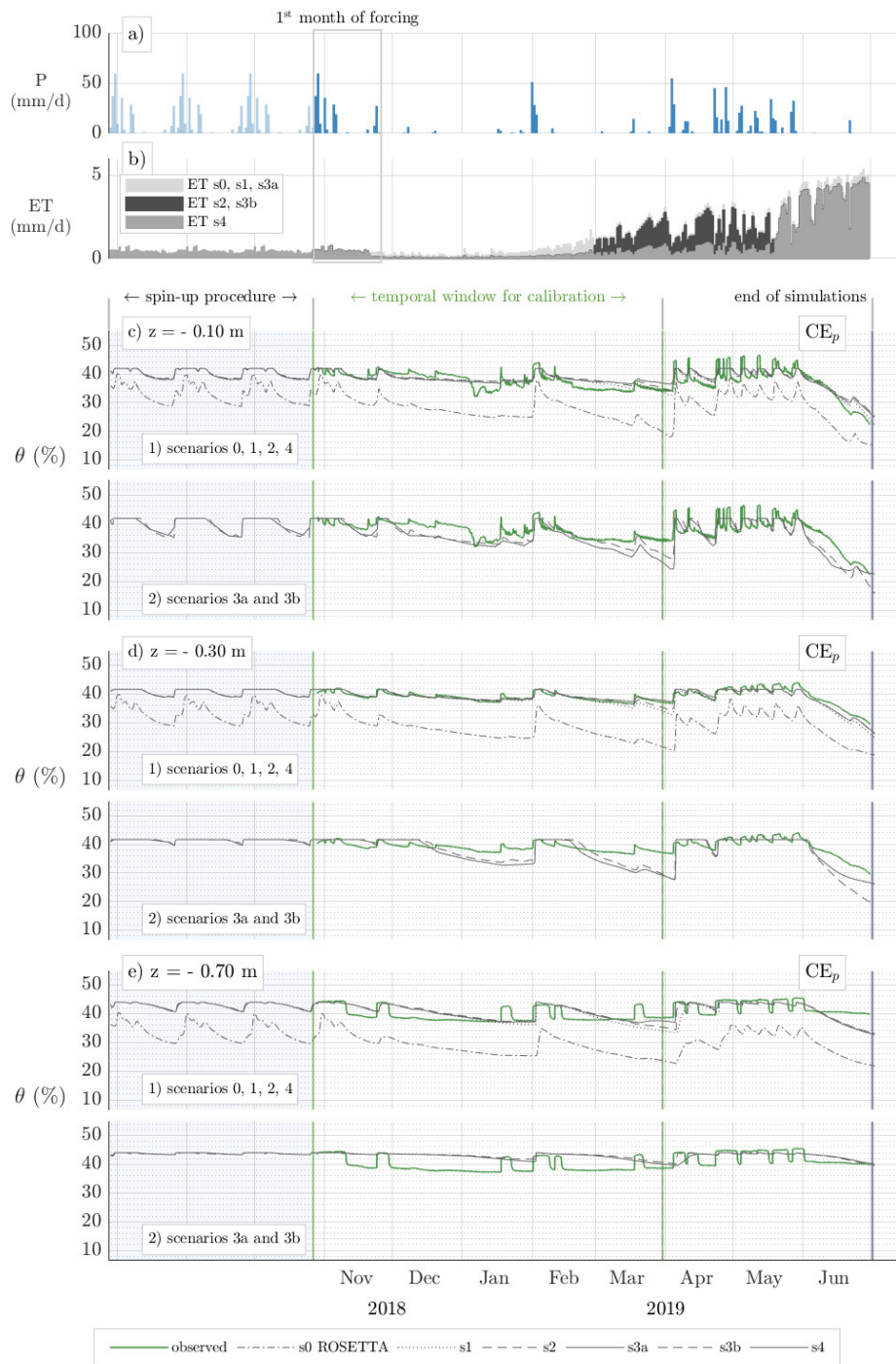


Figure 3.7: Results of the rainfall infiltration modelling in terms of water content ( $\theta$ ) at the experimental parcel of Colnù East ( $CE_p$ ) compared with rainfall ( $P$ ) and evapotranspiration ( $ET$ ) forcing.

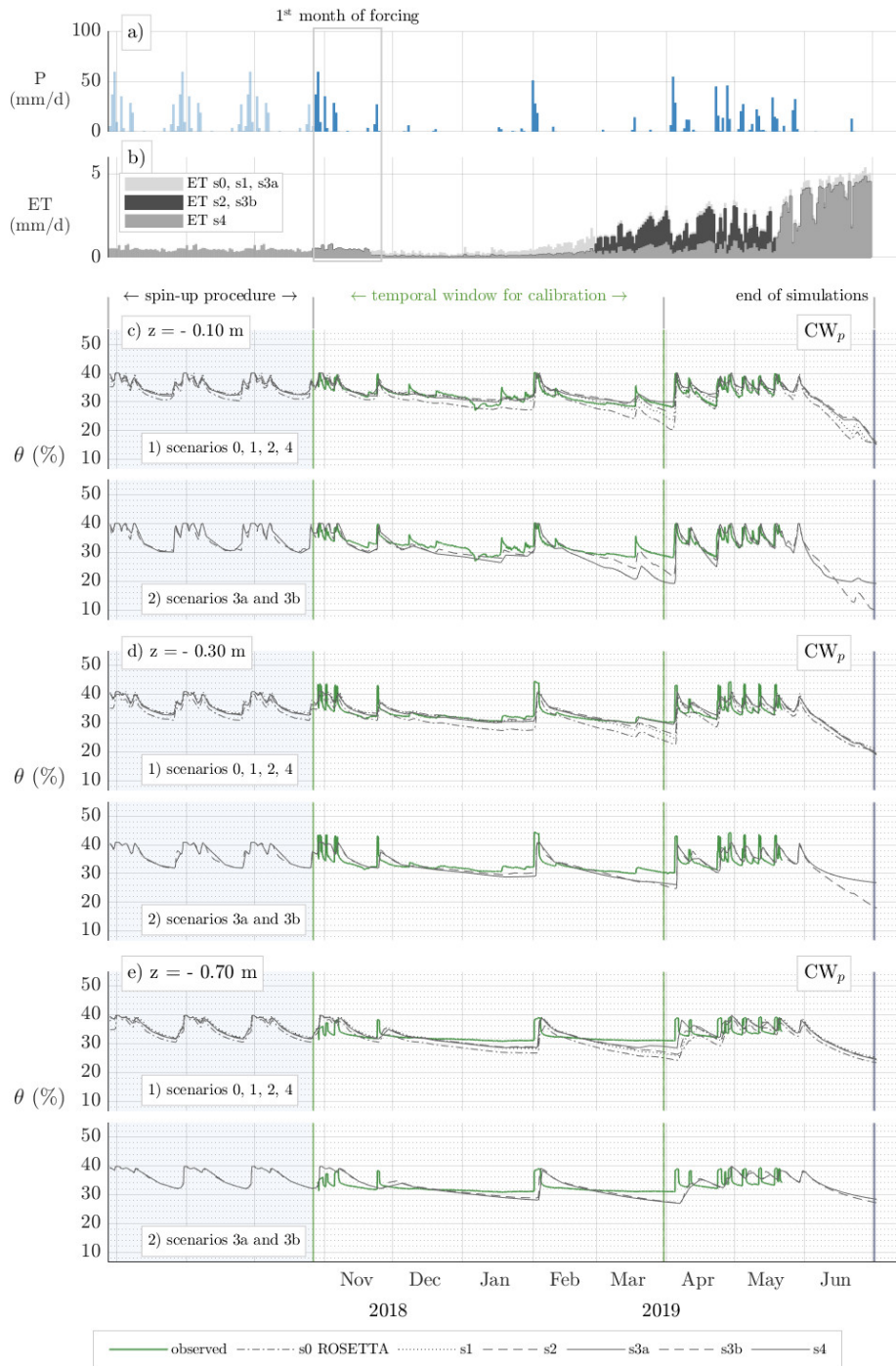


Figure 3.8: Results of the rainfall infiltration modelling in terms of water content ( $\theta$ ) at the experimental parcel of Colnù West ( $CW_p$ ) compared with rainfall ( $P$ ) and evapotranspiration ( $ET$ ) forcing.

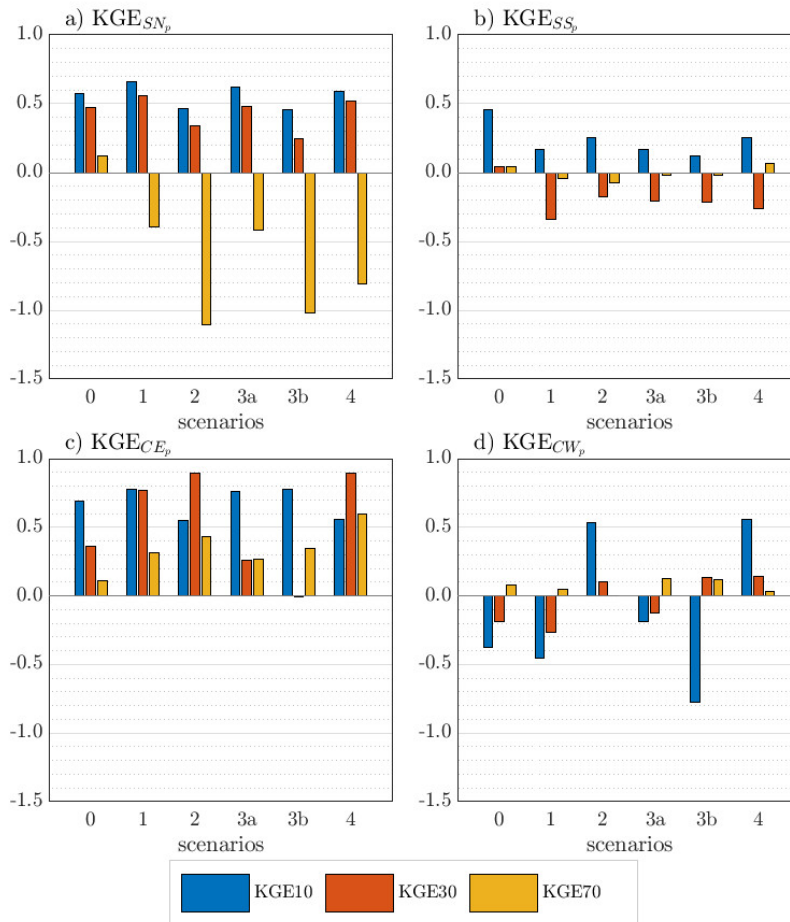


Figure 3.9: Comparison between the Kling-Gupta efficiency coefficients (Gupta et al., 2009) calculated to evaluate the goodness of fit of the soil water-content trend modelled in the tested scenarios (Table 2.6).

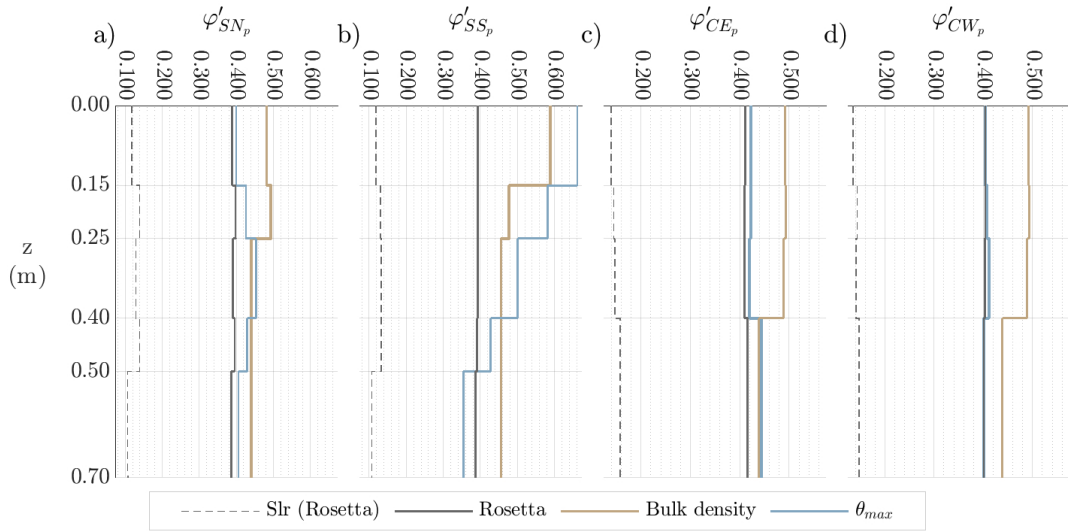


Figure 3.10: Porosity ( $\varphi$ ) values from Table 3.2 vs depth ( $z$ ). Values of  $\varphi$  were initially derived for all parcels using the ROSETTA code (a, b, c and d). Values of  $\varphi'$  were derived from bulk densities for the Settolo site (a and b) and water content at saturation for the Colnù site (c and d).

slightly overestimating the water content peaks of April and May 2019. All the calibration procedures developed in s1, s2 and s4 improved the capability of the model to simulate  $\theta$  values closer to the measured ones but made worse the temporal behavior. In the scenarios 3a and 3b the permeability  $k$  only was subjected to calibration while the other two hydraulic parameters,  $\alpha$  and  $n$ , were derived from the water retention curve obtained in the laboratory analysis (section 2.2). The difference between the two scenarios lies on the configuration of the two ET parameters,  $K_c$  and  $Z_e$ . In Scenario 3a  $K_c$  was considered, as for s1, equal to the unity and constant throughout the period covered by the simulation while  $Z_e$  was set at its minimum. This affected the  $\theta$  trend at -0.10 m with the overestimation of the superficial evaporation and therefore the underestimation of the observed values of the soil water content. In s3b  $K_c$  and  $Z_e$  were considered as for the Scenario 2, hence the former was set equal to 0.3 for the three months after the pesticide application and the latter was set constant and equal to 0.30 m. This ET configuration improved the modelling of the  $\theta$  trend at -0.10 m



### 3.1. Pointwise-scale results

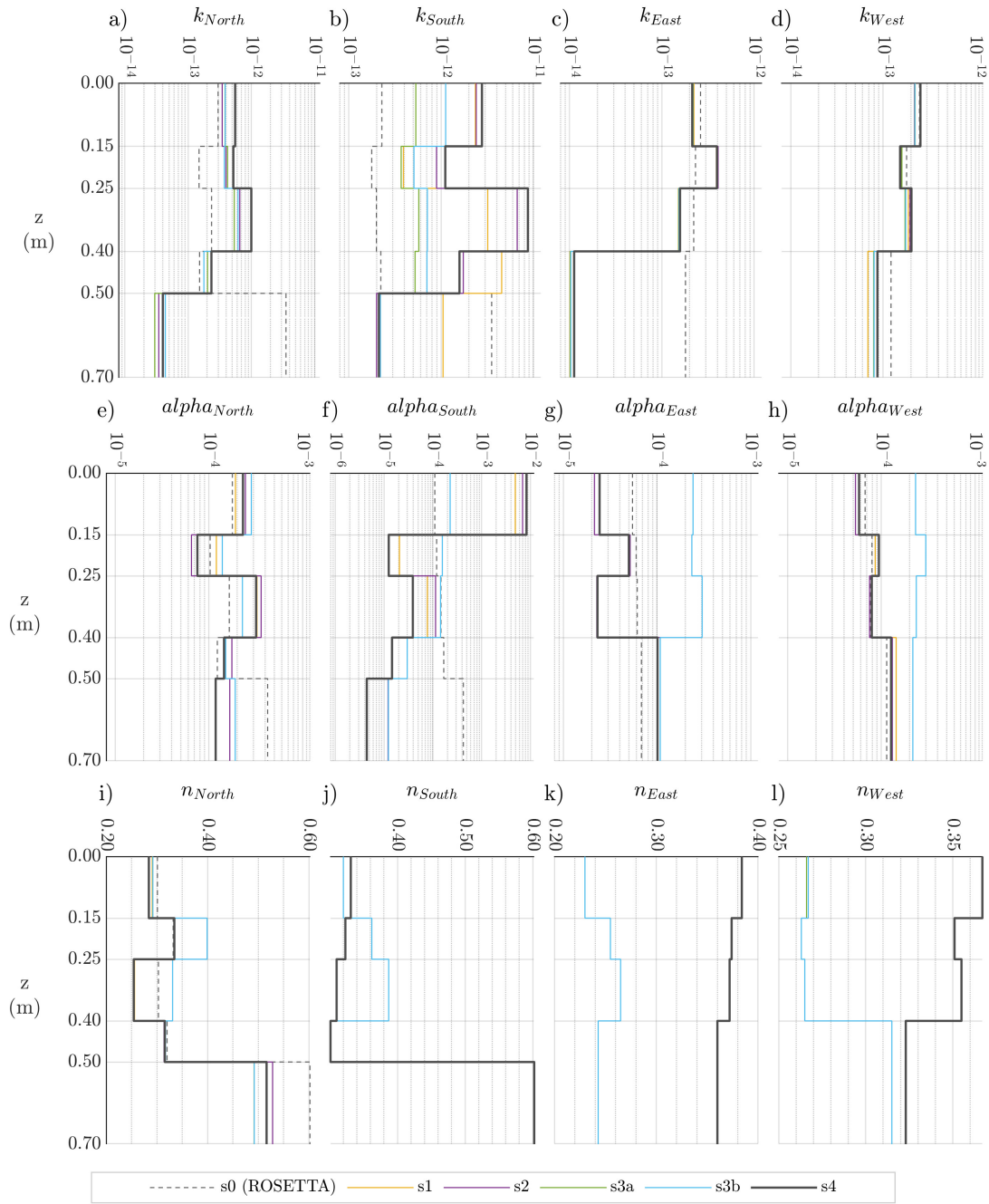


Figure 3.11: Hydraulic parameters permeability  $k$  and water retention curve coefficients  $\alpha$  and  $m$  vs depth  $z$ .

and -0.30 m during the dry periods while at -0.70 m it remained unchanged. Overall, the small differences observed between the results of the s3a and s3b scenarios and the other scenarios characterized by the hydraulic parameters calibration, suggest a higher sensitivity of the model to the permeability than to the water retention curve coefficients  $\alpha$  and  $n$ . As highlighted by the Figures 3.5, 3.6, 3.7, and 3.8, the differences between the scenarios, except for the Scenario 0, are minimal and make it difficult to evaluate the model performances based on the graphical representation of the results only. The KGE coefficients computed by comparing the  $\theta$  values simulated and observed at the three depths (0.10 m, 0.30 m, and 0.70 m) of each site parcel, are reported in Figure 3.9 ( $-\infty < \text{KGE} \leq 1$ , where the unity represents the optimum). In Scenario 0, the efficiency of the model in simulating the  $\theta$  observed behaviors, was confirmed, in three out of four cases, also showing a good consistency of the results along the depth. By comparing the KGE values from Scenario 0 and 1, it is manifest that the latter was affected by the calibration of the estimated hydraulic parameters, like at the  $\text{SN}_p$  where the fitting sought during the calibration phase for the  $\theta$  values gauged at -0.10 and -0.30 m, negatively affected the behavior of the simulated values at -0.70. Consistent performances along the depth were observed for the scenarios 3a and 3b at Settolo while at Colnù the improvement of the simulations at deeper positions were achieved at the expense of the goodness of the ones computed at shallower depths (Figure 3.9 c and d). The KGE computation highlighted different scenarios performances depending on the parcel considered, even within the same experimental site. As an example, the set of parameters of Scenario 2 (time varying  $K_c$  and constant 0.30 m deep  $Z_e$ ), negatively affected, respect to the Scenario 1, the  $\theta$  simulations in  $\text{SN}_p$ , in  $\text{CE}_p$  at -0.10 m and in both  $\text{SS}_p$  and  $\text{CW}_p$  at -0.70 m but it improved the results for these latters at -0.10 m and -0.30 m as well as for  $\text{CE}_p$  at -0.70 m and -0.30 m (Figure 3.9). Among the simulations achieved by calibrating the entire set of hydraulic parameters, the s4 results obtained by considering a time varying  $Z_e$ , were always better, with the only exception of the  $\text{SS}_p$

at -0.30 m, than the ones obtained in Scenario 2 by setting it constant in time. This supports the hypothesis that the effects of the herbicide on the transpiration activity of the plant's roots cannot be neglected at this scale.

### 3.1.3.2 Tracer evolution

The parameters calibrated in the scenarios 2 and 4, showing the best overall results in terms of KGE, were used to simulate the bromide infiltration. The diffusion coefficient was set equal to  $1\text{E-}09\text{ m}^2/\text{s}$  (la Cecilia et al., 2018) assuming that the advective process prevailed according to the mainly coarse soil texture (see section 3.1.2.1). With reference to all the parcels, Figures 3.12 and 3.13 show the bromide concentration modelling results compared to the observed data and both the observed and simulated water content behaviors. The meteorological forcing (rainfall data and computed evapotranspiration) is reported in the upper part of the figures. From a general point of view, given the difficulties related to the modelling of on-site experiments, the results are good, mainly at the Colnù site. The observed temporal behavior of the tracer concentration was well reproduced by both the considered simulation scenarios, underestimating the tracer concentration only in the surficial layer (up to -0.10 m) of both the Colnù parcels and in  $\text{SS}_p$  at -0.30 m. The tracer application was simulated as a step injection (see section 2.3.2) that represented a schematization only of the real physical process. Probably for this reason, observed and modelled concentration show the maximum differences in the surficial layer of both the experimental sites. A very good agreement between simulated and observed concentrations was obtained just below -0.30 m during the time-period spanning from the application (November 2018) to the beginning of February 2019 (Figures 3.12e and 3.13e), with exception of the  $\text{SN}_p$  where an abrupt reduction of concentration was measured in the months just following the application. Similar discrepancies with the modelled results, that is an overestimation of the observed concentrations, are generally manifest at -0.70 m, where the tracer results strongly reduced respect to the



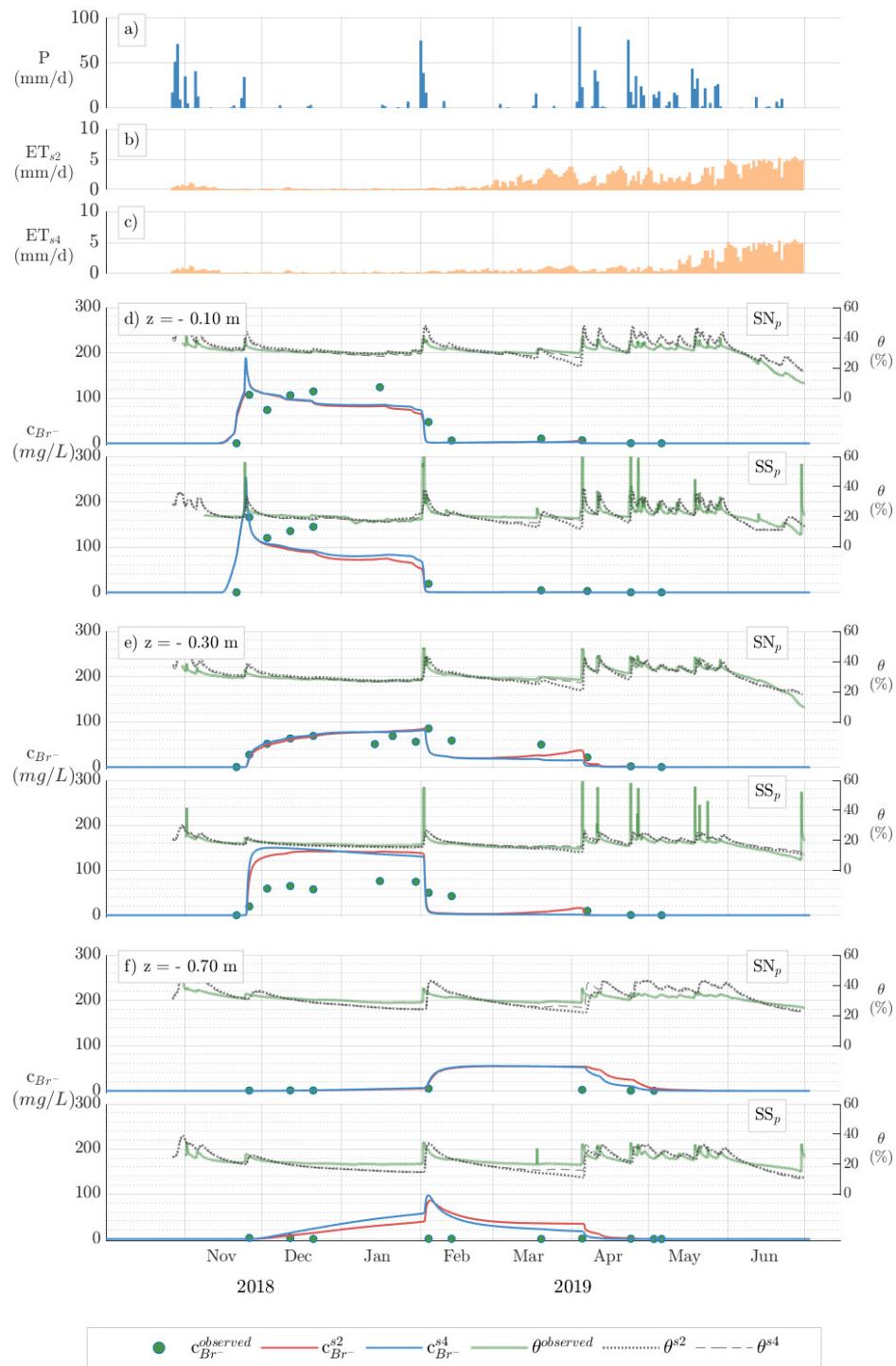


Figure 3.12: Comparison between the tracer concentration values measured at the Settolo site and the results of the tracer infiltration modelling achieved for s2 (red line) and s4 (blue line).

### 3.1. Pointwise-scale results

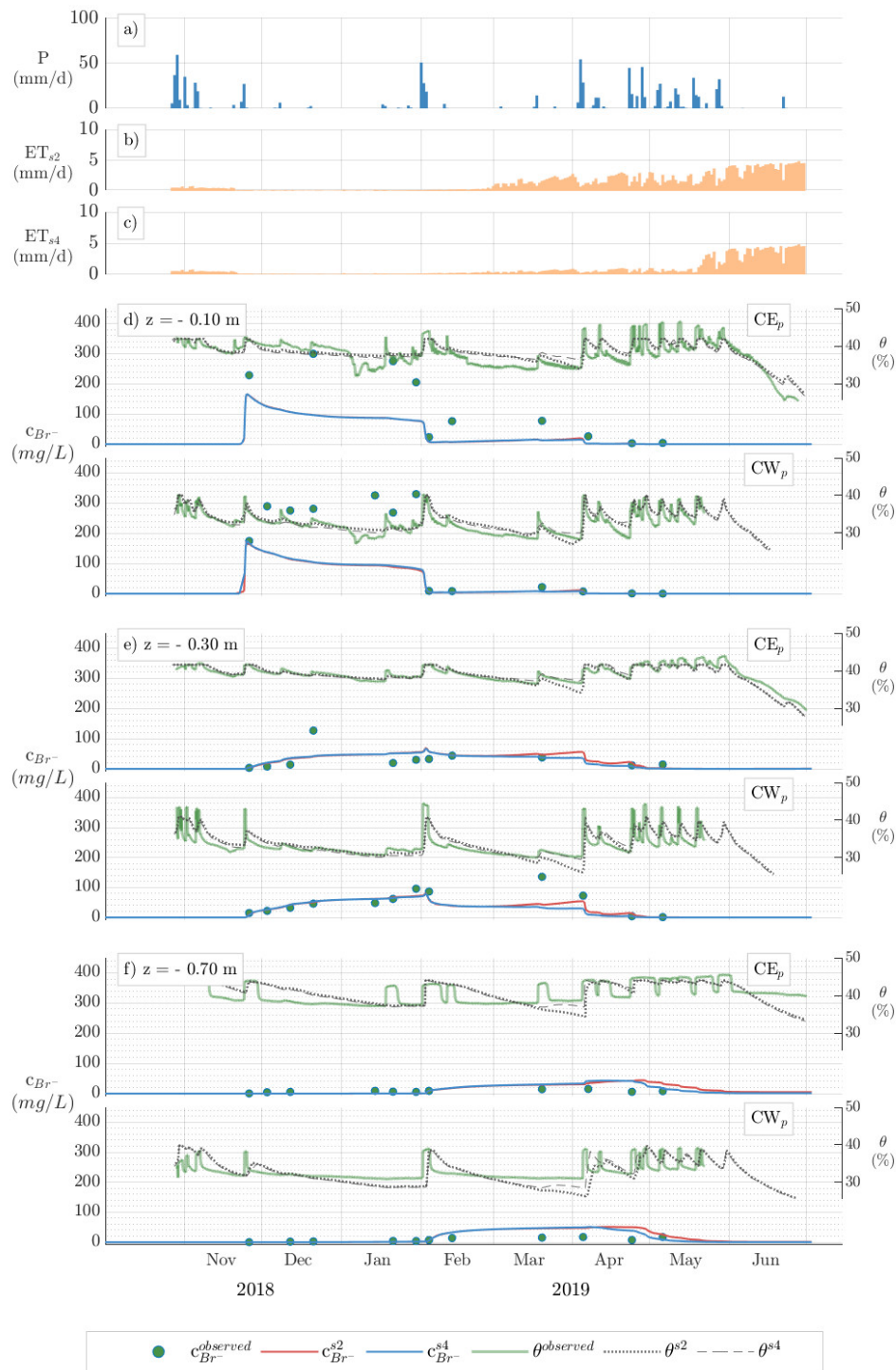


Figure 3.13: Results of tracer infiltration modelling compared with water content behavior. Observed values are reported in green while the other lines are the s2 and s4 modelling results.

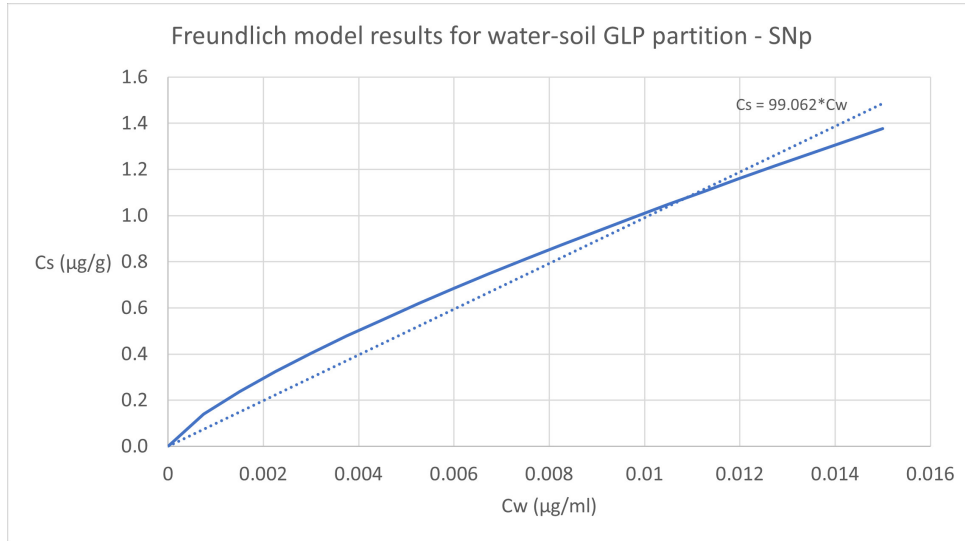


Figure 3.14: Comparison between the Freundlich model result for GLP water-soil partition for  $SN_p$  using site-specific experimental data (Mencaroni et al. (2021) – blue line). Linear interpolation to obtain the coefficient  $K_d$  for the BRTSim adsorption modelling is reported as dotted line.

simulated concentrations. The limit represented by the one-dimensional model may be the cause of this, being the real evolution of the infiltration process affected by three dimensional structures of the soil even in the first meter below the surface. This over-estimation is more pronounced at Settolo where the maximum concentrations observed at -0.70 m, 5.00 mg/l and 2.42 mg/l for  $SN_p$  and  $SS_p$  respectively, resulted much lower than the corresponding values observed at the depth of 0.30 m, equal to 85.12 mg/l and 75.92 mg/l respectively. As previously mentioned, the  $SS_p$  values at -0.30 m is strongly reduced respect to the 150 mg/l observed at -0.10 m, and this is consistent with the strong heterogeneity observed in the Settolo site texture.

### 3.1.3.3 Glyphosate evolution

The GLP evolution was simulated using the hydraulic parameters calibrated in the Scenario 4 only, being negligible the differences on the tracer transport simulations between scenarios 4 and 2 as shown in the previous section. The site-specific GLP partition co-

### 3.1. Pointwise-scale results

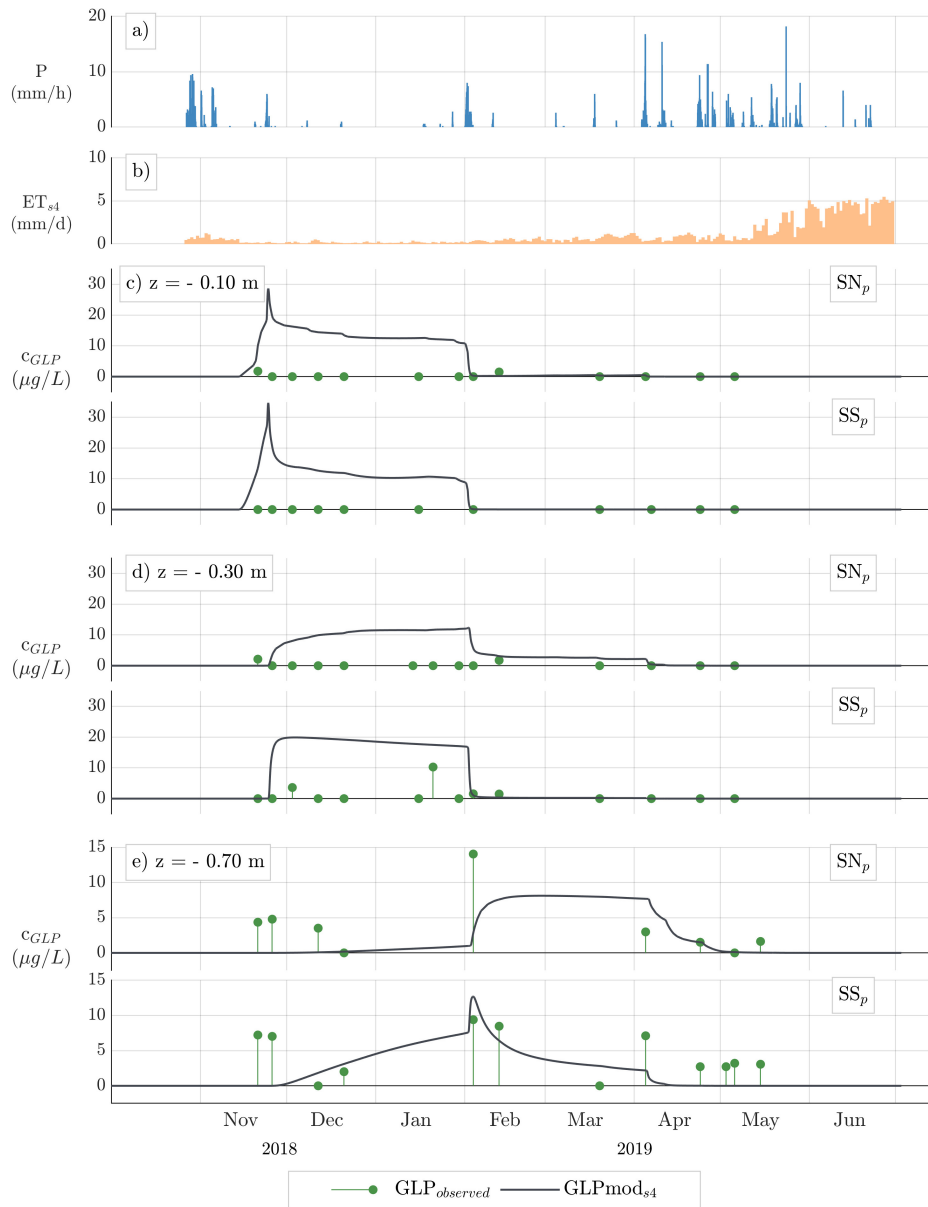


Figure 3.15: Comparison between the GLP concentration values measured at the Settolo North parcel ( $SN_p$ ) and the results of the GLP infiltration modelling.

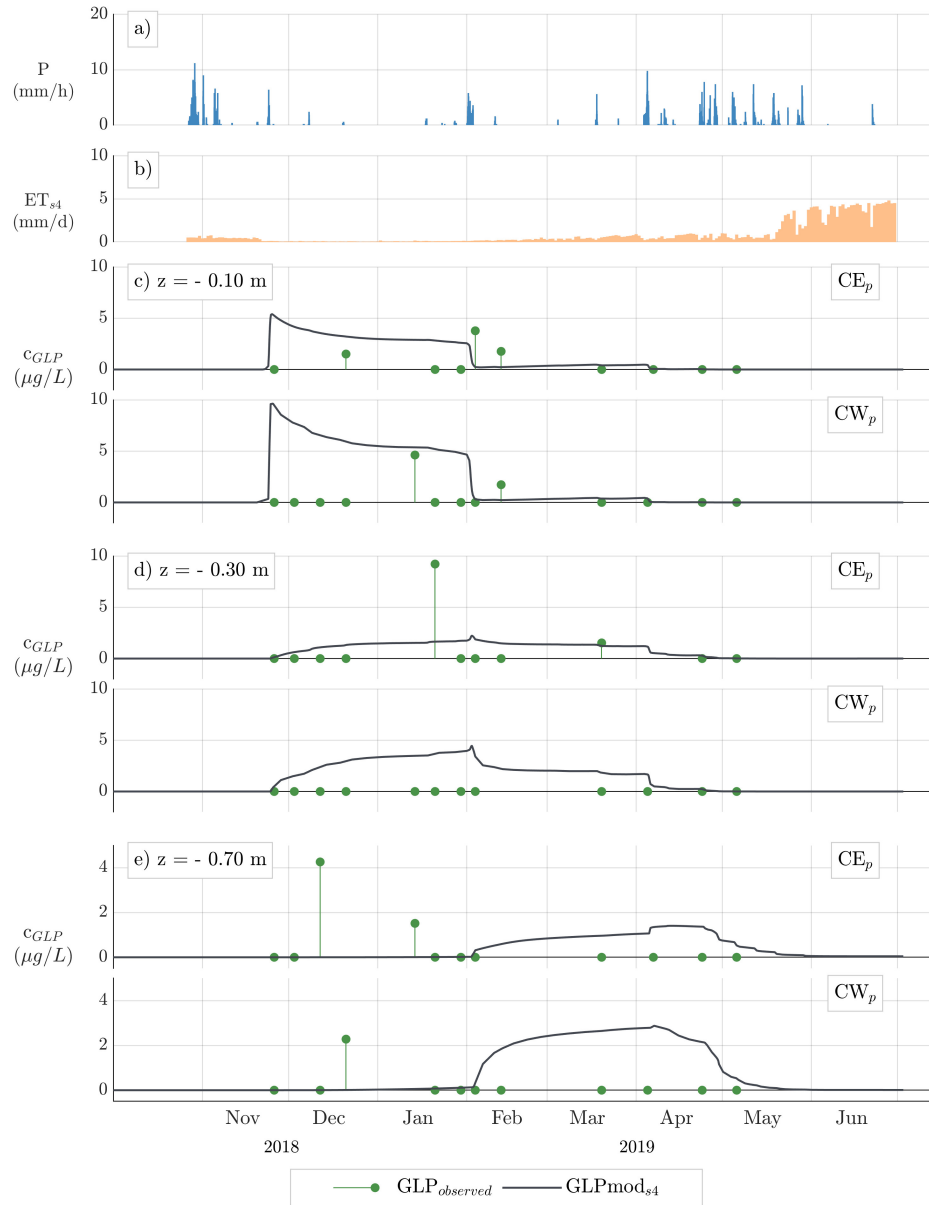


Figure 3.16: Comparison between the GLP concentration values measured at the Colnù East parcel ( $CE_p$ ) and the results of the GLP infiltration modelling.

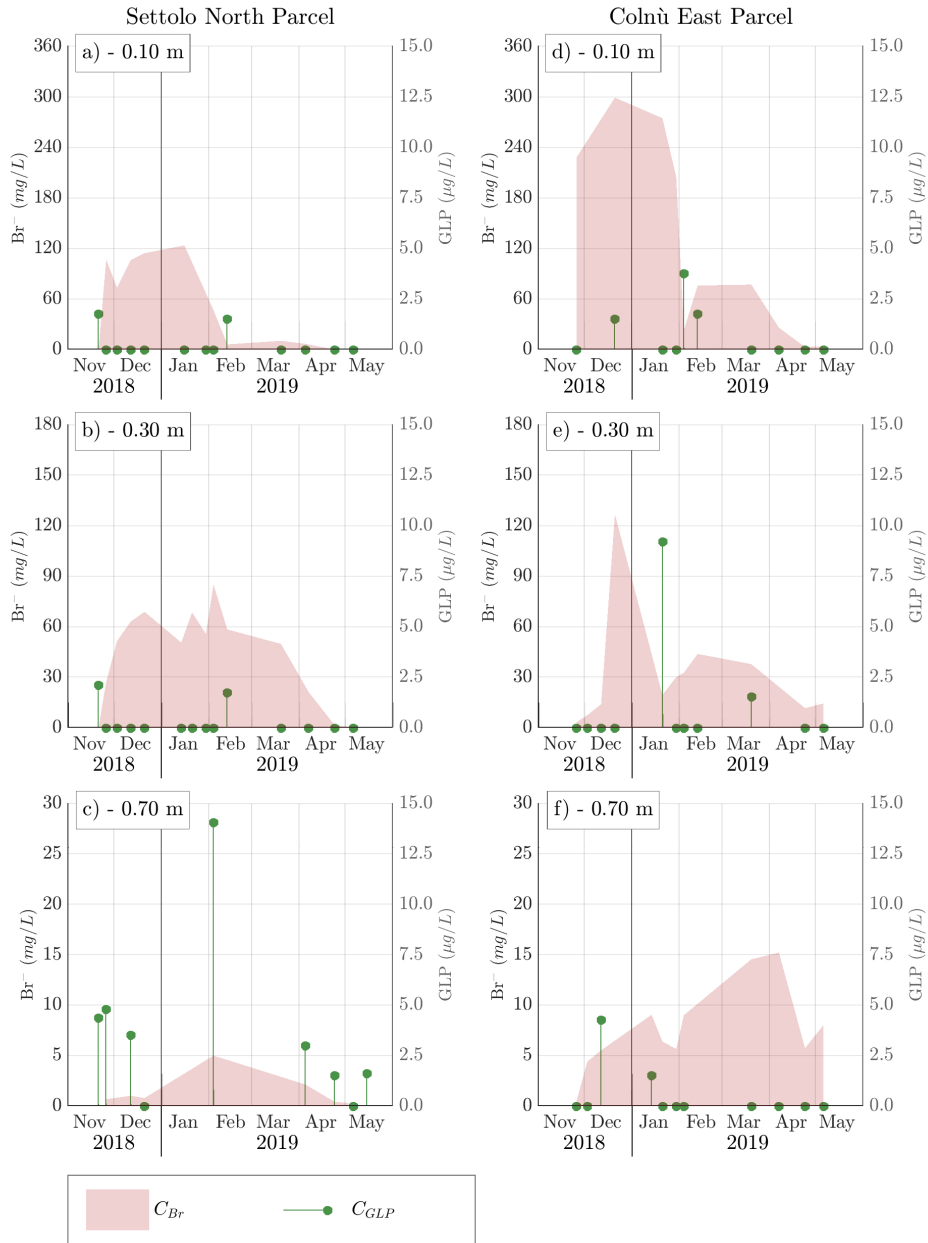


Figure 3.17: Comparison between Glyphosate and KBr evolutions along the vertical in  $SN_p$  and in  $CE_p$ .

Table 3.3: Log-values of the linear partition coefficient  $K_d$  [microg/g\*ml/microg] used in the GLP evolution modeling (data from Mencaroni et al. (2021)).

parameter	$SN_p$	$SS_p$	$CE_p$	$CW_p$
$\log_{10}K_d$	2.00	2.04	2.85	2.54

efficients achieved by Mencaroni et al. (2021) were adopted in the simulations, whereas the kinetics for biodegradation were assumed according to the work by la Cecilia et al. (2018), where the analyzed site shows pedologic features similar to the Colnù ones. Strictly speaking, the adsorption coefficients  $K_d$  reported in Table 1 represent the angular coefficients of the linear relationships adopted in the simulations, that well describe the Freundlich soil-water partition models in the range of GLP concentrations observed in the field (Mencaroni et al, 2021). The  $K_d$  values show evident differences between the two sites, highlighting a not negligible variability between the two parcels of the Colnù site too. The mean value of  $K_d$  for the Colnù site resulted five times larger than the one of the Settolo site, being the parcels specific values recorded in the former site one the twice of the other. The comparisons between numerical simulations and observed data are reported in Figures 3.15 and 3.16 for the Settolo and the Colnù sites respectively. Even if the spatial-temporal evolution of the herbicide is not accomplished by the numerical simulations results, the upper layer in Colnù and the deeper ones in Settolo show some reasonable results in terms of the reproduced concentration peaks. Generally speaking, most part of the GLP measurements are below the limit of quantification, while the model suggests a continuous evolution, in time and along the vertical, of not negligible herbicide concentration values. However, in sporadic cases spotted after the more intense rainfall events, the observed values show unexpected spikes of concentration. Just as an example, an increase of concentration along the vertical direction is observed in both the Settolo parcels between -0.30 m and -0.70 m during the period between November and December after an intense rainfall event. This fact, together

with the general discrepancy previously mentioned, between observed and simulated concentrations, suggests that the evolution of the pesticide along the vertical cannot be modelled as an advection-dispersion process only. The presence of high fractions of GLP adsorbed to the soil matrix highlighted by the laboratory analyses, hints a different mechanism of transport. During the more intense rainfall events the grains of limited dimensions with adsorbed GLP can move along the preferential pathways enhanced by the soil heterogeneity. This is manifest also from Figure 3.17 where the GLP and the bromide evolutions show relevant differences for the  $SN_p$  up to the depth of 0.70 m where the finest soil particles washed out by the more intense precipitation events are collected by the sampling system (pan lysimeters). Similar considerations cannot be developed for the Colnù site where the porous cups prevented the collection of colloidal particles and where discrepancies with the advective / diffusive one-dimensional model may be ascribed to the presence of three-dimensional preferential paths due to the soil heterogeneity. In both cases, the results suggest that a interpretative and/or forecasting model of PPPs evolution should be developed considering the heterogeneous characteristics of the soil in three-dimension and, for chemical species characterized by a high adsorption rate, like GLP-based herbicide here considered, the influence of the colloidal transport inside the heterogeneous formations.

#### 3.1.4 Final remarks

- The hydraulic parameters governing the process of rainwater infiltration into the soil, assumed as the main driving mechanism for the herbicide transport, were calibrated with a one-dimensional model based on experimental data.
- Observed  $\theta$  and KBr concentration values were well simulated up to a depth of 0.30 m BGL.
- Below 0.30 m, discrepancies between observed and modelled values pointed out the



limits of the 1-D modelling suggesting the presence of preferential flow-pathways due to soil heterogeneity and flow movements different from the vertical one.

- Lab analysis showed that GLP is mostly adsorbed to the topsoil acting like a barrier to infiltration. However, high GLP concentrations were spotted at -0.70 m in the site of Settolo indicating possible infiltration events through soil preferential pathways.
- The use of parcel-specific values of the GLP partition coefficient in the numerical simulations of the GLP evolution, gave reasonable results in terms of the reproduced GLP concentration peaks.
- The lack of consistence of more than one GLP observed value with the advection-dispersion model predictions, hints a different mechanism of transport
- The herbicide is adsorbed to the finest soil particles that, displaced by the most intense rainfall events, are transported through preferential pathways. Only a small fraction is dissolved in the infiltrating rainwater
- The achieved results at the point-wise scale, suggest the needing to develop a more complex interpretative model leaving the description obtained with one-dimensional advection-dispersion.
- The different GLP behaviors observed in the monitoring points within the same area, suggests a dependency of vertical mobility on the spatial heterogeneity of the properties of the soil.

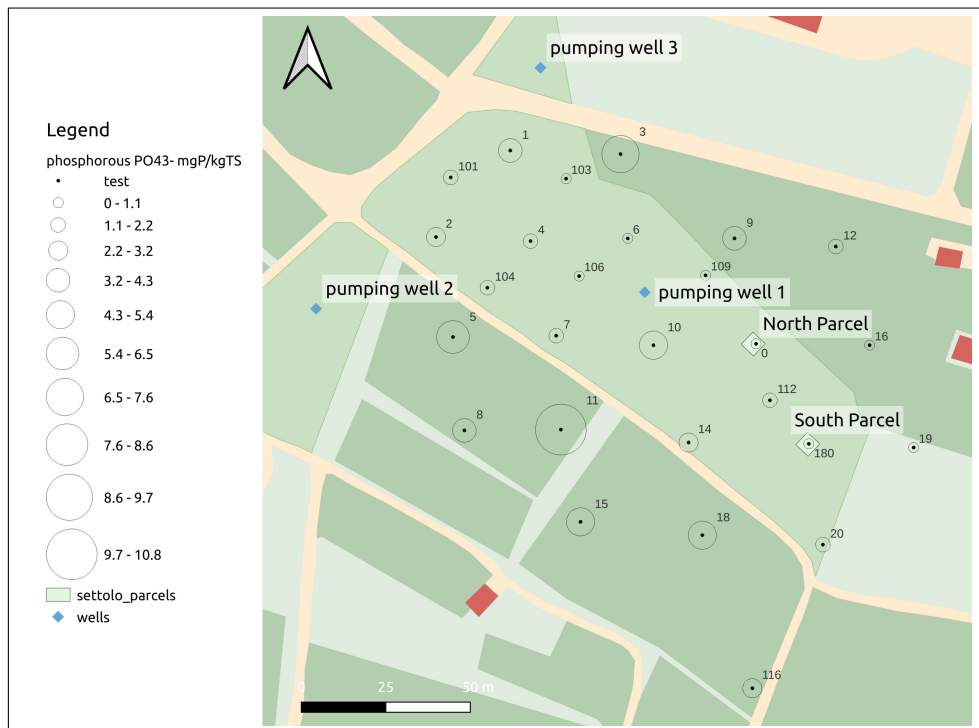


Figure 3.18: Soluble phosphorus  $PO_4^{3-}$  concentrations in the topsoil of the Settolo site.

## 3.2 Field-scale results

### 3.2.1 Results of the experimental surveys

The experimental data collected during the surveys - infiltration tests (plus soil sampling at the Settolo site) - provided themselves a first picture of the spatial heterogeneity of the soil properties, both physical and chemical, observed within the two experimental sites.

#### 3.2.1.1 Soil sampling

Table 3.4 and Figures 3.18 - 3.19, show the results of the laboratory analysis on the collected topsoil samples. As expected, higher concentration values of the soluble phosphorus were found on average in the topsoil samples collected within the vineyards, being the vines periodically subjected to treatments with growth regulators PPPs (fertilizers).

Table 3.4: Results of the analyses developed on the top-soil samples collected at the Settolo site.

sampling position	TS <sup>1</sup> % dry sample	VS <sup>2</sup> % <sub>TS</sub>	TOC <sup>3</sup> %C <sub>TS</sub>	PO <sub>4</sub> <sup>3-*</sup> mgP/kgTS
1	92	6.30	<1	3.90
101	85	3.90	<1	1.20
2	94	3.80	<1	2.30
103	82	4.30	<1	<1
4	96	2.60	<1	1.90
104	83	4.40	1.00	2.00
6	81	4.70	<1	<1
106	82	4.60	<1	<1
7	95	3.30	<1	1.80
109	79	3.70	<1	<1
10	93	4.40	<1	4.70
0	88	3.40	<1	<1
14	95	3.90	<1	3.20
112	83	5.70	<1	1.90
180	86	3.40	<1	<1
20	87	3.70	<1	1.60
3	84	4.60	<1	7.20
9	79	7.70	1.50	3.30
12	88	4.90	<1	1.80
16	88	4.40	<1	<1
19	87	3.30	<1	<1
5	83	5.50	2.30	5.90
8	82	3.40	1.30	3.60
11	83	3.50	<1	10.80
15	85	3.60	<1	5.00
116	77	7.80	1.10	2.40
18	80	3.40	<1	4.60
mean	85.8	4.38	1.44	3.64
st. dev.	5.3	1.25	0.46	2.32

<sup>1</sup> Total Solids (what remains in the sample after evaporating the water).

<sup>2</sup> Volatile Solids expressed as a percentage of the dry sample (value that can be correlated to the quantity of organic substance expressed as a percentage of the weight of the dry sample).

<sup>3</sup> Total Organic Carbon: actual percentage of organic carbon in the dry sample.

\* Concentration of soluble phosphates expressed as phosphorus in the dry sample

During the surveys, values of 10.8 and 7.3 mgP/kgTS were observed in the vineyards located west and north-east to the base well respectively, increasing the risk of GLP leaching. In the buffer area around the well, the highest phosphorus concentration was the half (4.7 mgP/kgTS), being the non-cultivated area only subjected to grass mowing. The  $\text{PO}_4^{3-}$  concentrations observed in the vineyards could have been affected by the sampling period. In fact, the soil sampling activity was developed in the first week of August, distant in time from the spring fertilization treatment of the vines. Each year vineyards are subjected to two fertilization treatments, the first one is developed in spring, in the months April-May depending on the climate conditions, while the second is carried out in autumn, just after the grape harvest. Phosphorus is contained in form of  $\text{P}_2\text{O}_5$  in both two-components - with Nitrogen - and three components - with Nitrogen and Potassium - fertilizers, to enhance the development of roots, flowers, seeds, and fruits (Dittmar et al., 2009). In wine-making practices it is suggested a phosphorus concentration of 140 grams per vine plant per fertilization treatment (Skinner et al., 1988), while the reference dose per hectare indicated by the Wine-making Protocol varies in the range 200-500 kg/ha. Moreover, phosphorus in soil can also derive from degradation product of glyphosate residues, increasing the availability of a more ready bio-degradable source of nutrients for the soil micro-organisms (Sun et al., 2019). For these reasons, this element remains a valuable parameter for future surveys. The laboratory analysis on the soil samples showed a general low concentration of soil organic matter in the topsoil of the investigated area, resulting in this way potentially more vulnerable to pesticide leaching. However, the obtained data were too few for a reliable prediction, also in terms of its spatial distribution. Only five measures resulted above the TOC limit of quantification, making it impossible to determine any pattern or appreciable differences between different plots, as it was for the  $\text{PO}_4^{3-}$  concentration values. Similar results were observed for volatile solids (VS). The VS measure is commonly developed in environmental engineering when very low TOC concentrations are expected/found, as a

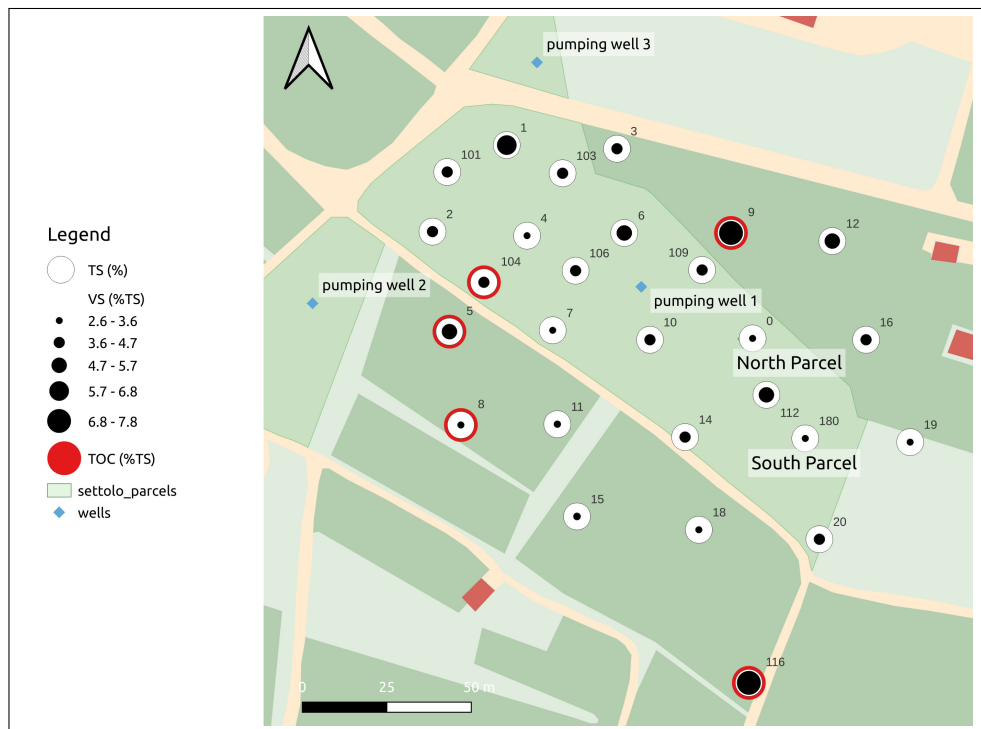


Figure 3.19: Total Organic Carbon (TOC) and the Volatile Solids (VS) spatial distributions at the Settolo site.

Table 3.5: Summary of the univariate statistics developed on the top-soil analyses results (Settolo site).

measure	Total Solids [%]		Volatile Solids [%TS]		TOC [%TS]		$PO_4^{3-}$ [mgP/kgTS]	
	well area	vineyards	well area	vineyards	well area	vineyards	well area	vineyards
<b>Min.</b>	79.00	77.00	2.600	3.300	0.0000	0.0000	0.000	0.000
<b>1st Qu.</b>	82.75	81.00	3.625	3.450	0.0000	0.0000	0.000	2.100
<b>Median</b>	86.50	83.00	3.900	4.400	0.0000	0.0000	1.700	3.600
<b>Mean</b>	87.56	83.27	4.131	4.736	0.0625	0.5636	1.531	4.055
<b>3rd Qu.</b>	93.25	86.00	4.450	5.200	0.0000	1.2000	2.075	5.450
<b>Max.</b>	96.00	88.00	6.300	7.800	1.0000	2.3000	4.700	10.800

backup estimation of the organic content of the soil. Also in this case, the VS fraction was always quantified, as showed in Figure 3.19, but it did not highlight any significant differences in concentration between the vineyards and well buffer area (Table 3.5).

### 3.2.1.2 Infiltration tests

During the tests performed with the double-ring infiltrometers, differences of the soil infiltration capacity  $f$  between the distributed surveys positions, were manifested already from the first minutes of each test. This, by evaluating the number of re-fills required to prevent the complete emptying of the two rings - proportional to the volume of infiltrating water - and of the real-time  $f$ , by equation 2.2. The development of the tests on-site, permitted to appreciate an evident heterogeneity of the infiltration capacity even within plots destined to the same activity (agricultural and non-agricultural). Figures 3.20 and 3.21 show the two sites maps with examples of infiltration tests results obtained in different positions within the investigated areas that permitted the identification of plots characterized by similar infiltration behaviors. In each graph reported around the site map, the blu line indicates the water depth  $h$  inside the infiltrometer, while the blu dots indicates the values of infiltration rate  $f$ . At the Settolo site, the buffer area around the base well (highlighted in Figure 3.20 with a yellow contour line, and hereinafter referred to as 'well area') was characterized on average by infiltration tests

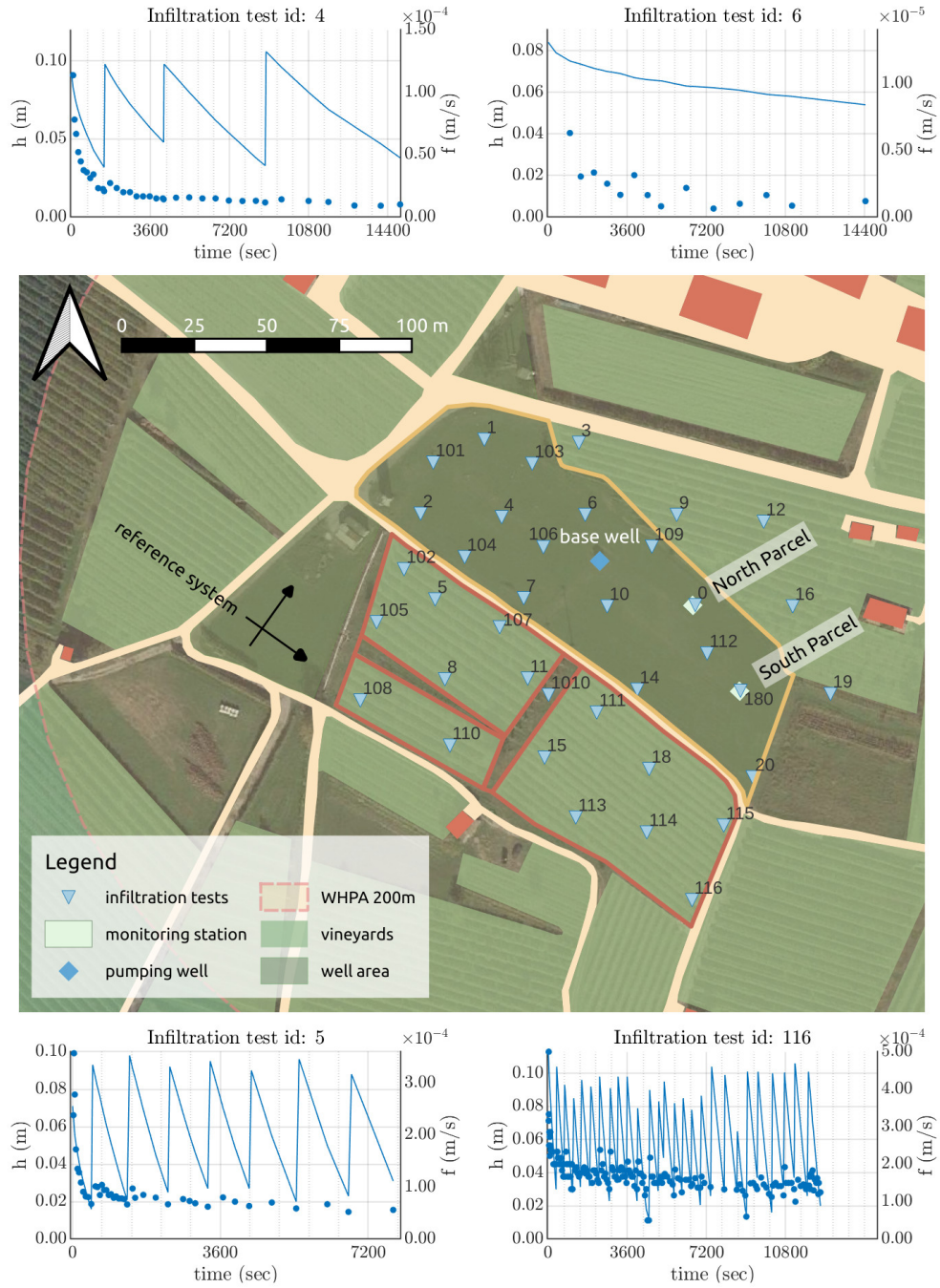


Figure 3.20: Overview of the infiltration tests results achieved at the Settolo site. The two macro-areas characterized by similar values of soil infiltration capacity are outlined in yellow, 'well area', and orange, 'south vineyards'.

similar to test 4, requiring 3 to 4 refills of the two rings during the test and showing an asymptotic value of  $f$  approaching  $1.5 \times 10^{-5}$  m/s. However, at around 25 meters east from test 4, test 6 showed a much slower infiltration rate, requiring no refill all along the test duration and reaching  $f$  values close to  $5 \times 10^{-7}$  m/s. This large difference (more than one order of magnitude) was a first important hint in the definition of the characteristic correlation length of the area in the structural analysis reported in the following section. South-West and South respect to the buffer area of the well, test 5 and test 116 both showed infiltration rates characteristic of the vineyards in which they were performed. The vineyards are outlined in the map of Figure 3.20 with a orange contour line and hereinafter referred to as 'south vineyards'. Both tests there showed a much steeper curve of infiltration during the first minutes and required 4 and 8 times respectively the water volume required on average for the tests performed within the well area. Considering that test 116 was performed by refilling the infiltrometer 26 times, and that the volume needed for one refill is around 25 to 30 liters, the total volume was not much lower than  $0.7 \text{ m}^3$ . The constant values of  $f$  reached with the two tests were around  $1 \times 10^{-4}$  to  $1.5 \times 10^{-4}$ , one order of magnitude larger than the one observed on average within the well area. A similar subdivision of the investigated area was also ascertained for the Colnù site, based on the preliminary experimental evidences achieved with the infiltration tests. In this case, however, the larger differences in soil infiltration capacity rates were observed between two plots both destined to vines cultivation. In the vineyard located north in the site map of Figure 3.21, hereinafter referred to as 'north vineyard', the trend of the soil infiltration capacity resulted on average similar to the one observed with the test 7005, approaching values of field-saturated hydraulic conductivity lower than  $6 \times 10^{-6}$  m/s. In fact, most of the tests performed in the north vineyard area needed less than  $0.1 \text{ m}^3$  of water each for the infiltrometer re-filling along the entire test duration. As highlighted by the results obtained with the test 2024 - and as observed in the well area of the Settolo site - also in the case of this vineyard very low



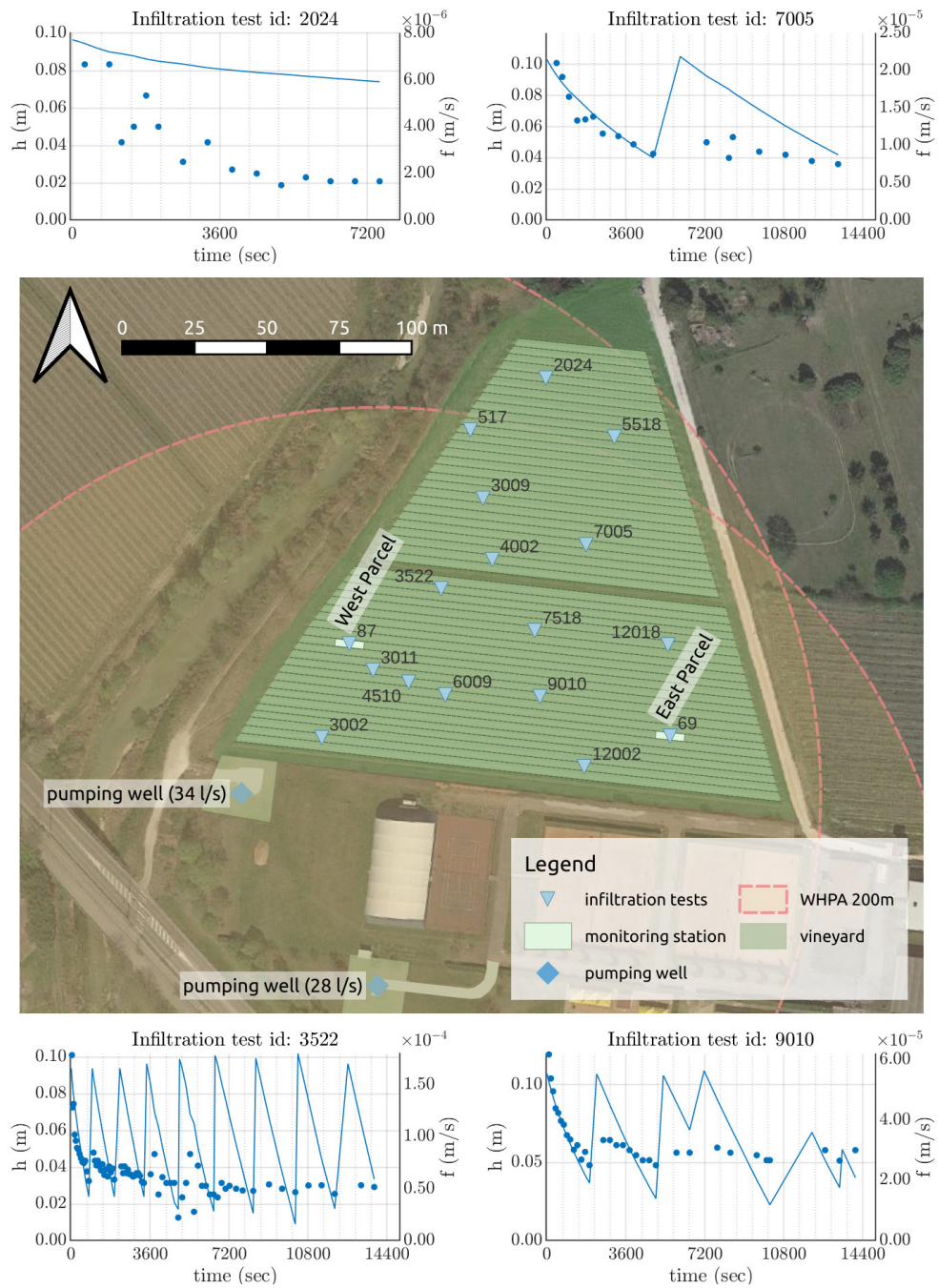


Figure 3.21: Overview of the infiltration tests results achieved at the Colnù site

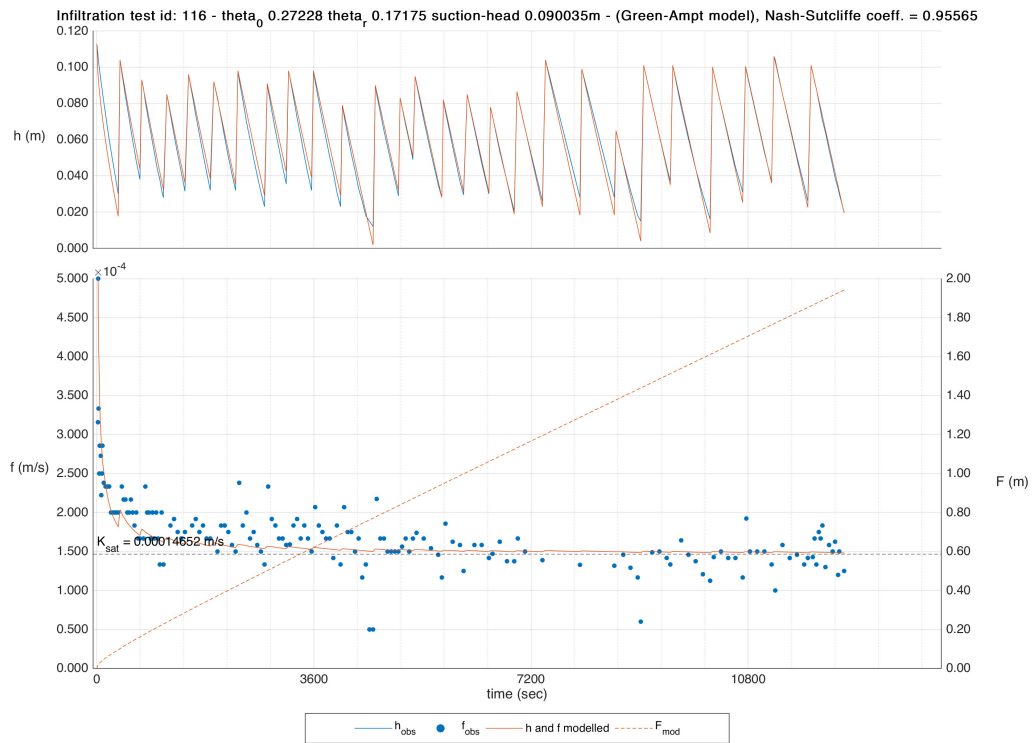


Figure 3.22: Example of calibration result for the Green-Ampt model parameters, initial water content  $\theta_0$ , effective hydraulic conductivity,  $K_e$ , and suction head at the wetting front  $\psi_{wf}$ . Infiltration test n.116.

rates of infiltration were measured, manifesting difference up to an order of magnitude respect to the asymptotic value of  $f$  observed in test 5518 developed at a distance of 50 meters. Higher infiltration rates were observed on average within the 'south vineyard', hosting the two site parcels organized with the monitoring stations. The results of the tests 3522 and 9010 are reported as reference of the range of infiltration rates observed within the plot.

### 3.2.2 Results of the infiltration tests modeling

The analysis of the infiltration tests developed by using the Green-Ampt model, permitted the evaluation, by calibration of the hydraulic parameters of the model as showed by the example reported in Figure 3.22, of the field-saturated hydraulic conductivity,

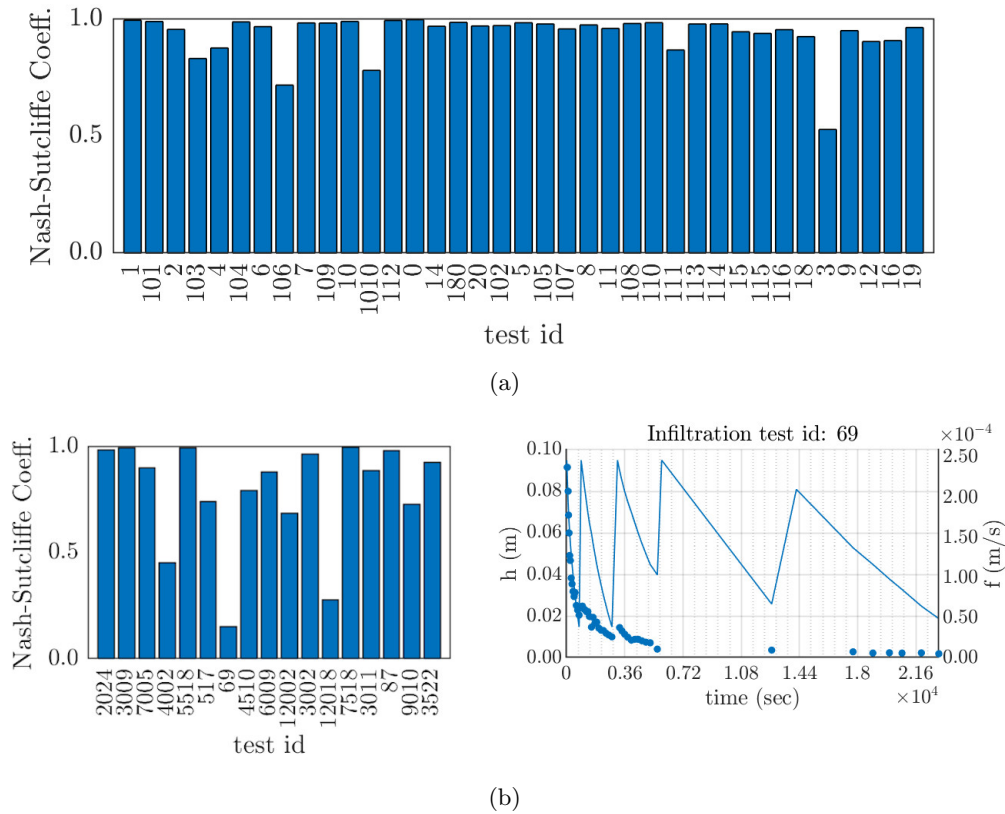
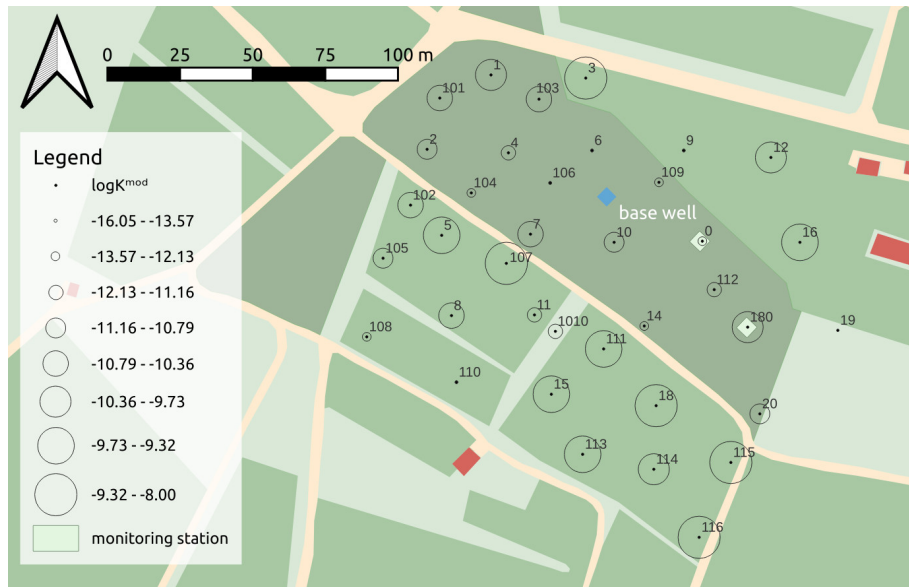


Figure 3.23: Nash-Sutcliffe Efficiency coefficients for the simulated infiltration tests at a) Settolo and b) Colnù. Figure b) also reports the infiltration test 69, presenting a significant variation in the infiltration rate in the first phases of the test.

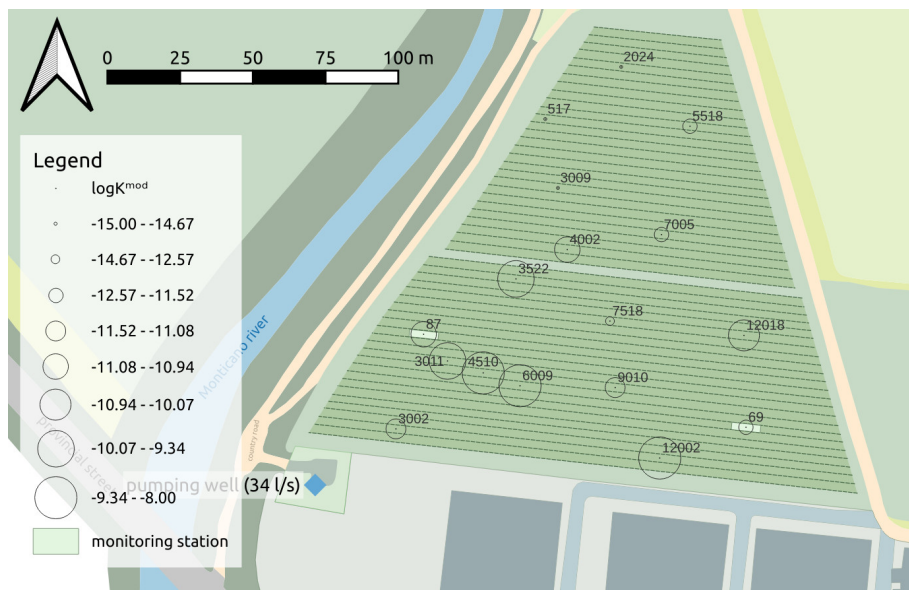
$K_{fs}$ . In most cases, the modeled values of water depth  $h$  and infiltration rate  $f$ , both showed with orange lines in the reported example, simulate very well the observed behaviors of the corresponding experimental values. The goodness of fit was ascertained for each test simulation by computing the Nash-Sutcliffe efficiency coefficient (NSE - ranging from  $-\infty$  to 1 where 1 is the optimum). The NSE values, reported in Figures 3.23a and 3.23b, show that the analysis of the infiltration tests results developed using the Green-Ampt model, worked very well for the tests developed in both sites. Among 54 simulated infiltration tests, only 3 tests fall below a coefficient value of 0.5 and they all belonged to the ensemble of surveys performed at the Colnù site. The low fitting of the model in that cases was due to a different behavior of the infiltration curve in the

first part of the test, probably caused by the presence of preferential flow-paths in the agricultural soil that cannot be simulated with the Green-Ampt model. Figure 3.23b reports the test 69, developed in the same position of the monitoring station  $CE_p$  (see section 2.2.3), showing a very steep infiltration curve in the first 1.5 hour and a strong decrease of the infiltration rate afterwards. For these tests, the field-saturated hydraulic conductivity  $K_{fs}$  was assumed equal to the constant value of infiltration rate  $f$  reached at the end of the test. A first spatial characterization of the infiltration tests modeling results  $K_{mod}$  was developed in QGIS using rule based symbology. The developed site maps are reported in Figures 3.24a and 3.24b. They agree, by showing circles around the surveys positions proportional to the  $\log K_{mod}$  values, with the hypotheses of i) the presence of areas within the sites characterized by similar infiltration capacity and of ii) a higher permeability, on average, of the ones destined to the vine cultivation.

**Univariate analysis** Table 3.6 reports the hydraulic parameters of the Green-Ampt model calibrated for each infiltration test developed at the two sites. The table is accompanied with Figures 3.25 and 3.26 results of a univariate analysis on the  $\log K_{mod}$  values for the two sites respectively. Both histograms, representing the probability distribution of  $\log K_{mod}$ , highlight a mild negative skewness (toward higher values) meaning that within both the sites there is a larger probability to observe high soil infiltration capacities. This tendency appears stronger within the Settolo site, as showed by the cumulative distribution function (cdf) plotted as a red line overlying the histogram. This is manifest also by the values of the position measures *mean* and *median* reported in Table 3.7). Within the same table, it is noticeable that the area south vineyards, presents a higher difference, respect to the well area, between the two measures of position. This is due to the lower values of soil infiltration capacity observed in tests 108 and 110 (Figure 3.24a, developed in the small vineyard located further southwest respect to the well area. This results show that a higher variability of the infiltration capacity can



(a)



(b)

Figure 3.24: Spatial characterization of the  $\log K_{mod}$  distribution at a) the Settolo site b) the Colnù site.

Table 3.6: Infiltration tests modeling results.

N.	Settolo site					Colnù site				
	test id	$\theta_0$	$\psi_{wf}$	$K_{mod}$	$\log K_{mod}$	test id	$\theta_0$	$\psi_{wf}$	$K_{mod}$	$\log K_{mod}$
1	1	0.348	0.124	3.258e-05	-10.33	2024	0.197	0.209	4.238e-07	-14.67
2	101	0.380	0.114	2.605e-05	-10.56	3009	0.183	0.223	3.082e-07	-14.99
3	2	0.339	0.126	1.899e-05	-10.87	7005	0.203	0.202	4.505e-06	-12.31
4	103	0.357	0.115	2.058e-05	-10.79	4002	0.204	0.205	1.779e-05	-10.94
5	4	0.320	0.128	1.207e-05	-11.32	5518	0.199	0.220	3.462e-06	-12.57
6	104	0.289	0.125	4.090e-06	-12.41	517	0.220	0.200	3.836e-07	-14.77
7	6	0.303	0.103	7.470e-07	-14.11	69	0.160	0.217	9.922e-06	-11.52
8	106	0.271	0.113	1.216e-06	-13.62	4510	0.143	0.236	1.476e-04	-8.82
9	7	0.245	0.120	2.564e-05	-10.57	6009	0.157	0.210	1.126e-04	-9.09
10	109	0.241	0.111	1.344e-06	-13.52	12002	0.153	0.224	8.803e-05	-9.34
11	10	0.217	0.123	1.533e-05	-11.09	3002	0.138	0.251	1.538e-05	-11.08
12	1010	0.241	0.109	1.150e-05	-11.37	12018	0.123	0.281	3.465e-05	-10.27
13	112	0.318	0.086	1.352e-05	-11.21	7518	0.132	0.264	2.587e-06	-12.86
14	0	0.340	0.086	1.643e-06	-13.32	3011	0.146	0.236	4.218e-05	-10.07
15	14	0.273	0.103	5.401e-06	-12.13	87	0.134	0.259	1.675e-05	-11.00
16	180	0.244	0.098	3.862e-05	-10.16	9010	0.145	0.232	1.445e-05	-11.14
17	20	0.178	0.135	1.611e-05	-11.04	3522	0.192	0.177	4.564e-05	-9.99
18	3	0.330	0.152	1.073e-04	-9.14					
19	9	0.274	0.141	5.247e-07	-14.46					
20	12	0.315	0.107	3.295e-05	-10.32					
21	16	0.266	0.117	6.209e-05	-9.69					
22	102	0.352	0.107	3.057e-05	-10.40					
23	5	0.302	0.112	6.319e-05	-9.67					
24	105	0.337	0.106	1.498e-05	-11.11					
25	107	0.270	0.107	1.072e-04	-9.14					
26	8	0.241	0.119	2.057e-05	-10.79					
27	11	0.204	0.131	9.652e-06	-11.55					
28	108	0.207	0.125	1.331e-06	-13.53					
29	110	0.221	0.108	8.437e-07	-13.99					
30	111	0.268	0.098	7.971e-05	-9.44					
31	113	0.306	0.093	8.178e-05	-9.41					
32	114	0.305	0.095	4.483e-05	-10.01					
33	15	0.271	0.105	5.970e-05	-9.73					
34	115	0.217	0.111	9.898e-05	-9.22					
35	116	0.272	0.090	1.465e-04	-8.83					
36	18	0.219	0.109	1.674e-04	-8.69					
37	19	0.190	0.117	1.072e-07	-16.05					

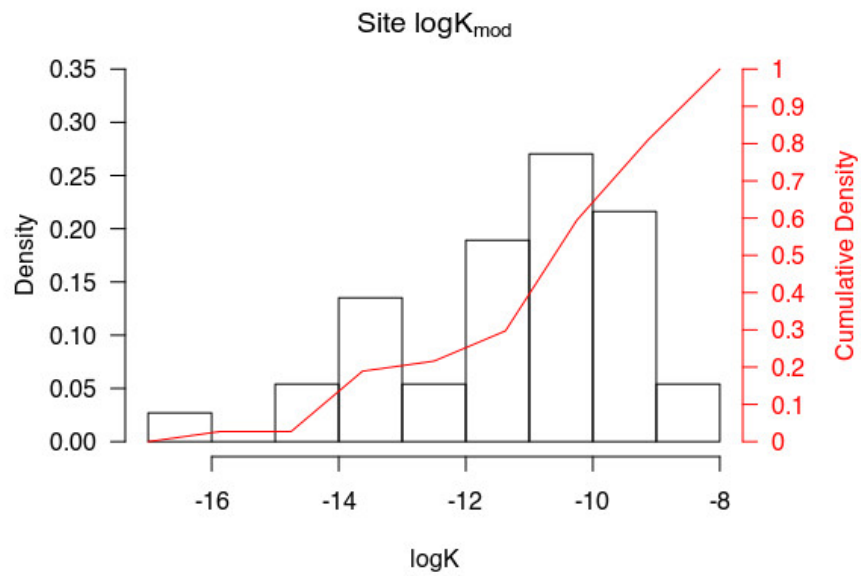


Figure 3.25: Histogram of  $\log K_{mod}$  obtained for the Settolo site.

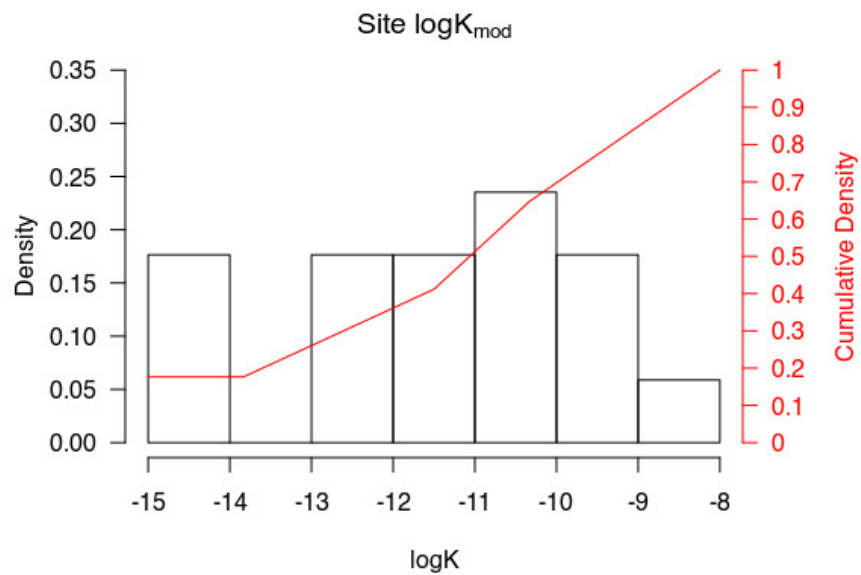


Figure 3.26: Histogram of  $\log K_{mod}$  obtained for the Colnù site.

Table 3.7: Descriptive statistics summary.  $K_{mod}$  values obtained for the Settolo site.

area	unit	Min.	1st Qu.	Median	Mean	3rd Qu.	Max.
whole area	$K_{mod}$	1.072e-07	5.401e-06	2.057e-05	3.718e-05	5.970e-05	1.675e-04
	$\log K_{mod}$	-16.049	-12.129	-10.792	-11.178	-9.726	-8.695
well area	$K_{mod}$	7.470e-07	3.478e-06	1.442e-05	1.462e-05	2.185e-05	3.862e-05
	$\log K_{mod}$	-14.11	-12.64	-11.15	-11.69	-10.74	-10.16
south vineyards	$K_{mod}$	8.437e-07	1.411e-05	5.226e-05	5.867e-05	8.608e-05	1.675e-04
	$\log K_{mod}$	-13.986	-11.175	-9.869	-10.430	-9.364	-8.695

Table 3.8: Descriptive statistics summary.  $K_{mod}$  values obtained for the Colnù site.

area	unit	Min.	1st Qu.	Median	Mean	3rd Qu.	Max.
whole area	$K_{mod}$	3.082e-07	3.462e-06	1.538e-05	3.274e-05	4.218e-05	1.476e-04
	$\log K_{mod}$	-14.993	-12.574	-11.082	-11.498	-10.074	-8.821
north vineyard	$K_{mod}$	3.082e-07	3.937e-07	1.943e-06	4.478e-06	4.244e-06	1.779e-05
	$\log K_{mod}$	-14.99	-14.75	-13.62	-13.38	-12.38	-10.94
south vineyard	$K_{mod}$	2.587e-06	1.492e-05	3.465e-05	4.816e-05	6.684e-05	1.476e-04
	$\log K_{mod}$	-12.865	-11.113	-10.270	-10.473	-9.666	-8.821

be expected in areas destined to vineyards. The probability distribution reported in Figure 3.26 for the Colnù site, shows a large variance, likely influenced by the presence of numerous low values. These are the  $\log K_{mod}$  values obtained for the infiltration tests developed in the north vineyard. The increasing trend of the cdf results in this way less steep compared to the one obtained for the Settolo site, characterized by the presence of agricultural and non-agricultural plots.

### 3.2.3 Results of the geostatistical analysis

To obtain a robust definition of the experimental semi-variogram and the variogram model fitting, the universally recognized *rule-of-thumb* principles suggest that:

- a) variogram values that corresponds to distances farther than the half of the maximum distance between two regional variable realizations should be not considered;
- b) the minimum number of regional variable realizations in the sample should be larger than 50.



Based on these indications, the available data in Colnù are not enough to develop a reasonable geostatistic analysis. For this reason, despite an attempt developed using the SAGA code (see Section 2.3.2.1), no results are reported in this thesis work. For the Settolo site, the infiltration tests were developed in 37 measurement positions, that is less than the proper minimum number of data. Anyway, we decided to present the following geostatistical analysis as preliminary result of a "in-progress-work". The descriptive analysis evidences, useful for any subsequent geostatistical analysis and estimation, are probably the more reliable result, at this time, that can be obtained from the collected data.

**Exploratory data analysis and spatial characterization** To detect any recognizable pattern in the spatial distribution of the  $\log K_{mod}$  values, a second spatial characterization was developed for the Settolo site using the interpolation method based on the Thiessen-Polygons (section 2.3.2.1). Figure 3.27 shows the result of this interpolation that assigns the point-wise value of the test to the surrounding area by geometrical criterion. This interpolation, although not reliable from a physical view-point, being the real trend of the spatial variable much more scattered, can be useful for the estimation of the parameters necessary in the computation of the experimental variogram (see the following paragraph). In particular, the TP interpolation highlighted a low- $\log K$  structure ( $K_{mod} = 7.5E-07$  m/s,  $\log K_{mod} = -14$ ) located within the well area. This follows an apparent direction at an angle of  $45^\circ$  respect to the axis of the investigated area (directed from North-West to South-East). Starting from the road dividing the two areas of the Settolo site, the structure seems to turn south after 60 meters, toward the two site parcels organized with the monitoring stations. A similar analysis was developed for the vineyards located South-West respect to the well area, highlighting a direction of spatial correlation in agreement with the axis of the investigated area (North-West to South-East). Along this direction the soil infiltration capacity seems to increase, from

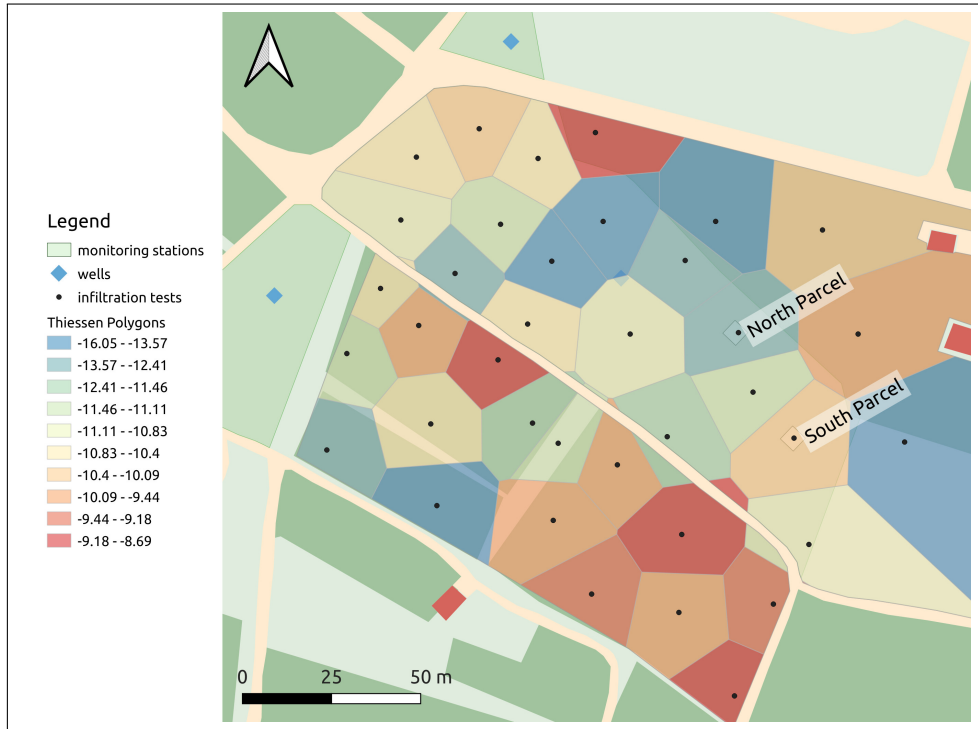


Figure 3.27: Spatial interpolation of the  $\log K_{mod}$  values at the Settolo site using the Thiessen Polygons method (TP).

West to East, from  $K_{mod} = 2E - 05$  m/s ( $\log K_{mod} = -10.8$ ) to  $K_{mod} = 1.5E - 04$  m/s ( $\log K_{mod} = -8.8$ ). For the Colnù site, the spatial characterization consisted of two interpolations, using, as reported in Section 2.3.2.1, the Triangulation-based Natural Neighbor Interpolation and the Thiessen Polygons methods combined together (NNI-TP), and the Inverse Distance Weighting (IDW) method. By comparing the obtained  $\log K_{mod}$  interpolations reported in Figure 3.28, the one developed using NNI-TP (left-side of the figure) seems to provide a better spatial estimation, in the case of a limited number of data, compared to the IDW method (right-side of the figure). The former highlights with colors blue and red two distinct macro-areas of low- $\log K$  and high- $\log K$  respectively. By using this method, the maximum and the minimum  $K_{mod}$  values -  $K_{mod} = 1.5E - 04$  m/s,  $\log K_{mod} = -8.8$  and  $K_{mod} = 3E - 07$  m/s,  $\log K_{mod} = -15$  - were assigned to the middle-west area of the *south vineyard* and to the north area

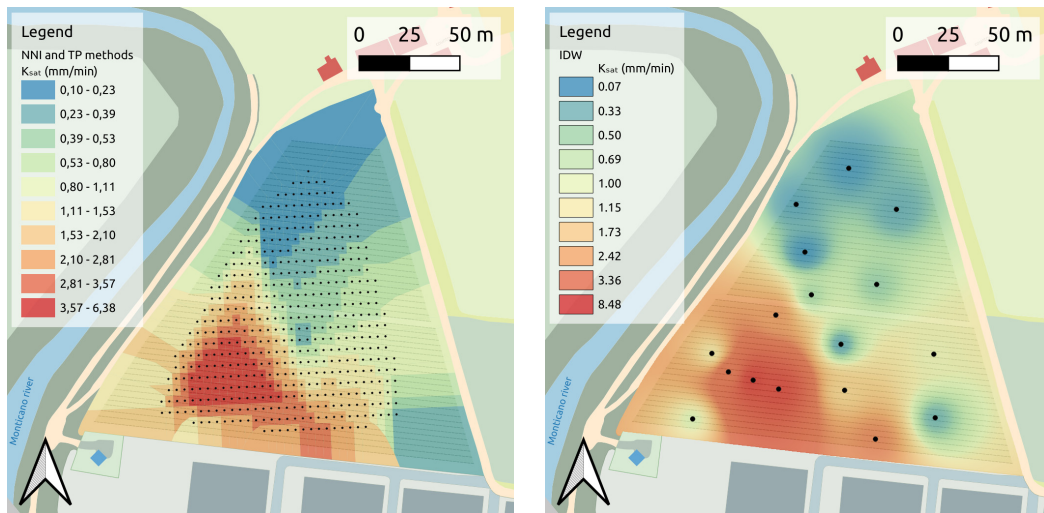


Figure 3.28: Spatial interpolations of the modeled hydraulic conductivity,  $K_{mod}$ , developed for the Colnù site.

of the *north vineyard*, highlighting a decreasing trend of  $K$  along the South-West to North-East direction within the experimental site. On the other hand, the interpolation developed with the IDW method did not highlight a clear trend of the investigated property. The obtained result gave a less reliable "bubble-effect" estimation of  $K$  around the known values. This is probably due to the limited number of available points and to the characteristics of the method, which tends to estimate the hydraulic conductivity in far positions from the known values with  $\log K_{mod}$  values that are close to the mean  $\log K_{mod}$  of the entire area.

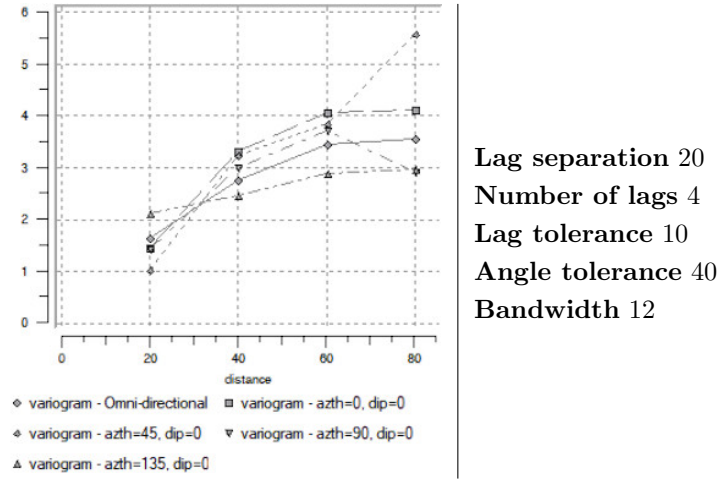
**Structural analyses for the investigated area at the Settolo site** The information achieved by the exploratory data analysis were used for the development, using the dedicated SGeMS tool, of the experimental variogram of the ensemble of spatially defined  $\log K_{mod}$  values. This, being us aware of the low number of points available for this type of analysis (e.g., Journel and Huijbregts 1976 and Vieira et al. 1981).

Prior to the structural analysis, the coordinates of the experimental points were pre-processed. The surveys positions at the Settolo site lay in domain that develops itself

along the northwest-southeast diagonal. With this arrangement of the data, things get difficult when some geostatistical methodologies, such as point estimation methods like Kriging (De Marsily, 1986), are intended to be used. This because they perform estimations based on a research grid prior defined. In the SGeMS code this grid can be only be defined following Cartesian directions leaving in the case of ensemble of points distributed along a diagonal direction - as for the hydraulic conductivity values observed at the Settolo site - large portions of empty space (without points). In this scenario, Kriging requires a large search area, resulting in an oversampling in the areas containing the data and errors in the development of the estimation. For these reasons a new Cartesian reference system was set-up by roto-translation of the points coordinates. The origin of the new reference system lays just outside of the investigated area and the axes are rotated clockwise by an angle of 35.5 degrees, as reported in Figure 3.29.

The parameters used for the whole area of the Settolo site, comprising both the well area and the south vineyards area, are reported in Table 3.9 along with the result achieved using the SGeMS code. Considering the spatial characterization obtained with the Thiessen Polygons and discussed above, the lag separation and the number of lags by which the code solves the equation 2.12, were properly adjusted to obtain the spatial analysis of all the domain. The plot on the left side of the table, shows the increments of variance computed at increasing lag separation by steps of 20 meters (see section 2.3.2.1). The variograms computed along four different angles, plotted in the graph, show a very small nugget effect while the asymptotic value of variance is reached for distances larger than 60 meters. The results of the variograms computation along different angles are reported in Table 3.10 in separated plots. The scatter plots show the increments of the variance (reported as red crosses) along the different computation directions. The resulting trends, even if only described by four intervals, hinted a non-isotropic distribution of the correlated values with higher correlation along the azimuth angle  $45^\circ$  and lower correlation along  $135^\circ$ . A 25% difference observed between the

Table 3.9: Experimental Variograms computed along  $0^\circ$ ,  $45^\circ$ ,  $90^\circ$ ,  $135^\circ$  directions and the parameters values used for the computations.



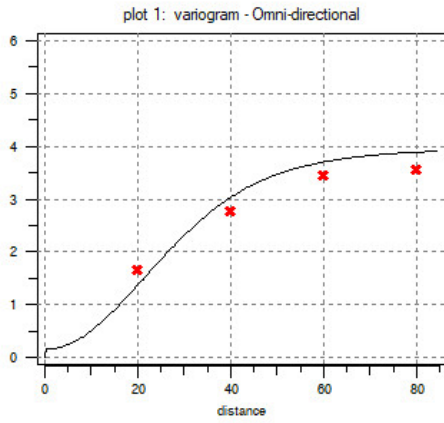
maximum variance reached along the same angles, highlighted the presence of a zonal anisotropy (Goovaerts et al., 1997). In the fitting of the variogram model, performed using SGeMS, this was accounted by calibrating a two-structures Gaussian model. The compact formula of the model is reported in the same table while the fitting results are reported in the experimental variogram plots with black lines.

Considering the low density of the experimental variogram points, the Gaussian model was chosen only because it well fitted the small nugget effected observed in the graph of Table 3.9 as well as the large increment of variance observed in plots 2, 3, and 4 (Table 3.10). A first attempt to evaluate the magnitude of the soil infiltration capacity-spatial correlation length  $l$  inside the site was also carried out. This by means of the equation:

$$l = \frac{1}{\sigma^2} \int_0^{\infty} (\sigma^2 - \gamma(h)) dh \quad (3.1)$$

where  $\sigma^2$  is the ensemble variance,  $\gamma(h)$  is the variogram, and  $h$  is the lag-distance in the horizontal plain. The estimation of the correlation length, i.e. the distance inside which the variable is perfectly correlated, resulted, as a preliminary indication, lower than 25 meters.

Table 3.10: Experimental variogram and variogram model for the Settolo site (entire investigated area).

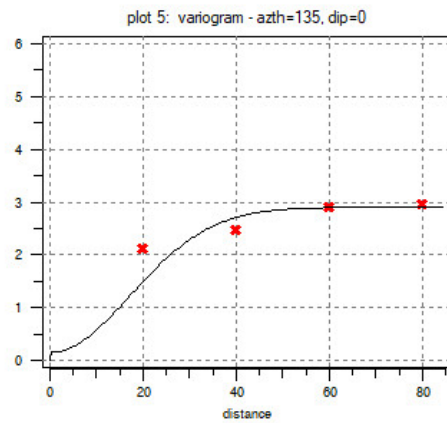
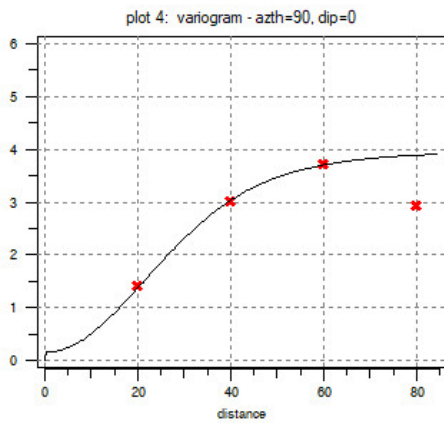
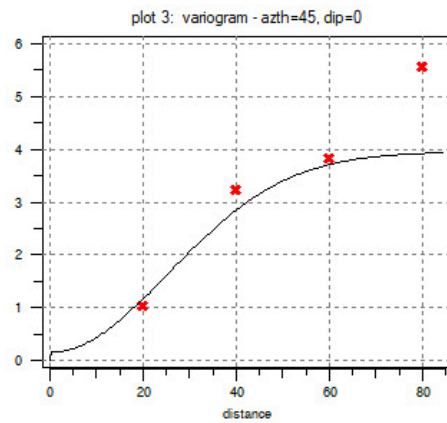
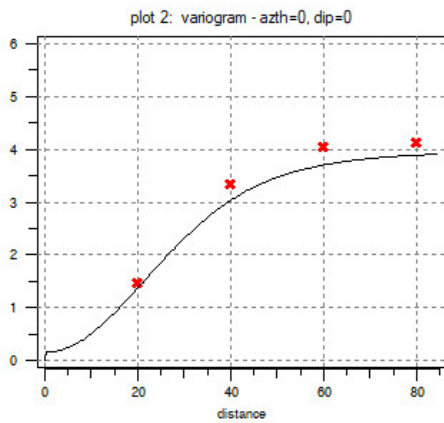


**Variogram Model:**  

$$\gamma(\vec{h}) = 0.15 + 2.75 \cdot \text{Gau}(\vec{h}) + 1.05 \cdot \text{Gau}(\vec{h})$$

**Str 1.**  
 Ranges, Max = 64.0, Min = 42.4,  
 Angle 45°

**Str 2.**  
 Ranges, Max = 8640, Min = 58,  
 Angle 135°



### 3.2.3.1 Estimation results

The analysis of the spatial correlation for the soil-infiltration capacity values observed within the Settolo site, led to the development of a further spatial interpolation of the sparse data testing the geostatistical estimation algorithm Ordinary Kriging. As underlined at the beginning of the section, the results has to be considered preliminary. In other words, the available data were used to test the procedure of geostatistical analysis and validation of the kriging estimation algorithm based on the Gaussian variogram model.

**Estimation considering the entire area** Figure 3.29 shows the result obtained by applying, in a first attempt, the Ordinary Kriging algorithm to the entire area interested by the infiltration tests, without distinction on the land use of the different site plots. The map, showing in orange the areas affected by a higher infiltration capacity and in blue-green the ones characterized by a lower permeability, is accompanied with the scatter-plot showing the result of the cross-validation. This provides a measure of the uncertainty of both variogram model and kriging estimation. As expected, the resulting correlation coefficient appears low ( $R = 0.39$ ) indicating that the algorithm heavily relies on hard data (i.e. the known values of the regional variable). In the cases in which one of them was missing, the algorithm not always estimated the corrected  $\log K$  value in the same position. That results in a low reliability for the other values estimated in not surveyed areas. By discarding the cross-validation results for the outlier test 19 (south-outside of the well area) and the north-east vineyard tests 3, 9, 12, and 16, developed at the boundary of the area, the correlation coefficient increases, reaching a mild correlation ( $R' = 0.62$ ). Also in this case, this coefficient variation can be addressed to the limited number of tests (4) developed in the northeastern vineyard, compared to the 32 ones carried out in the remaining investigated area.

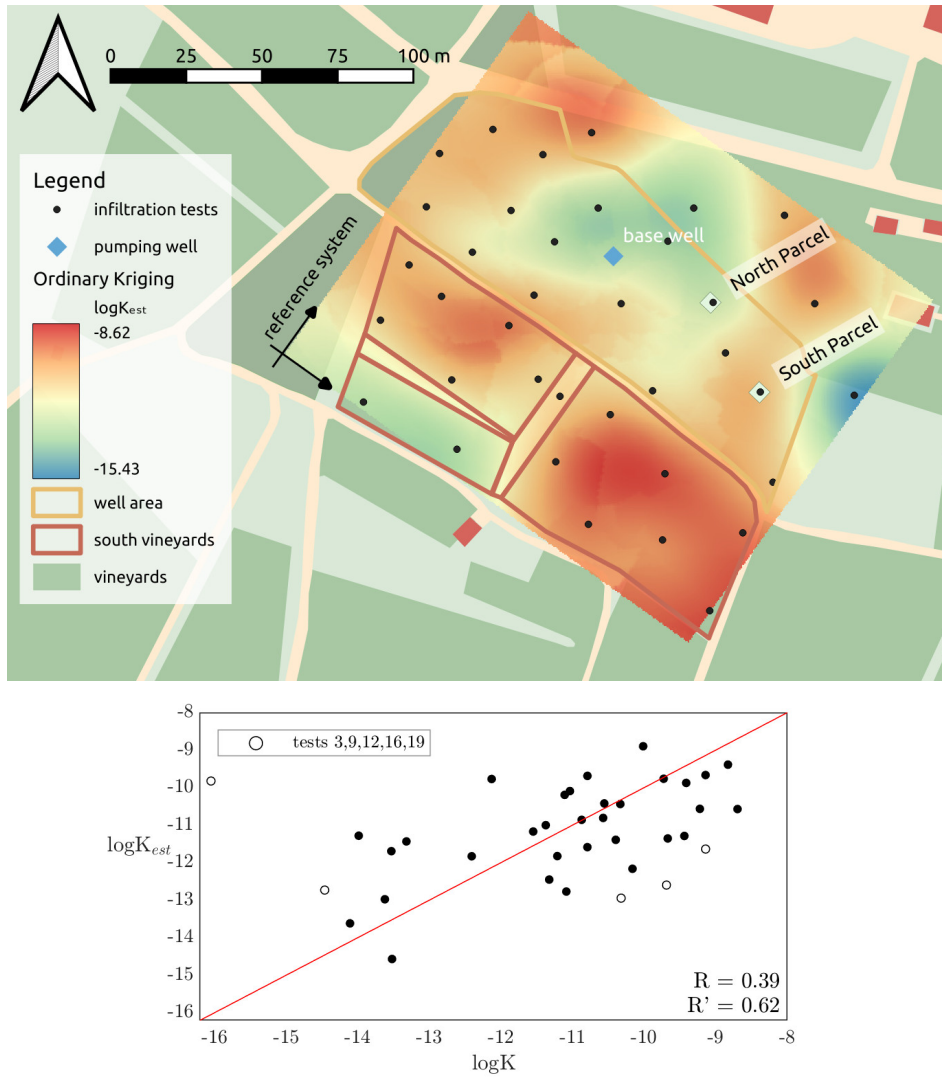


Figure 3.29: Spatial interpolation by Ordinary Kriging of the  $\log K_{mod}$  values obtained at the Settolo site and Cross-validation result.



Table 3.11: Parameters for the definition of the experimental variograms based on the values of  $\log K_{mod}$  obtained in the well area and in the south vineyards area.

area	Lag separation	Number of lags	Lag tolerance	Angle tolerance	Bandwidth
well area	19	4	9.5	45	12
south vineyards	21	3	9	40	11

**Well area and South vineyards area** Just as an exercise, the geostatistical analysis developed considering the entire sample of observations, was repeated by dividing the sample in two ensembles of measures, collected inside the well area and inside the south vineyards respectively. This, to test the geostatistical analysis in areas characterized by the same use: non-agricultural, in the former case, and agricultural, in the latter case. Consequently, the estimation grid was subdivided in two minor grids, framing each one of them the reciprocal area. By using the parameters listed in Table 3.11, the structural analyses were repeated for the two sub-groups of measurement points. The estimation results, developed by using the Ordinary Kriging, are showed in Figure 3.30. What catches the eye, quite rapidly, is now the net separation between the two areas. By dividing the areas, despite the number of available points, the algorithm seems to better estimate the high infiltration capacities observed south respect to the road dividing the two areas. Before, in the case of a unique estimation for the entire area, these values were underestimated by the smoothing character of the Ordinary Kriging, misled by the lower  $\log K_{mod}$  values localized in the well area. This estimation improvement for the area occupied by the vineyards can be red from the correlation coefficient in the plot linked to the estimation map. Slightly lower the correlation coefficient achieved in the cross-validation developed for the well area. This could have been caused by the overestimation, by the Ordinary Kriging, of some low values of soil-infiltration capacity observed within the well area. However, being the number of points far from sufficient for a proper geostatistical analysis, as showed in Tables 3.12 and 3.13, and Figure 3.31, the structural analyses and the approximately fitted variogram models, cannot be considered satisfactory. Accordingly, these results must be considered only as preliminary.

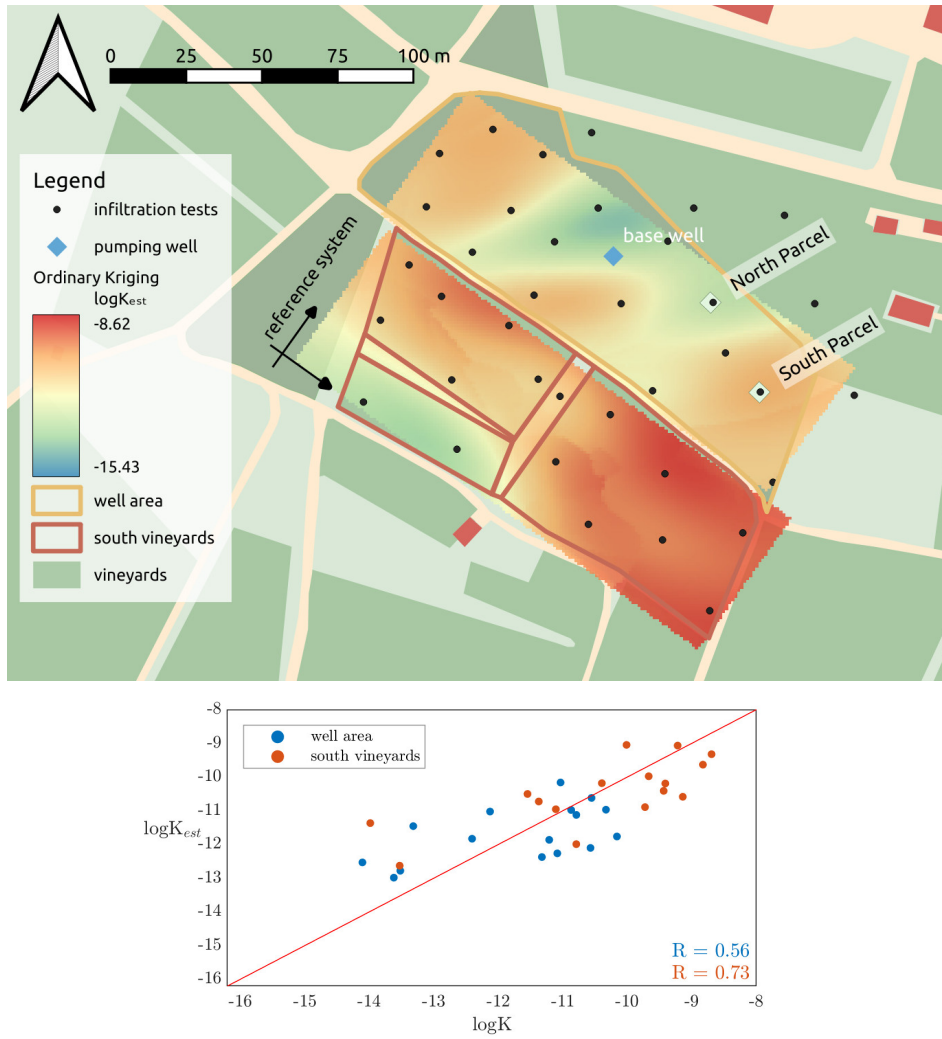
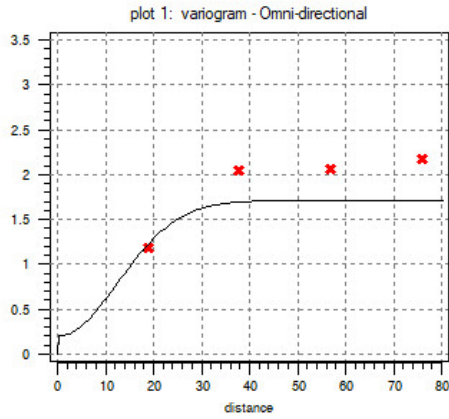


Figure 3.30: Spatial interpolation by Ordinary Kriging of the  $\log K_{mod}$  values subdivided in the two macro-areas of the Settolo site and Cross-validation result.

Table 3.12: Experimental variogram and variogram model for the well area of the Settolo site.



**Variogram Model:**  
 $\gamma(\vec{h}) = 0.2 + 1.51 \cdot \text{Gau}(\vec{h})$   
**One-structure model**  
 Ranges, Max = 57.0, Min = 23.6,  
 Angle 45°

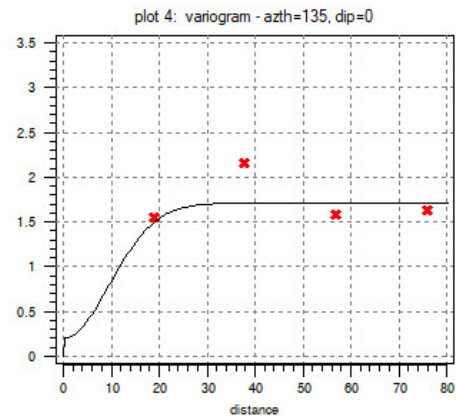
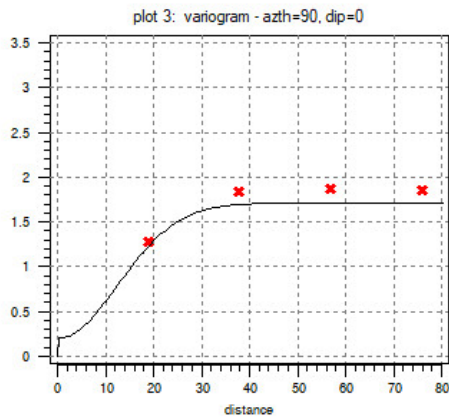
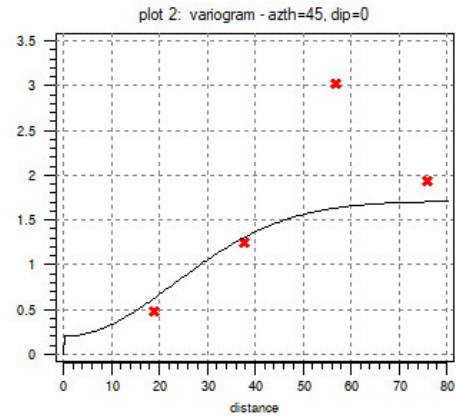
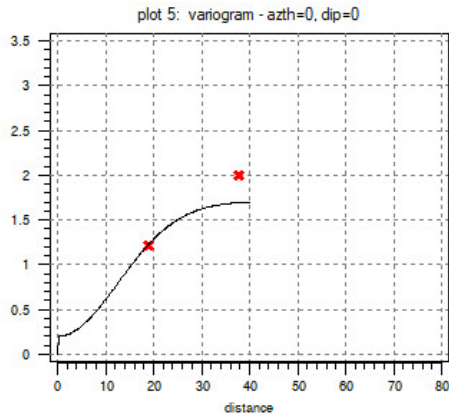
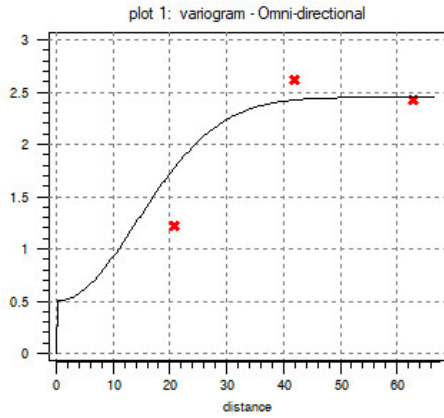
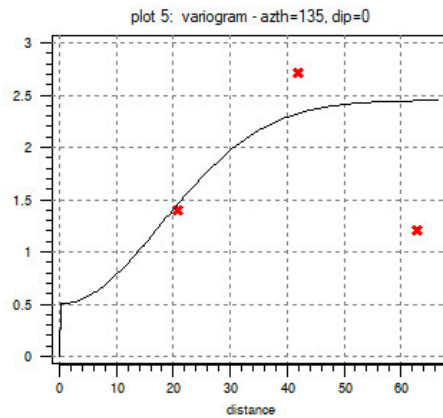
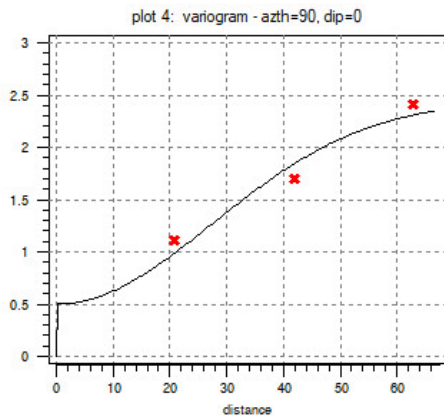
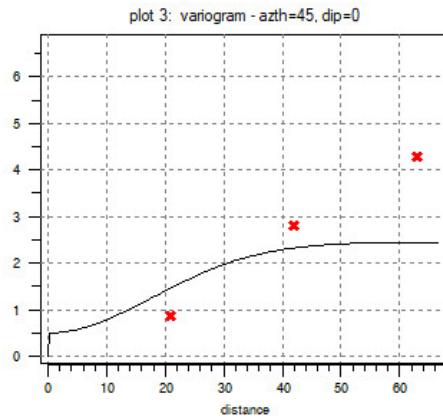
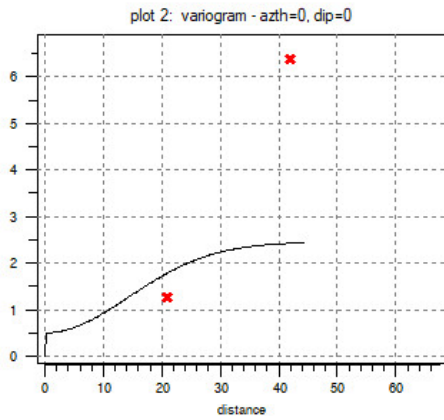


Table 3.13: Experimental variogram and variogram model for the south vineyards area of the Settolo site.



**Variogram Model:**  
 $\gamma(\vec{h}) = 0.5 + 1.95 \cdot \text{Gau}(\vec{h})$   
**One-structure model**  
 Ranges, Max = 67.2, Min = 35.0,  
 Angle 90°



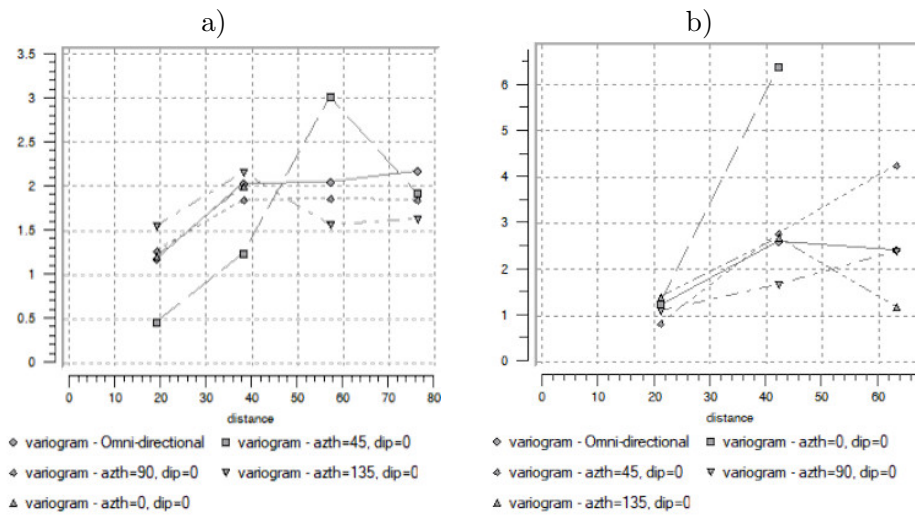


Figure 3.31: Experimental variograms computed for the measure points inside a) the well area b) the south vineyards area

### 3.2.4 Results of the groundwater quality monitoring activity

In the saturated part of the phreatic aquifer of the Settolo site, the groundwater quality control developed using the multi-parametric probe HL4 Hydrolab has not highlighted until now the occurrence of any pollution phenomenon. A total of 17090 measures, and counting, of the the standard water quality indicators, conductivity, temperature, and pH, the index parameters oxidation-reduction potential, ORP, ammonium ion,  $\text{NH}_4^+$  and nitrate,  $\text{NO}_3$ , were collected with an averaged frequency of 30 minutes in a time-period of around 680 days (excluding the time periods needed for the maintenance and to perform the periodic sensors calibrations), from February the 28<sup>th</sup>, 2020 until now. Except for sporadic cases as the one reported as example in Figure 3.32, in which the sensors or the probes detect low traces of the monitored parameters, no deviations from the admissible quality values required for groundwater were observed. Figure 3.33 show the trend of the parameters measured along the depth of the installation borehole in a survey performed in November 11<sup>th</sup>.

The survey highlighted that the parameters (with the exception of the conductivity only) are affected by minimum variations up the depth of 30 meters, that is the working limit for the HL4 probe.

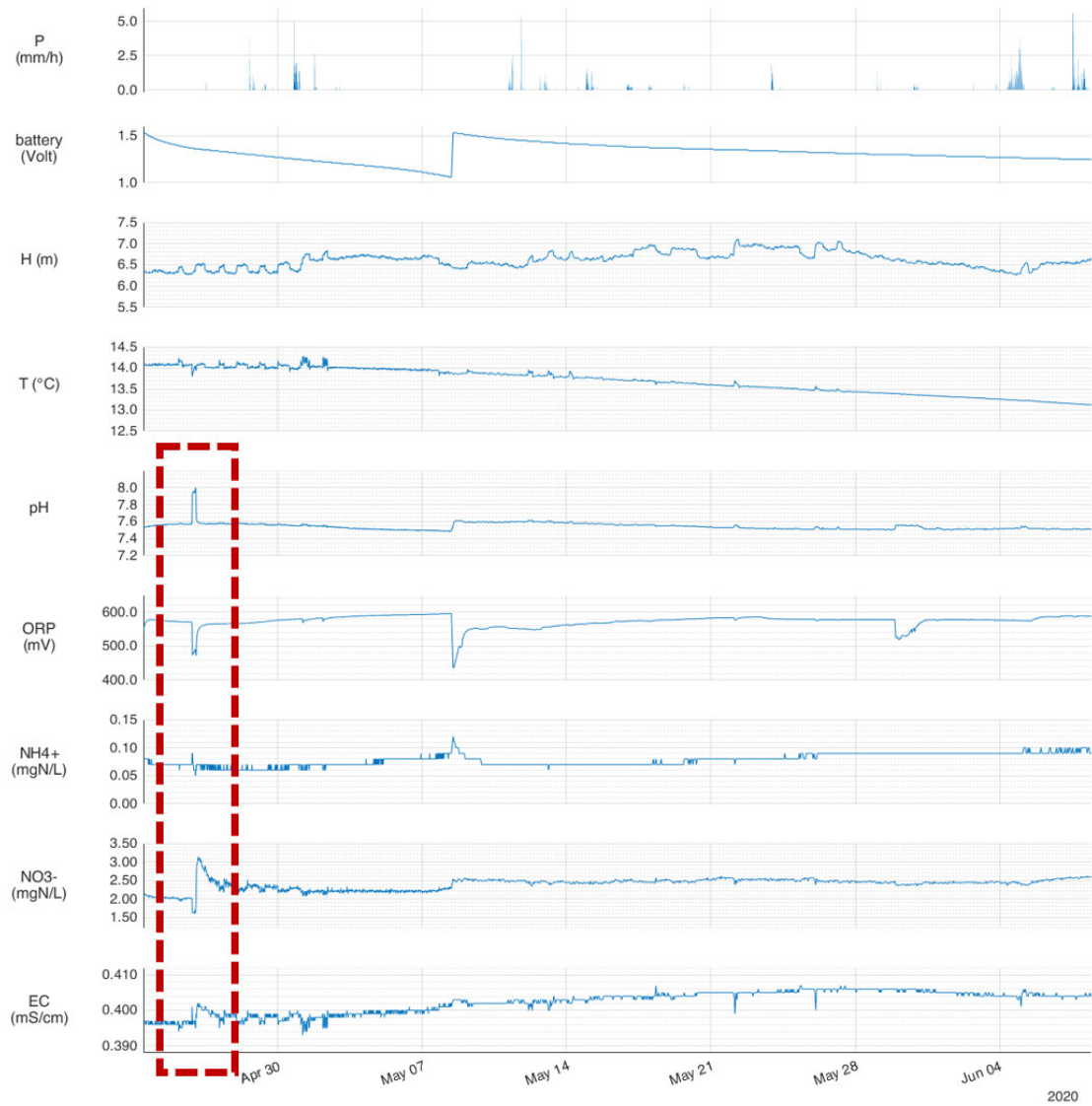


Figure 3.32: Example of groundwater quality monitoring developed with the HL4 multi-parameter.

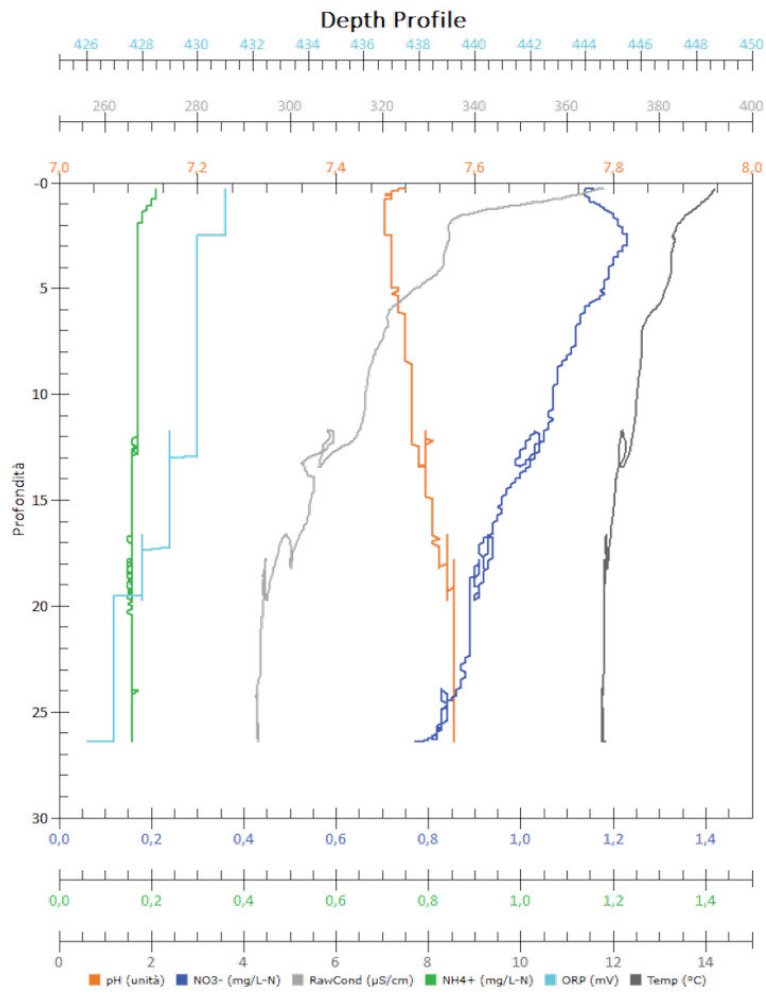


Figure 3.33: Example of depth profile measurement developed by dipping the HL4 multi-parameter probe in the borehole of installation.



### 3.2.5 Final remarks

- Higher concentration values of the soluble phosphorus were found on average in the topsoil samples collected within the vineyards increasing the risk of GLP leachability, being the phosphorous negatively correlated to the value of the herbicide soil-adsorption coefficient
- The laboratory analysis on the soil samples showed a general low concentration of soil organic matter in the topsoil of the investigated area. the backup measure VS was always quantified but it did not highlight any significant differences in concentration between the vineyards and well buffer area
- The infiltration tests developed in different positions within the investigated areas showed a large spatial heterogeneity of the soil infiltration capacity and permitted the identification of sub-areas within the experimental sites characterized by similar infiltration behaviors.
- The numerical analysis of the infiltration tests results developed using the Green-Ampt model to estimate the soil hydraulic conductivity values, worked very well for the tests developed in both sites.
- A poor fitting of the model was observed only in three cases due to a different behavior of the infiltration curve in the first part of the test. This was probably caused by the presence of preferential flow-paths in the agricultural soil that cannot be simulated with the simplified Green-Ampt model.
- In the case of the two experimental sites, the spatial characterization of the soil infiltration capacity by means of Thiessen Polygons (TP) method and Natural Neighbor Interpolation (NNI) method, provided important hints on the correlation structures present within the experimental sites.

- A preliminary structural analysis, developed at the Settolo site by computing the experimental variogram, evidenced a correlation length for the  $\log K_{mod}$  values of about 25 meters
- The geostatistical estimation of the  $\log K_{mod}$  spatial distribution within the Settolo site using the algorithm Ordinary Kriging, achieved better results by developing the analysis in separated wine-growing areas and not-cultivated areas
- At this time, the groundwater monitoring activity carried out in the saturated part of the phreatic aquifer of the Settolo site, has not highlighted any pollution phenomenon

### 3.3 Province-scale results

In the following sections, the results of the geospatial analysis developed on the basis of the PPPs sales data and on the land-use geospatial data, are presented maintaining the order presented in the dedicated Materials and Method section (§ 2.3.3).

#### 3.3.1 PPPs distribution analysis

Figure 3.34 report the results of the distribution analysis of vine-specific PPPs in the province of Treviso in graphical form. In the map of the study area, each municipal territory was colored according to the units of PPPs sold, highlighting a higher concentration of the registered sales in the northeastern municipalities. By reporting in the map also the extension of the territories interested by the vine cultivation (grey color), it is evident that the PPPs sales in the Treviso province were principally related to products suitable for the wine-making practices. This hypothesis is confirmed by the information showed in Figures 3.34a and 3.34b. The first one shows that the vast majority of sold PPPs (almost 280 in 2019) were fungicides. The second, reporting on a logarithmic bar-plot the active substances contained in the first 13 best-selling products - in this order: Sulfur, Metiram, neutralized copper sulphate lime - Bordeaux Mixture, Cimoxanil, Ametocradin, Acetamipirid, Cyazofamid, Copper hydroxide, Copper oxychloride, Dimetomorph, Potassium phosphonate, Glyphosate, Phosethyl Aluminum - , also shows that the majority are fungicides, with the exceptions of glyphosate, which as already mentioned is a herbicide, and acetamipirid, which is an insecticide. Sulfur is the best-selling substance, followed by Metiram, and both are fungicides used in the vine integrated defense. Moreover, the first 8 sales all refer to active substances distributed on leaf or plant, a treatment commonly developed in vineyards. The only one used for weeding, and therefore applied directly on the ground, is glyphosate. This is in line with the real context because the main diseases affecting the vineyard are bacterial or

### 3.3. Province-scale results

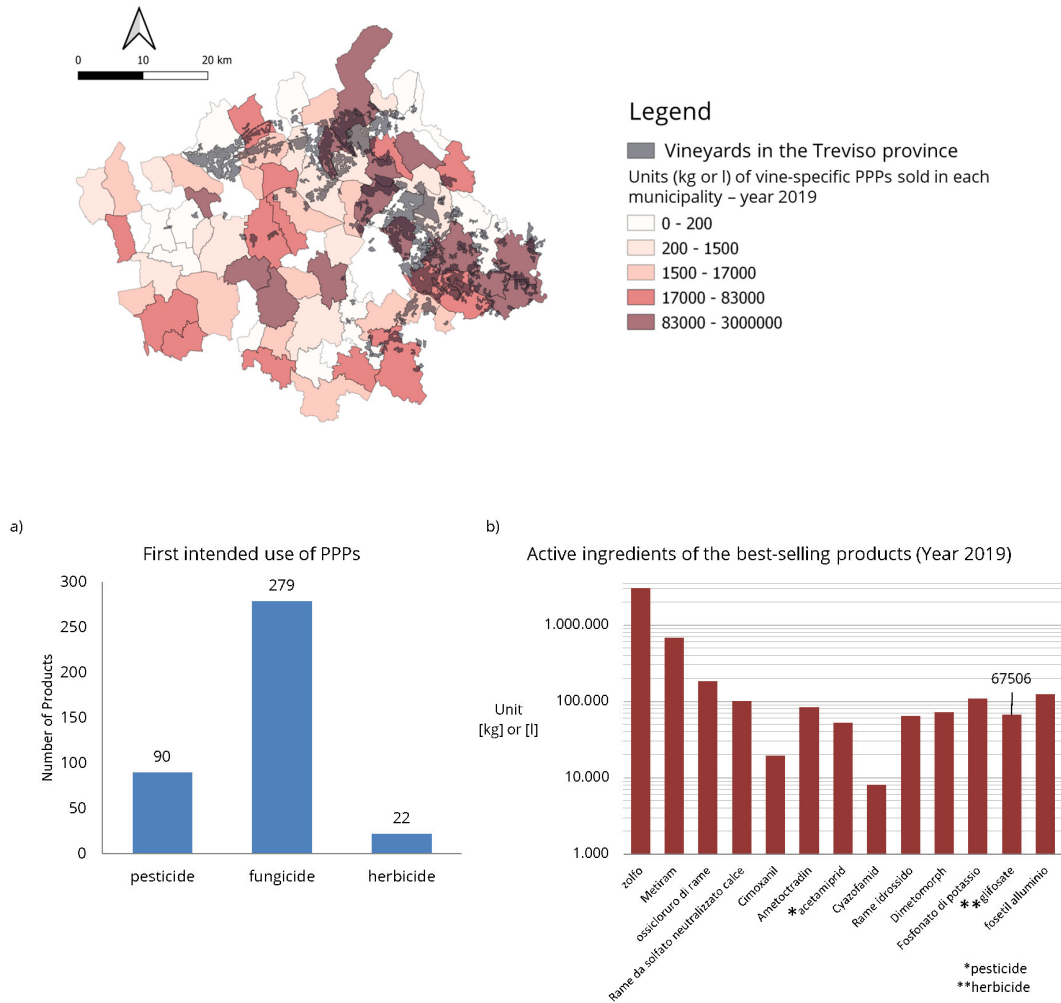


Figure 3.34: Map of the PPPs sales spatial distribution and analysis of the class of use (bar-graphs *a* and *b*).

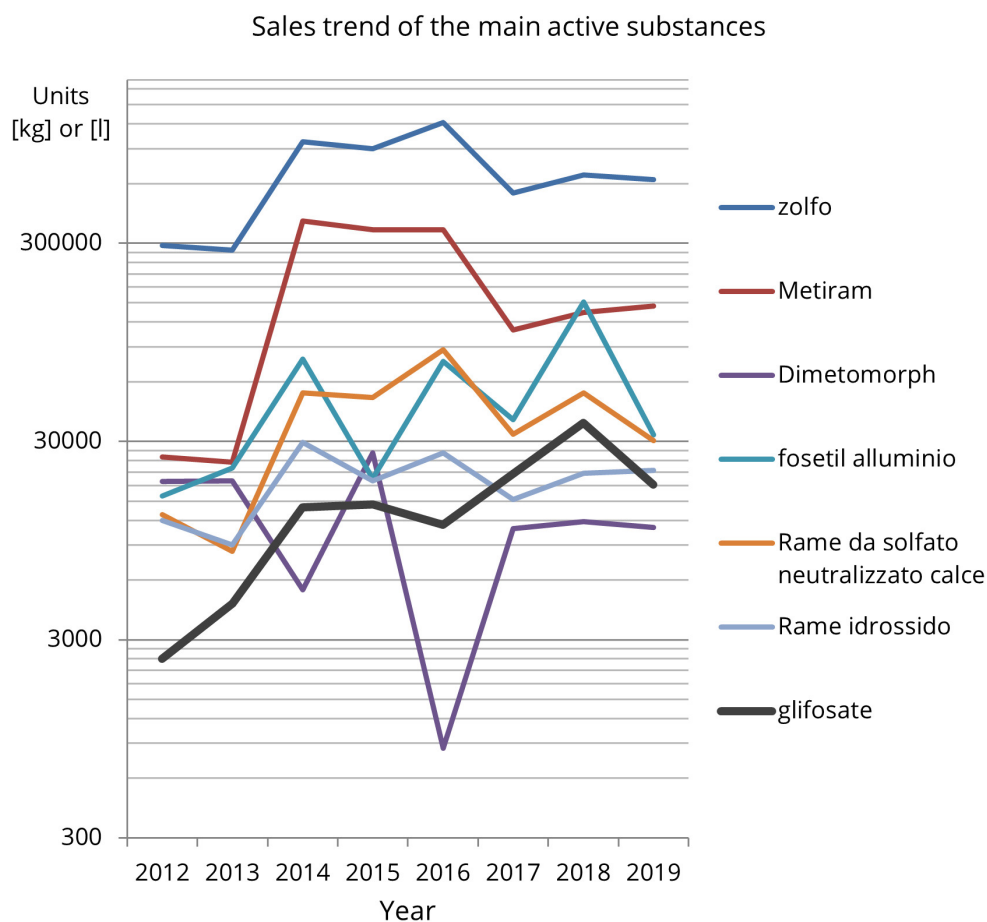


Figure 3.35: Sale trends for the seven best-selling products.

fungal. Sales data collected in the time period 2012-2019 permitted to analyze the PPPs trend over time, as reported in Figure 3.35 showing in a logarithmic graph the history of sales from 2012 of the 2019 top-seven active substances. In the study area, sulfur is also in this case the active substance most sold in all the observed years and appears to be slightly on the rise reaching alone the 62% of the total vine-specific PPPs sales in 2019. Glyphosate shows the higher increment in the sales, increasing more than 10 times between 2012 and 2019. The widely used herbicide, labeled as "GHS09: Dangerous for the environment" in the CLP hazard classification, was banned in the DOCG territories in 2019 but its use is still allowed, at this time, in Europe until the end of 2022.

### 3.3. Province-scale results

Table 3.14: Features and Hazard classification for the best-selling products in the wine-growing areas of the Treviso province

Product information				Active substances in the product		Hazard analysis					
Reg. id	Name of the commercial product	Suitable for biologic agriculture	Type First intended use	Principal active substance	%	GHS05	GHS06	GHS07	GHS08	GHS09	Hazard class
13	THIOPRON	v	fungicide	zolfo	57.3			v			3
206	ALBENE	v	insecticide	olio minerale	78.1					v	4
1155	CHEMOL	v	insecticide	olio minerale paraffinico	80						1
1156	CHEMOL	v	insecticide	olio minerale paraffinico	80						1
1583	MICROTHIOL DISPERS	v	fungicide	zolfo	80						1
1714	KERB 80 EDF	x	diserbante	propizamide	80				v	v	5
1850	IDRORAME FLOW	x	fungicide	Rame da solfato tribasico	15.2					v	4
1903	SULFURENE	v	fungicide	zolfo	35			v			3
2923	TIOVIT JET	v	fungicide	zolfo	80						2
3082	OLEOTER ESTATE	v	insecticide	olio minerale paraffinico	85	v			v		5
3102	OLEOTER	v	insecticide	olio minerale	80						1
3503	AGRUMIN	v	diserbante	olio minerale	5.88				v		5
3640	CUPROSTAR	v	fungicide	Rame idrossido	12					v	4
4012	RELDAN 22	x	insecticide	clorpirifos-metile	21.4			v	v	v	5
4710	ALIETTE	x	fungicide	fosetil alluminio	80			v			3
5152	TIOSPOR WG	v	insecticide	zolfo	80			v			3
6704	TIOLENE 80 WG	v	fungicide	zolfo	80			v			3
6873	IDRORAME 193	v	fungicide	Rame da solfato tribasico	15.2					v	4
6945	TOPAS 10 EC	x	fungicide	Penconazolo	10.1			v	v	v	5

#### 3.3.2 Hazard analysis results for the vine-specific PPPs

Table 3.14 reports an excerpt of the hazard analysis developed according to the active-substances CLP hazard classification (see section 2.3.3). In the Table, the hazard analysis for the best-selling products in the wine-growing areas of the Treviso province is accompanied with information on the percentage of the principal active substance contained and the use for which the product was developed (class of use). According to this latter parameter, 71% of the products contain fungicides active substances, 23% are made with insecticides or acaricides active substances, while the remaining, only 6%, contain herbicides active substances. The lower percentage of herbicides compared to the others depends on the directives established by the Winemaking Protocol, in which the use of these PPPs is recommended in few cases, preferring in most cases the mechanical weeding. After the assignment of the hazards class as shown in the table above, the Corine Land Cover 2018 geospatial data, giving the extension of the land destined to

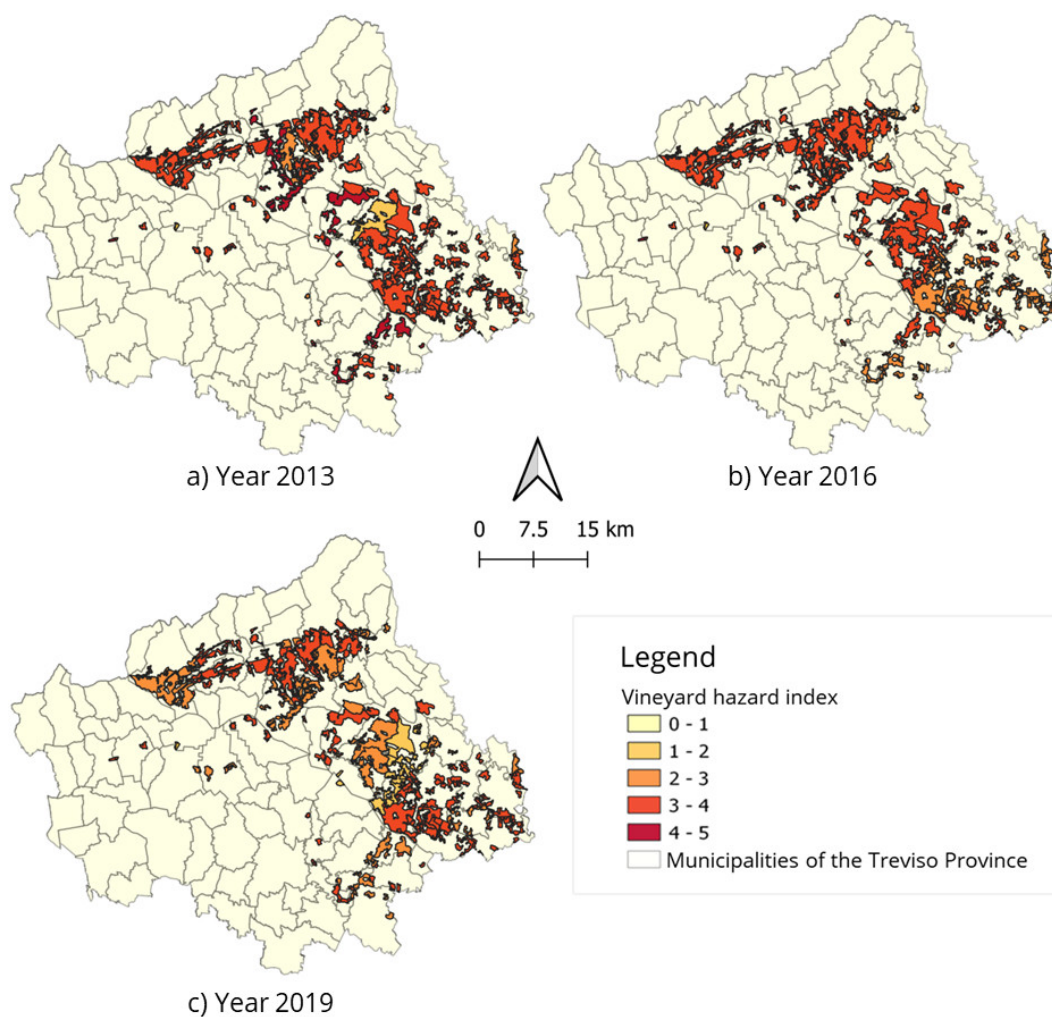


Figure 3.36: Hazard maps developed for the wine-growing areas of the Treviso Province.

vineyards, was used to develop the hazard maps reported in Figure 3.36 for the years 2013, 2016 and 2019. The maps indicate the hazard of the wine-growing areas based on the amount and the hazard class of the vine-specific PPPs applied. The hazard level is indicated with colors ranging from yellow, for null or low hazard areas, to dark red, for very-high hazard areas. According to the available data and the hazard classification adopted for the PPPs, in 2016 the majority of wine-growing areas were characterized by a high hazard level while in 2019 areas with medium and high hazard levels were equally distributed. In 2013 the overall hazard level of the vineyards, was in the middle of the

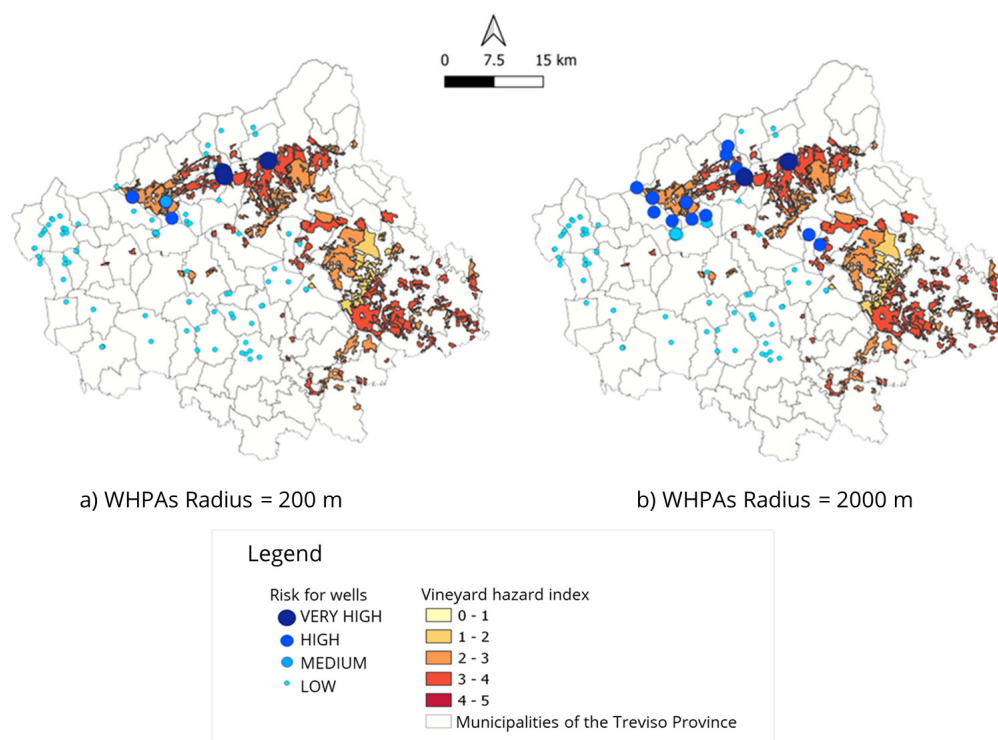


Figure 3.37: Vulnerability map for the wells of the Treviso Province.

ones observed in years 2016 and 2019. However, since the complete national regulation on the PPPs sales registration was available to the regions in 2014 only (see section 1.2), missing PPPs sales data in years 2012 and 2013, limit the reliability of the hazard map developed for this latter. Considering the sales data collected along the entire period 2012-2019, although the quantity of PPPs sold in the province is increasing, the total hazard, on average, is decreasing. This result can be linked to the gradual changeover of many wine-makers to the more profitable and advertised biological market. From 2013 to 2016, the biological cultivated hectares increased from 11741 to 18549 hectares in the Veneto region (source <http://dati.istat.it/index.aspx?queryid=31926>).



### 3.3.3 Vulnerability of WHPAs

The geographical information obtained from the wine-growing hazard maps were used to develop a vulnerability map for the georeferenced wells exploiting the phreatic aquifers of the study area for drinking water supply. The vulnerability was defined according to the level of superimposition between the extension of the vineyards, characterized by the hazard indexes, and the extension of the wellhead protection areas, defined by geometrical criterion. Figure 3.37a shows that already by considering the WHPAs most often inadequate, i.e. defined by a circular area around the well having a radius of 200 meters, in the developed geospatial analysis 4 wells have a *very high vulnerability*, 6 wells have a *high vulnerability*, 1 well has a *medium vulnerability*, and all of them are located in the DOCG area. This last result supports quite well the problem statement presented at the beginning of this thesis work, being the DOCG area for the Prosecco production an example of highly exploited agricultural territory that, however, is also strategic for the extraction of drinking water for human consumption. In fact, the remaining wells distributed within the Treviso province present a *low vulnerability*. In absence of more detailed data on the real extension of the WHPAs within the study area, a second vulnerability map was developed by precautionary assuming a radius of the geometrical criterion equal to 2 km. Even if this dimension could seem overestimated, the example of the Settolo site WHPA, stretched along a distance larger than 1 km considering an isochrone of 60 days as boundary, support the assumption that the WHPAs can be much more extended than 200 meters. In this scenario, developed also considering the numerous PPPs loss phenomena that could happen during the plants treatments (e.g. wind drift), 23 wells that before were classified with a low vulnerability, present now a medium or high vulnerability (Figure 3.37b). By properly define the WHPAs - approximately in between the two considered scenarios - the vulnerability map can provide a clear picture of the PPPs-specific actions required for each well to minimize the risk for drinking water supplied for human consumption.

### 3.3.4 Final remarks

- PPPs sales in the Treviso province are mainly related to products suitable for wine-growing practices
- Most vine-specific PPPs are fungicide and the sale of these products is increasing. This result is in agreement with the major adversities that affect the vine, which are fungal and bacterial
- Based on the hazard of the vine-specific PPPs, in 2019 medium hazard and high hazard wine-growing areas were equally distributed
- Although the quantity of sold PPPs is increasing the sales-weighted hazard index of the wine-growing areas is decreasing
- In the scenario of WHPAs defined by the 200 m radius geometrical criterion, 4 wells have a *very high vulnerability*, 6 wells have a *high vulnerability*, 1 well has a *medium vulnerability*, and all of them are located in the DOCG area.
- In the precautionary scenario of WHPAs defined by the 2 km radius geometrical criterion, 4 wells have a *very high vulnerability*, 22 wells have a *high vulnerability*, 8 well has a *medium vulnerability*

## Chapter 4

# Conclusions

In this work the impact of the agronomic activities on the wellhead protection areas has been studied at three different spatial scales connected each-other, i) point-wise scale, ii) field scale, and iii) provincial scale. At the point-wise scale the possible interaction between agronomic activities and WHPA was studied by analyzing the leaching capability in the vadose zone of the active substance glyphosate (GLP). This to understand the mechanisms governing the evolution of the plant protection products from the ground surface, where they may deposit, toward the saturated part of the phreatic aquifers. The experimental evidence achieved in two experimental sites, Settolo and Colnù, located in the Treviso province, showed that GLP, subjected to hydrological forcing only, is mostly adsorbed to the topsoil, which acts like a barrier to infiltration. However, in the same experimental campaign, high concentrations of the herbicide were found at the depth of 0.70 m after the more intense rainfall events. A one-dimensional model was used to analyze and predict this GLP evolution, assuming the rainwater infiltration as the main driving mechanism of the herbicide infiltration process. The hydraulic parameters of the soil, governing the infiltration process, were calibrated based on the temporal trends of the soil-water content measured in the same site-parcels (two for each site) treated with the herbicide. The concentration values of a non-reactive tracer,

---

potassium bromide, applied to the soil in solution with the herbicide, were used to test the infiltration-advection coupling capability of the model. In the developed simulations related to the rainwater infiltration process and the non-reactive transport of the tracer, observed soil water content and potassium bromide concentrations were well simulated by the calibrated model up to a depth of 0.30 m BGL. Below this depth, discrepancies between observed and modelled values pointed out the limits of the one-dimensional modelling suggesting the presence of preferential flow-pathways due to soil heterogeneity and flow movements different from the vertical one. In the numerical simulations of the herbicide evolution, the parcel specific values of the Freundlich partition coefficient were used to model the adsorption process affecting the mobility of the herbicide. This because not negligible differences were observed between the coefficient values between the two experimental sites and between parcels, as in the case of Colnù, belonging to the same site. However, The lack of consistence of numerous GLP concentration values with the advection-dispersion model predictions provided by the one-dimensional model, hints a different mechanism of transport. The herbicide is adsorbed to the finest soil particles that, displaced by the most intense rainfall events, are transported through preferential pathways. Only a small fraction is dissolved in the infiltrating rainwater. For these reasons, the achieved results at the point-wise scale, suggest the needing to develop a more complex interpretative model leaving the description obtained with one-dimensional advection-reaction. At the field scale the research activity was addressed to the analysis of the spatial heterogeneity of the soil properties affecting the glyphosate mobility. This was manifest by different GLP behaviors observed in parcels belonging to the same experimental site. At this purpose, three soil properties were selected, based on i) the correlation analysis developed between the parcel-specific GLP adsorption coefficients and the soil properties observed at the same parcel by laboratory analysis on soil samples collected during the first experimental campaign, and ii) the experimental evidence on the infiltration process acquired during the activity developed at the

point-wise scale. The selected properties were the soluble phosphorus, the total organic carbon, and the soil-infiltration capacity, being still recognized the water infiltration process as driving mechanism of the herbicide infiltration after the first point-wise analysis. A total of 54 surveys were developed at the two experimental sites, consisted of 54 infiltration tests and 27 soil samplings. Among the three soil properties investigated, soil infiltration capacity and soluble phosphorous show a large spatial heterogeneity also within plots destined to the same land use. Higher concentration values of the soluble phosphorus were found on average in the topsoil samples collected within the vineyards, thus increasing the risk of GLP leachability, being the phosphorous negatively correlated to the value of the herbicide adsorption coefficient. The distributed infiltration tests showed a large spatial heterogeneity of the soil infiltration capacity and permitted the identification of areas within the experimental sites characterized by similar infiltration behaviors. To properly estimate the field-saturated hydraulic conductivity starting from the infiltration tests results, these were analyzed using the Green Ampt model. The simplified infiltration model worked well for the tests developed within the two sites showing discrepancies with the experimental measures only in three cases. This is due to an outlier behavior, compared to the other 51 tests, of the infiltration curve in the first part of the test and this is probably caused by the presence of preferential flow-paths in the agricultural soil of the Colnù site that cannot be simulated with the simplified Green-Ampt model. The obtained spatially defined  $K_{mod}$  values were then analyzed by geostatistical tools to find the correlation length characterizing the spatial heterogeneity of the property. This length, in the Settolo site, was found not to be greater than 25 meters. The structural analysis (experimental variogram) computed for the group of  $\log K_{mod}$  values in the Settolo site, was used to test the estimation of the property in areas not covered by the surveys, by using the geostatistical algorithm Ordinary Kriging. This highlighted once again the result already achieved with the spatial characterization of the infiltration results, that better results are achieved by develop-

---

ing the analysis in separate wine-growing areas and not cultivate areas. To widening the perspective on the PPPs residues potentially affecting the groundwater quality, an extensive monitoring activity was developed using a multiparametric probe installed in 40 meters upstream to the base wall of the Settolo site. To date, the groundwater monitoring activity carried out in the saturated part of the phreatic aquifer of the Settolo site, has not highlighted any pollution phenomenon. At the provincial scale, the analysis of the plant protection products sale data in the province of Treviso, showed that PPPs sales are increasing and that, within the considered area, the sold PPPs are mainly destined to wine-growing practices. This is validated by the fact that the best-selling products are composed of fungicide active substances, being fungal and bacterial the main adversities affecting the vine plant. The CLP (Classification, Labelling and Packaging) labelling-based hazard analysis developed for the vine-specific PPPs, permitted the outlining, by assuming the use of the PPP in the municipality of sale, of a map showing the hazard of the wine-growing areas. The geographical analysis based on the level of superimposition obtained between the extension of the wellhead protection areas and the wine-growing areas, permitted to obtain a vulnerability map for wells dependent on the WHPAs extension. In a scenario developed assuming the WHPAs as defined by the 200 m radius geometrical criterion (D. Lgs 152/2006), 4 wells in the study area have a *very high vulnerability*, 6 wells have a *high vulnerability*, 1 well has a *medium vulnerability*, and all of them are located in the DOCG area. In absence of data on the proper extension of the WHPAs within the study area, a second vulnerability map was developed by assuming a radius of the geometrical criterion equal to 2 km. Even if this dimension could seem overestimated, it is now well known that WHPAs can be much more extended than 200 meters. In this scenario, developed also considering the numerous PPPs loss phenomena that could happen during the plants treatments (e.g. wind drift), 23 wells that before were classified with a low vulnerability, present now a medium or high vulnerability.

# Acknowledgments

I would like to thank Alto trevigiano services for having funded my thesis work and the related experimental activities.

I would like to thank the research groups of the DAFNAE department and the DICEA department, and everyone that has contributed to the development of the experimental activities in the field.

I would like to thank Professor Paolo Salandin, for his patience, trust, time, and commitment in supervising my research work

---



# Bibliography

- Allen, R. G., Pereira, L. S., Raes, D., Smith, M., et al. (1998). Crop evapotranspiration-guidelines for computing crop water requirements-fao irrigation and drainage paper 56. *Fao, Rome*, 300(9):D05109.
- Allison, F. E. (1966). The fate of nitrogen applied to soils. volume 18 of *Advances in Agronomy*, pages 219–258. Academic Press.
- Aparicio, V. C., De Gerónimo, E., Marino, D., Primost, J., Carriquiriborde, P., and Costa, J. L. (2013). Environmental fate of glyphosate and aminomethylphosphonic acid in surface waters and soil of agricultural basins. *Chemosphere*, 93(9):1866–1873.
- Arias-Estévez, M., López-Periago, E., Martínez-Carballo, E., Simal-Gándara, J., Mejuto, J. C., and García-Río, L. (2008). The mobility and degradation of pesticides in soils and the pollution of groundwater resources. *Agriculture, Ecosystems and Environment*, 123(4):247–260.
- Battaglin, W. A., Meyer, M. T., Kuivila, K. M., and Dietze, J. E. (2014). Glyphosate and its degradation product AMPA occur frequently and widely in U.S. soils, surface water, groundwater, and precipitation. *Journal of the American Water Resources Association*, 50(2):275–290.
- Baylis, A. D. (2000). Why glyphosate is a global herbicide: strengths, weaknesses and prospects. *Pest Management Science*, 56(4):299–308.

- 
- Bento, C. P., Commelin, M. C., Baartman, J. E., Yang, X., Peters, P., Mol, H. G., Ritsema, C. J., and Geissen, V. (2018). Spatial glyphosate and AMPA redistribution on the soil surface driven by sediment transport processes A flume experiment. *Environmental Pollution*, 234:1011–1020.
- Bittelli, M., Andrenelli, M., Simonetti, G., Pellegrini, S., Artioli, G., Piccoli, I., and Morari, F. (2019). Shall we abandon sedimentation methods for particle size analysis in soils? *Soil and Tillage Research*, 185:36–46.
- Bouwer, H. (1966). Rapid Field Air Entry Value and Parameters. *Water Resources Research*, 2(4):729–738.
- Burkart, M. and Stoner, J. (2008). Chapter 7 - nitrogen in groundwater associated with agricultural systems. In Hatfield, J. and Follett, R., editors, *Nitrogen in the Environment (Second Edition)*, pages 177–202. Academic Press, San Diego, second edition edition.
- Burri, N. M., Weatherl, R., Moeck, C., and Schirmer, M. (2019). A review of threats to groundwater quality in the anthropocene. *Science of The Total Environment*, 684:136–154.
- Carretta, L., Cardinali, A., Marotta, E., Zanin, G., and Masin, R. (2019). A new rapid procedure for simultaneous determination of glyphosate and ampa in water at sub  $\mu\text{g/l}$  level. *Journal of Chromatography A*, 1600:65–72.
- Childs, E. C. and Bybordi, M. (1969). The vertical movement water in stratified porous material: 1. Infiltration. *Water Resources Research*, 5(2):446–459.
- Conant, B., Cherry, J. A., and Gillham, R. W. (2004). A pce groundwater plume discharging to a river: influence of the streambed and near-river zone on contaminant distributions. *Journal of Contaminant Hydrology*, 73(1):249–279.

- Crestani, E., Camporese, M., and Salandin, P. (2015a). Assessment of hydraulic conductivity distributions through assimilation of travel time data from ERT-monitored tracer tests. *Advances in Water Resources*, 84:23–36.
- Crestani, E., Camporese, M., and Salandin, P. (2015b). Assessment of hydraulic conductivity distributions through assimilation of travel time data from ert-monitored tracer tests. *Advances in Water Resources*, 84:23–36.
- De Marsily, G. (1986). *Quantitative hydrogeology*.
- Deutsch, J. L. (2015). Experimental variogram tolerance parameters. *J. L. Deutsch (Ed.), Geostatistics Lessons*.
- Dittmar, H., Drach, M., Vosskamp, R., Trenkel, M. E., Gutser, R., and Steffens, G. (2009). *Fertilizers, 2. Types*. John Wiley & Sons, Ltd.
- Doherty, J. E. and Hunt, R. J. (2010). *Approaches to highly parameterized inversion: a guide to using PEST for groundwater-model calibration*, volume 2010. US Department of the Interior, US Geological Survey Reston.
- for Research on Cancer, I. A. (2017). Monographs on the evaluation of carcinogenic risks to humans 112, some organophosphate insecticides and herbicides. pages 1–452.
- Goovaerts, P. et al. (1997). *Geostatistics for natural resources evaluation*. Oxford University Press on Demand.
- Green, W. H. and Ampt, G. (1911). Studies on soil physics. *The Journal of Agricultural Science*, 4(1):1–24.
- Gupta, H. V., Kling, H., Yilmaz, K. K., and Martinez, G. F. (2009). Decomposition of the mean squared error and NSE performance criteria: Implications for improving hydrological modelling. *Journal of Hydrology*, 377(1-2):80–91.

- 
- Isaaks, E. H. and Srivastava, M. R. (1989). *Applied geostatistics*. Number 551.72 ISA.
- Journel, A. G. and Huijbregts, C. J. (1976). *Mining geostatistics*.
- Kjær, J., Ernsten, V., Jacobsen, O. H., Hansen, N., de Jonge, L. W., and Olsen, P. (2011). Transport modes and pathways of the strongly sorbing pesticides glyphosate and pendimethalin through structured drained soils. *Chemosphere*, 84(4):471–479.
- la Cecilia, D., Tang, F. H., Coleman, N. V., Conoley, C., Vervoort, R. W., and Maggi, F. (2018). Glyphosate dispersion, degradation, and aquifer contamination in vineyards and wheat fields in the Po Valley, Italy. *Water Research*, 146:37–54.
- la Cecilia, D., Tang, F. H., Coleman, N. V., Conoley, C., Vervoort, R. W., and Maggi, F. (2018). Glyphosate dispersion, degradation, and aquifer contamination in vineyards and wheat fields in the po valley, italy. *Water Research*, 146:37–54.
- Maggi, F. (2006). BRTSim . a general-purpose computational solver for hydrological , biogeochemical , and ecosystem dynamics.
- Maggi, F., la Cecilia, D., Tang, F. H., and McBratney, A. (2020). The global environmental hazard of glyphosate use. *Science of the Total Environment*, 717:137167.
- Mencaroni, M., Cardinali, A., Costa, L., Morari, F., Salandin, P., Zanin, G., and N, D. F. (2021). Mobility of glyphosate and ampa through different soil profiles of the prosecco wine production area. *Geoderma Regional*.
- Moore, I. D. and Eigel, J. D. (1981). Infiltration into two-layered soil profiles. *Transactions, American Society of Agricultural Engineers*, 24(6):1496–1503.
- Napoli, M., Marta, A. D., Zanchi, C. A., and Orlandini, S. (2016). Transport of Glyphosate and Aminomethylphosphonic Acid under Two Soil Management Practices in an Italian Vineyard. *Journal of Environmental Quality*, 45(5):1713–1721.

- Okada, E., Costa, J. L., and Bedmar, F. (2016). Adsorption and mobility of glyphosate in different soils under no-till and conventional tillage. *Geoderma*, 263:78–85.
- Okada, E., Costa, J. L., Bedmar, F., Barbagelata, P., Irizar, A., and Rampoldi, E. A. (2014). Effect of conventional and no-till practices on solute transport in long term field trials. *Soil and Tillage Research*, 142:8–14.
- Peruzzo, P. J., Porta, A. A., and Ronco, A. E. (2008). Levels of glyphosate in surface waters, sediments and soils associated with direct sowing soybean cultivation in north pampasic region of Argentina. *Environmental Pollution*, 156(1):61–66.
- Poiger, T., Buerge, I. J., Bächli, A., Müller, M. D., and Balmer, M. E. (2017). Occurrence of the herbicide glyphosate and its metabolite AMPA in surface waters in Switzerland determined with on-line solid phase extraction LC-MS/MS. *Environmental Science and Pollution Research*, 24(2):1588–1596.
- Remy, N., Boucher, A., and Wu, J. (2009). *Applied geostatistics with SGeMS: A user's guide*. Cambridge University Press.
- Schaap, M. G., Leij, F. J., and Van Genuchten, M. T. (2001). Rosetta: A computer program for estimating soil hydraulic parameters with hierarchical pedotransfer functions. *Journal of Hydrology*, 251(3-4):163–176.
- Shaw, E. (2005). *Hydrology in practice*. CRC press.
- Shepard, D. (1968). A two-dimensional interpolation function for irregularly-spaced data. In *Proceedings of the 1968 23rd ACM National Conference*, ACM '68, page 517–524, New York, NY, USA. Association for Computing Machinery.
- Sibson, R. (1981). A brief description of natural neighbour interpolation. *Interpreting multivariate data*.

- 
- Siebert, S., Burke, J., Faures, J. M., Frenken, K., Hoogeveen, J., Döll, P., and Portmann, F. T. (2010). Groundwater use for irrigation – a global inventory. *Hydrology and Earth System Sciences*, 14(10):1863–1880.
- Silva, V., Montanarella, L., Jones, A., Fernández-Ugalde, O., Mol, H. G., Ritsema, C. J., and Geissen, V. (2018). Distribution of glyphosate and aminomethylphosphonic acid (AMPA) in agricultural topsoils of the European Union. *Science of The Total Environment*, 621:1352–1359.
- Skinner, P., Cook, J., and Matthews, M. (1988). Responses of grapevine cvs. chenin blanc and chardonnay to phosphorus fertilizer applications under phosphorus-limited conditions. *Vitis*, 27:95–109.
- Stauffer, F., Guadagnini, A., Butler, A., Franssen, H.-J. H., Wiel, N. V. D., Bakr, M., Riva, M., and Guadagnini, L. (2005). Delineation of Source Protection Zones Using Statistical Methods. *Water Resources Management*, 19(2):163–185.
- Sun, M., Li, H., and Jaisi, D. P. (2019). Degradation of glyphosate and bioavailability of phosphorus derived from glyphosate in a soil-water system. *Water Research*, 163:114840.
- Székács, A. and Darvas, B. (2018). Re-registration Challenges of Glyphosate in the European Union. *Frontiers in Environmental Science*, 6(July):1–35.
- Tang, F. H., Jeffries, T. C., Vervoort, R. W., Conoley, C., Coleman, N. V., and Maggi, F. (2019). Microcosm experiments and kinetic modeling of glyphosate biodegradation in soils and sediments. *Science of The Total Environment*, 658:105–115.
- Tang, F. H., Lenzen, M., McBratney, A., and Maggi, F. (2021). Risk of pesticide pollution at the global scale. *Nature Geoscience*, 14(4):206–210.

- Thiessen, A. H. (1911). Precipitation averages for large areas. *Monthly weather review*, 39(7):1082–1089.
- Todorovic, G. R., Rampazzo, N., Mentler, A., Blum, W. E., Eder, A., and Strauss, P. (2014). Influence of soil tillage and erosion on the dispersion of glyphosate and aminomethylphosphonic acid in agricultural soils. *International Agrophysics*, 28(1):93–100.
- Trentin T. (2021). Setup of sensor network and modelling of the aquifer system in the high Venetian plain between Treviso, Padova and Venezia. *Ph.D. course of Science of Civil, Environmental and Architectural Engineering - XXXIII cycle*.
- van Genuchten, M. T. (1980). A Closed-form Equation for Predicting the Hydraulic Conductivity of Unsaturated Soils. *Soil Science Society of America Journal*, 44(5):892–898.
- Vieira, S. R., Nielsen, D. R., and Biggar, J. W. (1981). Spatial Variability of Field-Measured Infiltration Rate. *Soil Science Society of America Journal*, 45(6):1040–1048.
- Voronoi, G. (1908a). Nouvelles applications des paramètres continus à la théorie des formes quadratiques. deuxième mémoire. recherches sur les paralléloèdres primitifs. *Journal für die reine und angewandte Mathematik (Crelles Journal)*, 1908(134):198–287.
- Voronoi, G. (1908b). Nouvelles applications des paramètres continus à la théorie des formes quadratiques. premier mémoire. sur quelques propriétés des formes quadratiques positives parfaites. *Journal für die reine und angewandte Mathematik (Crelles Journal)*, 1908(133):97–102.
- Wauchope, R. D., Yeh, S., Linders, J. B. H. J., Kloskowski, R., Tanaka, K., Rubin, B., Katayama, A., Kördel, W., Gerstl, Z., Lane, M., et al. (2002). Pesticide soil sorption

---

parameters: theory, measurement, uses, limitations and reliability. *Pest management science*, 58(5):419–445.

Yang, X., Wang, F., Bento, C. P., Xue, S., Gai, L., van Dam, R., Mol, H., Ritsema, C. J., and Geissen, V. (2015). Short-term transport of glyphosate with erosion in Chinese loess soil — A flume experiment. *Science of The Total Environment*, 512-513:406–414.

Zovi, F., Camporese, M., Hendricks Franssen, H.-J., Huisman, J. A., and Salandin, P. (2017). Identification of high-permeability subsurface structures with multiple point geostatistics and normal score ensemble Kalman filter. *Journal of Hydrology*, 548:208–224.





